ALK1 SIGNALING IS REQUIRED FOR DIRECTED ENDOTHELIAL CELL MIGRATION IN THE PREVENTION OF ARTERIOVENOUS MALFORMATIONS

by

Elizabeth R Rochon

B.A. Biology, Rhode Island College, 2007

Submitted to the Graduate Faculty of

The Kenneth P. Dietrich School of Arts and Sciences in partial fulfillment

of the requirements for the degree of

Doctor of Philosophy

University of Pittsburgh

2015

UNIVERSITY OF PITTSBURGH

Kenneth P. Dietrich School of Arts and Sciences

This thesis was presented

by

Elizabeth R Rochon

It was defended on

March 27, 2015

and approved by

Jon Boyle, Ph.D., Associate Professor, Biological Sciences

Jeffery Hildebrand, Ph.D., Associate Professor, Biological Sciences

Neil Hukriede, Ph.D., Associate Professor and Vice Chair, Developmental Biology

Beth L. Roman, Ph.D., Associate Professor, Human Genetics

Committee Chair: Deborah Chapman, Ph.D., Associate Professor, Biological Sciences

ALK1 SIGNALING IS REQUIRED FOR DIRECTED ENDOTHELIAL CELL MIGRATION IN THE PREVENTION OF ARTERIOVENOUS MALFORMATIONS

Elizabeth R. Rochon, PhD

University of Pittsburgh, 2015

ALK1, a TGF-β type I receptor serine/threonine kinase, is critical for proper vascular development. Heterozygous loss of *ALK1* results in the vascular disorder, hereditary hemorrhagic telangiectasia type 2 (HHT2), which is characterized by the development of arteriovenous malformations (AVMs) and affects 1:8000 people worldwide. $alk1^{-/-}$ zebrafish develop embryonic lethal AVMs which form via a two-step mechanism. First, loss of *alk1* results in an increase in endothelial cell number in cranial arteries, which results in increased vessel caliber. In the second step, normally transient connections between arteries and veins are maintained as an adaptive mechanism to cope with an increased hemodynamic load. Using zebrafish as a tool to study the AVM formation due to loss of Alk1 signaling, I have found that Alk1 is required for directed arterial endothelial cell migration in opposition to blood flow. Embryos lacking *alk1* experience a redistribution of cells, with endothelial cells failing to efficiently migrate against the direction of blood flow and accumulating in more distal regions of *alk1*-dependent arteries. This altered cellular distribution causes an increase in arterial caliber and consequent retention of downstream arteriovenous connections, resulting in fatal AVMs.

Notch and ALK1 have been implicated in arterial specification and loss of function of either pathway causes AVMs. Furthermore, ALK1 can cooperate with Notch to upregulate expression of Notch target genes in cultured endothelial cells. These findings have led to the hypothesis that Notch and ALK1 collaboratively program arterial identity and prevent AVMs. I modulated Notch and Alk1 activities in zebrafish embryos and examined effects on Notch target gene expression and vascular morphology. Results demonstrate that control of Notch targets is context-dependent, with gene-specific and region-specific requirements for Notch and Alk1. Although loss of *alk1* increases expression of *dll4*, which encodes a Notch ligand, and enhanced Notch signaling causes AVMs, AVMs in *alk1* mutants could neither be phenocopied by Notch activation nor rescued by Notch inhibition. In conclusion, Alk1 is dispensable for acquisition and maintenance of arterial identity, and perturbations in Notch signaling cannot account or AVM development in *alk1* mutants.

TABLE OF CONTENTS

LIST OF TABLES

LIST OF FIGURES

PREFACE

I would like to begin by thanking Beth Roman for her outstanding mentorship throughout my graduate school career. She has been a model of integrity, hard work, honesty and perseverance. With her assistance, I have developed a solid base of knowledge and gained the tools I need to be successful in where ever my science career may take me. May she be rewarded for the quality of her efforts, the creativity of her ideas, the depth of her knowledge and the intensity of her need to understand, no one is more deserving.

I would also like to thank each of my committee members, Dr. Jon Boyle, Dr. Jeff Hildebrand, Dr. Neil Hukriede and especially Dr. Debbie Chapman, who provided my with much support and humor throughout this process. Each of them has been instrumental to my growth as a scientist, and the aid that they have provided to me has made this research possible. I will always remember their kindness and support.

A very special thanks to Dr. Suzanne Conklin. Her belief in my abilities and her persistence in urging me to apply to graduate school is the sole reason I am here today. Her presence in my life has changed the course of my life and for that I will never be able to repay her.

I have had the honor of working with many talented people in the lab who have touch my heart in many ways. A special thanks to Sarah Young (the best co-worker, mentor and friend), Paola Corti (who always has a balanced perspective on the world), Zak Kupchinski (Kupchinsky? Kupcinski? Fish whisperer), Derek Laux (my partner in crime and friend for life), Shane Wright (fastest learner and most supportive lab mate), Teresa Capasso (the sunshine in my life) and all of our other lab technicians, undergraduates and supportive help I've worked with throughout my years here at Pitt.

To my friends, thank you for your patience and love. I would like to thank each one of them for providing me with nothing but love and happiness over the past several years. You have been my family here in Pittsburgh and for that I am thankful.

To my family, your support has been the only reason I have been able to complete this journey. This accomplishment is ours, not just mine. Thank you.

LIST OF COMMONLY USED ABBREVIATIONS

AA1: first aortic arch

Alk1: activin receptor-like kinase

ALPM: anterior lateral plate mesoderm

AVM: arteriovenous malformation

BA: basilar artery

BCA: basal communicating artery

BMP: bone morphogenetic protein

CaDI: caudal division of the internal carotid artery

CCV: common cardinal vein

Coup-TFII: chicken ovalbumin upstream promoter transcription factor II

CrDI: cranial division of the internal carotid artery

CtA: central arteries

CV: caudal vein

DA: dorsal aorta

DLL4: delta-like ligand 4

dpf: days post fertilization

ECM: extracellular matrix

Edn1: endothelin-1

Efnb2: ephrinb2

ENG: endoglin

Fli1a: friend leukemia integration 1a

Gof: gain of function

HES1: hairy and enhancer of split

HHT: hereditary hemorrhagic telangiectasia

HIF-1α: hypoxia-inducible factor-1α

Hpf: hours post fertilization

HUVECS: human umbilical vein endothelial cells

ICA: internal carotid artery

KLF: krüppel-like factor

LDA: lateral dorsal aorta

Lof: loss-of-function

MO: morpholino

MOC: midbrain organizing center

MtA: metencephalic artery

MTOC: microtubule organizing center

NF-κB: nuclear factor kappa B

NICD: notch intracellular domain

NO: nitric oxide

OA: optic artery

PCS: posterior communicating segments

PECAM-1: platelet endothelial cell adhesion molecule-1

PHBC: primordial hindbrain channel

PLPM: posterior lateral plate mesoderm

PMBC: primordial midbrain channel

RBPJ: recombination signal binding protein for immunoglobulin kappa J

ROC: rostral organizing center

Shh: sonic hedgehog

Sih: silent heart

Tg: transgenic

TGFβ: transforming growth factor β

VECAD: vascular endothelial cadherin

VEGF: vascular endothelial growth factor

vSMC: vascular smooth muscle cell.

1.0   INTRODUCTION

1.1   VERTEBRATE VASCULAR DEVELOPMENT

1.1.1   Origins of the primitive vasculature

The circulatory system is one of the first organ systems to form in development and is responsible for the transport of gases, nutrients, hormones and metabolites throughout the embryo. In all vertebrate embryos, the first blood vessels arise via the process of vasculogenesis, the de novo formation of blood vessels from endothelial precursor cells known as angioblasts. The molecular mechanisms involved in angioblast differentiation are highly conserved among vertebrate species: members of the ETS and FOX transcription factor families are important for specifying endothelial cell lineages within mesoderm in fish, mice and humans [1].

Extraembryonically, blood islands arise within the yolk sac mesoderm of developing mammals and avians: the outer cells differentiate into endothelial cells, cells that line the vascular lumen, whereas the inner cells differentiate into red blood cells [2, 3].

In the embryo proper, cells within the posterior lateral plate mesoderm (PLPM) give rise to angioblasts that arrange into clusters by embryonic day (E)7.0 in mice [2], by the 10-somite stage in zebrafish [4] , and by the 1-somite stage in quail [5]. These cells migrate individually or as groups towards the midline, where they coalesce into cords and lumenize to form the trunk axial blood vessels [2, 4, 5].

1

Cranial vessels develop from anterior lateral plate mesoderm (ALPM) via a hybrid vasculogenic and angiogenic process. Instead of migrating to the midline, angioblasts migrate as discrete groups of cells to form large clusters; cells within these clusters proliferate and migrate via an angiogenesis-like sprouting mechanism to shape the cranial vessels. Specifically, within the developing zebrafish embryo, two sets of bilateral angioblast clusters form adjacent to the midbrain and the most rostral point of the ALPM. Sprouting from these clusters gives rise to the majority of cranial vessels [6]. A similar hybrid vasculogenic/angiogenic mechanism is involved in the formation of the pharyngeal arch arteries of mice and zebrafish: individual angiogenic clusters (one per arch artery) differentiate in the pharyngeal mesoderm and sprout dorsally to connect to the already patent dorsal aorta(e), and ventrally to give rise to the ventral aorta [7-9]. The ventral aorta connects directly to the outflow tract of the heart, thereby completing the initial primitive vascular loop.

1.1.2   Lumen Formation

Once a cord of endothelial cells has formed, it must hollow out to carry blood flow. While there is some evidence suggesting that cell hollowing (intracellular vacuole formation and fusion) may be involved in the formation of vessel lumens in vivo [10], a majority of the evidence now indicates that cord hollowing is the predominant mechanism by which vessels lumenize [11-13]. In the cord hollowing mechanism, apicobasal polarity is established via a Par3-mediated redistribution of junctional complexes away from the future apical surface and towards the periphery of endothelial cells within a cord [14].   Once polarity has been established, podocalyxin (PODXL) and CD34 are recruited to the apical surface [13]. These proteins, which

are members of the CD34-sialomucin family of proteins, are cell surface transmembrane proteins that mediate de-adhesion [15]. Additionally, PODXL/CD34 recruit moesin, which binds to F-actin, creating a network of actin filaments along the apical surface of the vessel and allowing further separation of apical surfaces via myosin-mediated contraction. Fluid passively enters the luminal space through paracellular gaps that are later resolved, resulting in an enclosed lumen [13].

1.1.3 Elaboration and remodeling of the primitive vasculature

Angiogenesis is the process by which the basic vessel architecture laid down during vasculogenesis is remodeled and expanded. Angiogenesis includes remodeling of capillary plexuses into hierarchical structures (Figure 1); sprouting of new vessels from existing vessels; and splitting of single vessels into multiple vessels (intussusception) [16].

During the activation phase of angiogenesis, basal lamina is degraded, mural cells detach and there is an increase in endothelial cell proliferation and migration. Vascular endothelial growth factor (VEGF) signaling is a critical regulator of angiogenesis and is required for nearly all aspects of vascular development. Signaling induces endothelial cell proliferation, migration and supports endothelial cell survival [17, 18]. There are five ligands in the VEGF family, VEGFA, VEGFB, VEGFC, VEGFD and placenta growth factor (PlGF), and three VEGF receptors, VEGFR1 (also known as FLT1), VEGFR2 (also known as FLK1 and KDRL), and VEGFR3 (FLT4). VEGFR2 and VEGFR3 are tyrosine kinases and ligand binding results in receptor dimerization and phosphorylation. VEGFA binding to VEGFR2 acts as the primary positive regulator of angiogenesis. Phosphorylation of VEGFR2 activates a complex network of

intracellular signal transduction pathways including phospholipase C gamma (PLCγ), mitogen-activated protein kinase (MAPK), protein kinase B (PKB or AKT), focal adhesion kinase (FAK), and nitric oxide (NO) signaling [17, 19, 20]. In mice, heterozygous loss of either *Vegfa* or *Vegfr2* is embryonic lethal due to decreased vascular density [21]. VEGFC and D interact with VEGFR3, and signaling through this receptor is critically important for lymphatic development and is involved in early venous specification [22, 23]. VEGFR1 has limited kinase activity [24] and acts primarily as a competitive inhibitor of VEGFR2 signaling by binding to VEGFA and VEGFB and acting as a ligand sink [25]. *Vegfr1*$^{-/-}$ mice die embryonically due to a hypervascular phenotype [26].

VEGF ligands and receptors are regulated by a wide variety of mechanisms. Hypoxia-inducible factor-1α (HIF-1α) upregulates VEGF signaling in response to tissue hypoxia, resulting in increased angiogenesis during tissue growth, development and wound repair [27]. ETS transcription factors (involved in angioblast specification as discussed above) can induce the expression of VEGF ligands and receptors [28]. Also Notch signaling is critical for regulating and restricting expression of specific VEGF receptors during sprouting angiogenesis [29-34].

An angiogenic sprout is composed of two different cell types, the tip cell and the stalk cell (Figure 2). Tip cells extend their filopodia towards an angiogenic stimulus and lead the sprout, while the stalk cells trail the tip cell and maintain a connection to the parent vessel and establish a vessel lumen [35, 36]. Microarray analysis of individual tip and stalk cells isolated by laser capture microdissection has revealed cohorts of genes that are differentially expressed in the two cell types [37]. *VEGFR2* is highly expressed in tip cells and permits cells to migrate towards VEGFA, which is expressed in nearby tissues in a morphogenetic gradient. Delta-like ligand 4 (*DLL4*), a membrane-bound ligand of the Notch pathway, is also preferentially

4

expressed in the tip cell and binds to Notch receptors in the neighboring stalk cell to active Notch signaling. Notch signaling represses expression of *VEGFR2* in stalk cells, thereby decreasing responsiveness to VEGFA [34, 38-41]. Cells with higher levels of VEGF signaling and lower levels of Notch signaling are found in the tip position [29]. However, tip and stalk cells do not have a fixed identity in an angiogenic sprout. Additional genetic interactions between Notch and VEGF signaling result in a transient induction of *DLL4* mRNA by VEGF [29, 42]. This tight regulation of *DLL4* results in fluctuating levels of *VEGFR2* expression. This results in a dynamic competition between overlapping cells within sprouts for the tip cell position [29, 43].
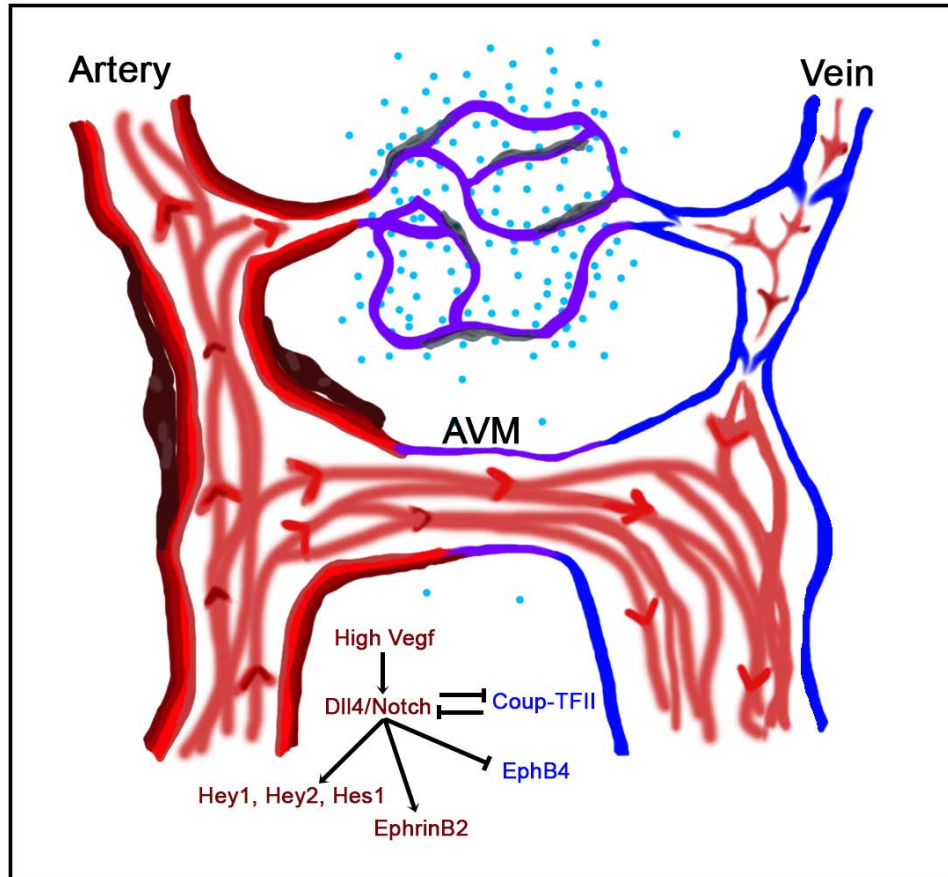
Figure 1: Arterial and venous differentiation and the formation of AVMs

Arteries (in red) are specified by Vegf-induced activation of Notch signaling, resulting in the expression of hey1, hey2, hes1 and ephrinb2. Notch/Dll4 signaling also represses the expression of ephb4 (a venous marker) in the arterial endothelium. Veins (in blue) express Coup-TFII, which represses Notch signaling in the venous endothelium and vice versa. High flow arteries have thick walls lined with vascular smooth muscle cells (brown cells) and flow into smaller caliber arterioles and finally into capillaries (purple), the location of oxygen and nutrient exchange (blue dots). Venules and then veins receive low magnitude flow and have valves to prevent backflow. AVMs are direct connections between arteries and veins, lacking an intervening capillary bed. These high flow shunts decrease oxygen and nutrient exchange. Also, veins that are downstream of these high flow shunts are enlarged. Impaired arterial venous specification has been implicated in AVM formation.

1.1.4   Vessel stabilization

During the resolution phase of angiogenesis, endothelial cells cease to migrate and proliferate and vessels are stabilized through the deposition of basal lamina and the recruitment of vascular smooth muscle cells (vSMCs) and pericytes, a type of vascular support cell [44]. Vascular mural cells function to support the endothelial cell layer and are able to contract and regulate vascular tone in response to environmental cues [45]. A number of signaling pathways are important for the resolution phase of angiogenesis. Platelet derived growth factor (PDGF) produced by endothelial cells attracts PDGFR-expressing pericytes and induces mural cell proliferation [46]. Additionally, sphingosine-1 phosphate (S1P)/S1P receptor 1 (S1PR1), angiopoetin1/Tie2 and Transforming growth factor β (TGFβ) signaling all contribute to vascular maturation through pericyte recruitment and/or extracellular matrix deposition [45].

1.1.5   Arterial and Venous Specification

Arteries and veins are genetically distinct prior to the onset of blood flow. Shortly after angioblasts are specified as endothelial cells they take on an arterial or venous (A/V) identity. In the trunk, sonic hedgehog (*shh*) expressed in the notochord induces the expression of *vegf* in the somites [47-49]. Vegf signaling induces *dll4* expression and Notch activation in the endothelium (Figure 1) [49]. It is thought that venous identity is the default identity, while Notch signaling confers an arterial identity through the regulation of *hey1*, *hey2* and *hes* genes [30, 50].

Additionally, Notch has been shown to regulate *ephrinB2* [30]. EphrinB2 is a ligand for the EphB4 receptor. EphrinB2/EphB4 are transmembrane proteins that signal through cell-cell

contact and label arterial and venous cells, respectively [51-53]. While Notch signaling induces *ephrinB2* expression in arterial endothelial cells, loss of Notch signaling results in the ectopic expression of *ephB4* in these same cells [30].
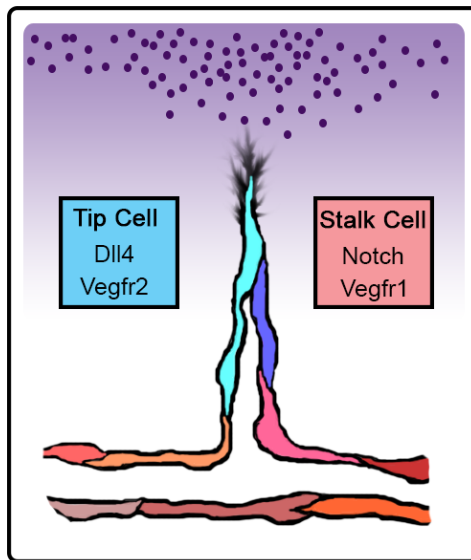
Figure 2: Angiogenic sprouts are composed of tip and stalk cells

Cells leading the way in a sprouting vessel extend filopodia as they migrate toward an angiogenic environmental cue (purple dots). Tips cells (cool colored cells) express high levels of dll4 and vegfr2 in relation to stalk cells (warm colored cells), which express notch and vegfr1. Stalk cells trail the tip cells, maintaining a connection to the parent vessel and forming a lumen. Interactions been Notch and Vegf pathways result in a dynamic competition between overlapping tip cells.

In addition to *ephB4* expression in venous endothelial cells, chicken ovalbumin upstream promoter transcription factor II (Coup-TFII), also known as nuclear receptor subfamily 2, group F, member 2 (Nr2f2) is an orphan nuclear receptor that is cell autonomously involved in determining venous identity [54]. Coup-TFII functions to downregulate Notch signaling in veins, and ectopic overexpression of coup-TFII in endothelial cells results in the fusion of arteries and veins [55, 56]. While it is thought that Coup-TFII functions to inhibit Notch signaling and repress arterial specification, Notch signaling has also been shown to block *Coup-TFII* expression during arterial differentiation (Figure 1), underscoring the complicated interactions involved in determining A/V identity that are not yet fully understood [57, 58].

While the identity of endothelial cells is genetically determined before the onset of blood flow, arterial and venous identity is reversible and highly plastic. In quail/chick grafting experiments, donor arterial or venous cells populate either type of vessel in a host embryo and take on the genetic identity of the host vessel [59, 60]. Additionally, time-lapse imaging of chick vessel development nicely demonstrates the plastic nature of vessel identity. As the vascular network remodels and arterial sprouts let go of a parent artery and reconnect to the venous plexus, they take on a distinct venous identity [61]. Hemodynamic forces also influence vessel identity. Arterial ligation in a chick embryo results in an arterial-to-venous identity change [61]. These results suggest that vessel identity is first determined through genetic mechanisms, but can be altered after the onset of circulation in response to blood flow as the vascular network remodels.

1.2 BLOOD FLOW AND MECHANOTRANSDUCTION

1.2.1 Hemodynamic forces in blood vessels

Prior to the onset of blood flow, vessel development is governed by local paracrine factors. Upon the onset of circulation, mechanical forces and endocrine factors influence vessel morphology, endothelial cell behavior and maintenance of arterial-venous identity.

There are three mechanical forces sensed by vessels: shear stress, cyclic strain, and hydrostatic pressure. Shear stress is a frictional force that acts directly on luminal surface of endothelial cells, parallel to the surface of the vessel. It is proportional to the flow rate and viscosity of the blood and inversely proportional to the vessel radius. Cyclic strain results in circumferential stretching of the vessel wall, whereas hydrostatic pressure acts perpendicular to and pushes outward on the vessel wall. Whereas shear stress is directly sensed only by endothelial cells, cyclic strain and hydrostatic pressure can be sensed by all cells in the vessel [62]. Of these forces, shear stress is the best studied. Vessels attempt to maintain normalized forces. In the face of increased blood flow rate (increased cardiac output) or viscosity, vessels will increase their radius to decrease the total shear forces experienced by the endothelial cells. Likewise, decreased shear forces result in decreased vessel caliber and in some cases, vessel regression [63-67].

Different types of shear stress have been shown to result in different biochemical responses. Straight vessels experience pulsatile laminar shear stress associated with high magnitude shear forces. Branched and curved vessels experience disturbed flow and low shear stress [62]. These different types of flow have different effects on gene expression and

endothelial cell behavior [68]. High pulsatile laminar shear stress activates Krüppel-like factor 2 (KLF2), a flow regulated transcription factor that favors vessel quiescence [69-71], while disturbed flow activates nuclear factor kappa B (NF-κB), resulting in an activated inflammatory response [72]. KLF2 inhibits the expression of NF-κB responsive genes, suggesting a mechanism by which an inflammatory response is silenced as the endothelium establishes a laminar shear flow pattern and the vessels become quiescent [73]. To accomplish these changes, the vessels need to be able to sense these different flow patterns and mechanical forces and then translate them into a biochemical response.

1.2.2   Mechanosensation of shear stress

It is not yet fully understood how shear stress is sensed nor how sensation is transduced to changes in gene expression and cell behavior. However, the primary cilium, cell-cell adhesion dynamics, the glycocalyx and nuclear hydrodynamic drag have all been implicated in vascular mechanosensation of shear stress (Figure 3) [62, 74].

1.2.2.1 Primary cilia

Primary cilia (Figure 3) are composed of microtubules arranged in a 9+0 pattern. They are nonmotile and reside on the apical surface of a cell. In endothelial cells, cilial bending results in a transient calcium influx that ultimately results in the production of NO, a potent vasodilator [75]. However it is unlikely that this is the primary means of mechanosensation. In regions of disturbed flow, some endothelial cells have a primary cilium [76, 77], whereas cells experiencing high physiological levels of shear stress dismantle their primary cilium [78-80]. Additionally,

while this mechanism would relay flow magnitude to the cell, it is unclear how the calcium influx could translate directional information [74].

1.2.2.2 Glycocalyx

The endothelial glycocalyx (Figure 3) consists of sulfated proteoglycans, hyaluronan and glycoproteins creating a gel-like layer that covers the apical membrane of endothelial cells [81]. The glycocalyx serves many functions including regulating vascular permeability and the formation of docking sites for plasma-derived molecules, creating microenvironments of growth factors and atheroprotective proteins [82]. In relation to mechanotransduction, it is thought that the glycocalyx is displaced in the direction of flow and transduces mechanical forces to the actin cytoskeleton via adherens junctions [83].

1.2.2.3 Adherens complex

Platelet endothelial cell adhesion molecule-1 (PECAM-1) and vascular endothelial cadherin (VECAD) are endothelial-specific proteins that localize to adherens junctions. Along with VEGFR2, these cadherins have been implicated in a flow-sensing complex that is critical in transducing shear stress into a biochemical response (Figure 3). PECAM-1 is thought to act as a direct mechanosensor because cultured endothelial cells incubated with PECAM-1 antibody-coated magnetic beads exhibit rapid PECAM-1 phosphorylation upon application of magnetic force, similar to that seen upon application of fluid shear stress. [84]. Through a mechanism that is not yet fully understood, shear stress leads to an accumulation of VEGFR2 at adherens junctions, and shear stress-induced phosphorylation of PECAM-1 results in ligand-independent phosphorylation of VEGFR2. With VECAD acting as a scaffolding protein, VEGFR2 initiates a

12

series of molecular events beginning with the activation of phosphatidylinositol-3-kinase (PI3K) and Akt [85]. Akt activation enhances NO production [86, 87], and increases activation of integrins [85], resulting in a cascade of molecular pathways that result in an endothelial cell response to flow.

1.2.2.4 Hemodynamic drag

In response to shear stress, endothelial cells become planar polarized, with the golgi apparatus and the microtubule organizing center positioned upstream of the nucleus with respect to the direction of flow (Figure 3). This arrangement has been shown to be dependent on PECAM-1/VEGFR2/VECAD mechanosensing complex [85]; however a direct mechanical push on the nucleus may also be a major factor in this polarization [74]. The bulge of the nucleus slightly protrudes into the lumen of the vessel and hydrodynamic drag pushes the nucleus downstream. The nuclear envelope, which is attached to the actin cytoskeleton, gradually rearranges as the location of the nucleus shifts. If the actin cytoskeleton is weakened by latrunculin treatment, there is less resistance to the downstream nuclear shift, and the endothelial cells polarize faster in the presence of flow [74]. In support of this model, a Nesprin-mediated link between the actin cytoskeleton and the nuclear envelope is necessary for shear stress induced endothelial cell polarization [88].
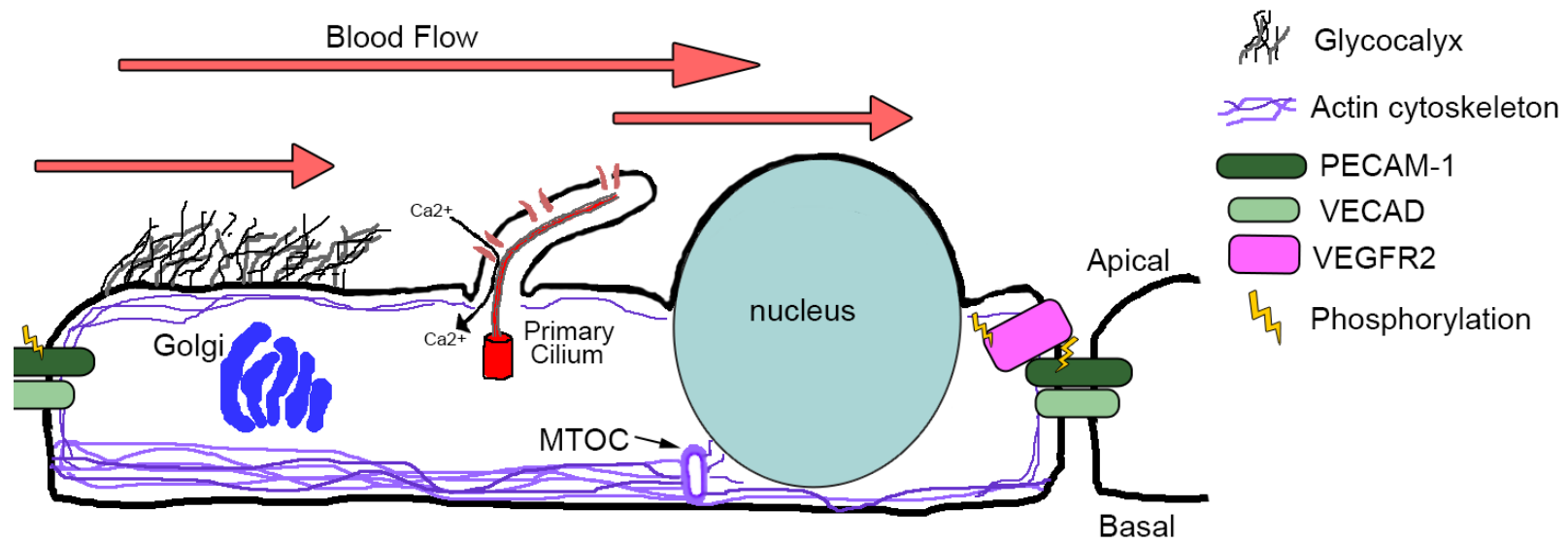
Figure 3: Mechanosensation of shear stress, four possible mechanisms

1: Primary cilia are displaced by blood flow resulting in a calcium influx, resulting in the production of NO. 2: The glycocalyx on the surface of endothelial cells bends in the direction of flow, transducing mechanical forces to the actin cytoskeleton via adherens junctions. 3: Shear stress activated PECAM-1 phosphorylates VEGFR2 and together with VECAD initiates signaling cascades that alter gene expression and cell behavior. 4: The nucleus bulges into the lumen of the vessel, experiencing hemodynamic drag, and orients itself downstream of the golgi apparatus and the microtubule organizing center, relaying both direction and strength of force to the actin cytoskeleton

1.3   ARTERIOVENOUS MALFORMATIONS

1.3.1   Anatomical and functional differences between different types of blood vessels

Arteries and veins (Figure 1) have developed structural features that reflect differences in the hemodynamic factors that each vessel type encounters. Arteries carry blood away from the heart and are designed to cope with high hemodynamic forces (pressure, shear stress, stretch): they have thick walls composed of several layers of smooth muscle and elastic fibers [16, 62]. Arteries lead to smaller caliber arterioles, which then ramify into a complex network of thin-walled capillaries [16]. Capillaries are sparsely supported by pericytes and serve as the site of nutrient and oxygen exchange [45]. As blood flows though the highly branched capillary bed, velocity decreases dramatically, and thus veins experience much lower magnitudes of hemodynamic force [89]. Accordingly, veins have thin walls and valves, which function to prevent back flow of blood.

1.3.2   Anatomy of AVMS

Arteriovenous malformations (AVMs) are direct, high flow connections between thick walled arteries and thin walled veins, lacking an intervening capillary bed. Over time, these connections become increasingly complex and tortuous, forming a tangled web of enlarged vessels, or nidus, which leads to a grossly enlarged draining vein. These malformations acquire a thick smooth muscle coat, thereby barring gas exchange (Figure 1) [90, 91]. Although the etiology of AVMs is

unclear, there is evidence to suggest that in some cases they arise due to failed regression of normally transient arterial/venous connections, or failed repulsion between arteries and veins due to improper arterial/venous (A/V) specification [53, 92].

1.3.3 Clinical consequences of AVMs

The clinical consequences of an AVM will depend on the location and size of the lesion. Generally, AVMs decrease gas exchange and cause localized ischemia, and these malformations may rupture due to the inability of veins to handle high magnitudes of mechanical forces [91]. Specifically, cerebral AVMs may cause localized ischemia or hemorrhagic stroke; pulmonary AVMs rarely rupture but can lead to cyanosis, brain abscess, transient ischemic attacks, and embolic stroke; and very high flow hepatic AVMs can lead to high output cardiac failure [93]. AVMs connecting small, mucocutaneous vessels are known as telangiectasias. Dermal telangiectasias may bleed but are primarily a cosmetic issue, whereas bleeding from GI and nasal telangiectasias can cause anemia and severe hemorrhage [94].

1.3.4 Genetic basis for AVMs

A majority of AVMs are sporadic, however, a subset of these vascular lesions is caused by genetic mutations. Capillary malformation-arteriovenous malformation (CM-AVM) is caused by heterozygous mutations in *Rasa1*, which encodes RAS p21 protein activator 1, and is characterized by multiple small capillary malformations [95]. Hypotrichosis-lymphedema-telangiectasia syndrome (HLTS) results from mutations in *Sox18*, a known regulator of *Dll4*, and

results in telangiectasias, lymphatic defects and renal failure [96]. Ataxia-Telangiectasia is an autosomal recessive mutation in *Ataxia-telangiectasia mutated* (*ATM*) gene. *ATM* is a serine/threonine protein kinase and is critical for normal repair of double stranded DNA breaks. As such, patients harboring mutations in this gene suffer from a wide array of symptoms including compromised immune systems, gonadal dysgenesis and telangiectasias [97]. Mutations in genes involved in the TGFβ signaling pathway are linked to the vascular dysplasia hereditary hemorrhagic telangiectasia (HHT) [98], the disease that is the main focus of my research.

1.3.5 Hereditary Hemorrhagic Telangiectasia

HHT, also known as Osler-Rendu-Weber syndrome, is a genetic disorder characterized by a predisposition to telangiectasias and AVMs. HHT is estimated to affect approximately 1:8000 individuals. However, due to the nonspecific symptoms (e.g. frequent nosebleeds) and variability in expressivity and age of onset of this disease, HHT is thought to be significantly underdiagnosed [98].

1.3.6 Genotype/phenotype correlations in HHT

Heterozygous mutations in members of the TGF-β signaling pathway are causally related to HHT. Mutations in Endoglin (*ENG*), a co-receptor in the pathway, result in HHT1 [99]. Mutations in *ACVRL1*, which encodes the TGF-β type I receptor, ALK1, result in HHT2 [100]. Additionally, mutations in *SMAD4*, a critical intracellular signal mediator within this pathway,

result in a combined juvenile polyposis-HHT syndrome [101]. Two additional loci on chromosomes 5q31.3-32 and 7p14 have been linked to HHT; however, the responsible genes within these loci have not yet been identified [102, 103]. HHT1 and HHT2 present with different phenotypic severity and location. HHT1 patients tend to experience more severe symptoms with an earlier age of onset. 49-75% of HHT1 patients present with pulmonary AVMs (PAVMs), 15-20% with cerebral AVMs (CAVMs) and 2-8% with hepatic AVMs (HAVMs). Between 60-72% of HHT1 patients have GI telangiectasias with approximately 18% of these patients experiencing bleeding [104-106]. HHT2 patients are typically diagnosed around the age of 40 and, compared to HHT1 patients, present with similar incidences of GI (gastrointestinal) telangiectasias/bleeding and lower incidences of PAVMS and CAVMs (5-44% and 0-2%). However, the incidence of HAVMs is between 28-84% in these patients [104-106]. The reason for the differences in the phenotypic severity and presentation between the two HHT sub-groups is unknown but may reflect differential tissue distribution or function of Endoglin and Alk1 [107].

1.3.6.1 ALK1 signaling

Overview of TGF-β family signaling

In TGF-β signaling, dimeric ligand binds to a heterotetrameric complex of type I and type II receptors. Upon ligand binding, the type II receptor phosphorylates the type I receptor. The type I receptor then phosphorylates Smad transcription factors. Once activated, Smad proteins bind to the common partner Smad, Smad4, and translocate into the nucleus to regulate the transcription of target genes (Figure 4). TGF-β superfamily signaling involves seven type I receptors (ALK1-

ALK7) and five type II receptors (ActRIIA, ActRIIB, BMPRII, TGFβII and AMHRII), all of which are serine/threonine kinases. Ligand binding to a heterotetrameric complex of type I and type II receptors can be facilitated by a type III receptor, ENG, which does not have enzymatic activity [108]. The family of TGF-β ligands is large and can be divided into multiple sub-families. Ligands in the TGF-β and activin subfamilies bind to receptor complexes that phosphorylate Smad2 and Smad3. Bone morphogenetic protein (BMP) ligands bind to different receptor complexes that phosphorylate Smad1, Smad5 and Smad9 [109].

Alk1 in vascular development

ALK1 is a transmembrane protein containing an extracellular N-terminal domain that binds ligand, a short, single pass transmembrane domain and a large intracellular domain. The intracellular domain contains three main motifs: a GS domain, a serine/threonine kinase domain and a cytoplasmic tail. The GS domain is phosphorylated by the type II receptor and contains a highly conserved TTSGSGSG motif [110, 111]. To date, 434 mutants in Alk1 have been identified, of which 50% have been found to be pathogenic (http://www.arup.utah.edu/database/hht/). Of these, 46% are missense mutations. Limited in vitro analysis of HHT2-associated *ALK1* mutations suggests that the majority of mutant proteins are localized to the cell surface and are able to bind to BMP9 (except for mutants in the extracellular domain), and that mutant protein does not affect activity of wild type protein [112, 113]. These data indicate that these mutations do not act as a dominant negative and suggest instead that phenotypes result from a haploinsufficiency [112].
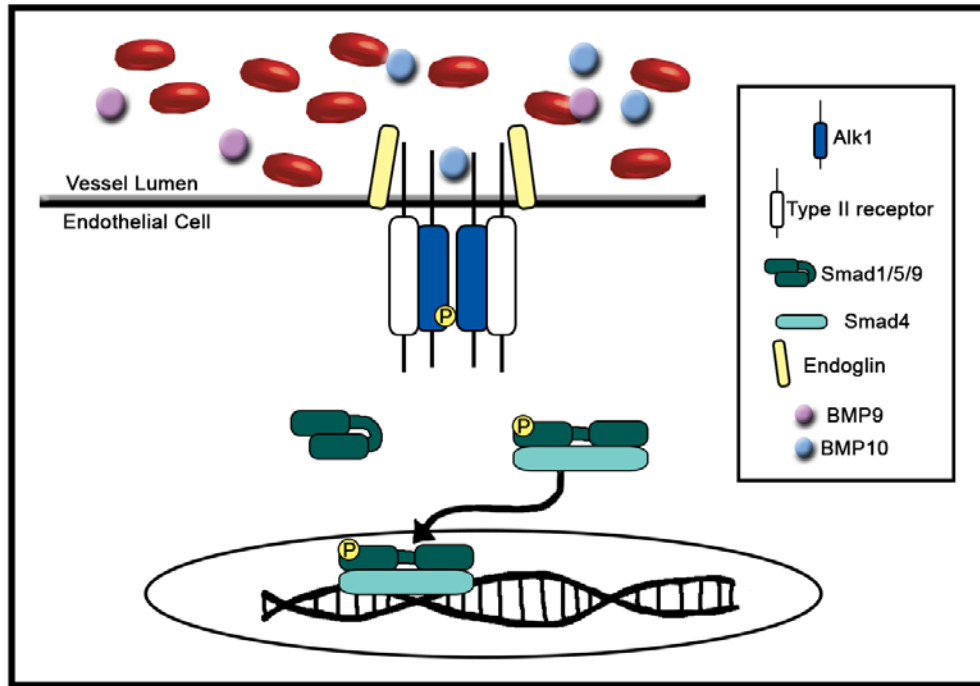
Figure 4: BMP/Alk1 signaling

Circulating Bmp9 or Bmp10 bind to a heterotetrameric complex consisting of two type I receptors (Alk1), two type II receptors (ActRIIA, ActRIIB or BMPRII) and the type III accessory receptor, Endoglin. Activated Alk1 phosphorylates Smad1/5/9, releasing it from an auto-inhibitory fold and allowing it to complex with Smad4, the common partner Smad. The activated Smad complex translocates to the nucleus where it binds DNA and affects the transcription of target genes.

Alk1 null mice are embryonic lethal at E11.5 due to enlarged vessels, impaired vascular remodeling, decreased vascular support cell coverage and AVMs [114, 115]. Heterozygous adults exhibit age-related dilated vessels, hemorrhage and bleeding within the GI tract [116]. Endothelial-specific deletion of *Alk1* during embryogenesis results in AVMs and is lethal by postnatal day 5 [117, 118]. Endothelial-specific deletion in adulthood is also lethal within 10-14 days of deletion due to vascular defects, mostly within the GI tract. However, development of dermal telangiectasias in these mice requires wounding. These data suggest that active angiogenesis is required for AVM and telangiectasia development in the absence of Alk1. [119, 120].

Zebrafish lacking *alk1* develop cranial AVMs in 100% of embryos by 36 hours post fertilization (hpf) and die by 5 days post fertilization (5 dpf). Heterozygous embryos have no phenotype and adults appear to be indistinguishable from their wild type siblings [92, 121]. While no apparent vascular phenotype has been observed in *alk1* heterozygous adults, the condition has not been studied thoroughly.

Endoglin in vascular development

ENG is an integral membrane protein that functions as a homodimer in conjunction with type I and type II TGFβ receptors to facilitate ligand binding [122]. BMP9 and BMP10 have been shown to bind directly to ENG [123, 124]. Homozygous mutant *Eng* mice die between E10.5-11.5 due to cardiac and vascular defects including enlarged vessels, impaired vascular remodeling and a decrease in vascular support cells [125-128]. However, these mice do not develop severe AVMs, as would be expected based on HHT1 patients. This is most likely due to cardiac defects resulting in early lethality. In support of this idea, neonatal endothelial-specific

deletion of *Eng* results in AVMs in a high percentage of mice [129], and adult mice harboring a single *Eng* mutation tend to develop age-related HHT-like phenotypes including nosebleeds, enlarged vessels and telangiectasias [126, 130, 131].

ALK1 Ligands, BMP9 and BMP10

BMP9 and BMP10 have recently been identified as the physiologically relevant ligands for ALK1 signaling and vascular development [112, 132-135]. BMP9 and BMP10 are highly related proteins, sharing 65% sequence identity at the protein level. Both proteins undergo very similar biosynthesis [112, 136]. Pre-pro-proteins are cleaved by convertase enzymes such as furin into a prodomain and mature peptide. After secretion, the prodomain remains associated with the mature peptide through non-covalent interactions. BMP9 is active when associated with the prodomain and able to bind to ALK1 and induce Smad1/5 phosphorylation [136]. However, BMP10 is latent until the prodomain is removed [137]. Although the metalloproteinase BMP-1 (unrelated to BMP ligands) can cleave the BMP10 prodomain in vitro [137], the mechanism by which BMP10 is activated in vivo is not understood. Perhaps mechanical forces, interactions with the extracellular matrix or accessory receptors are required to dissociate the prodomain from the BMP10 mature peptide in a physiologic setting.

In humans, *BMP9* is expressed in the liver (hepatocytes, biliary epithelial cells) and circulates in its biologically active form at 110 pg/ml in serum [133, 138, 139]. In mice, *Bmp*9 is also expressed in liver as early as E9.75 and is simultaneously detectable in serum. *Bmp9* null mice have no vascular defect and are viable [140]. BMP10 is produced by the heart [141], specifically within the ventricular cardiomyocytes as early as E8.5 then restricted to the atrial cardiomyocytes by E16.5 in mice [140], and is also detectable in mouse and human serum [112,

142], though in an inactive prodomain-bound complex [112]. BMP10 null mice die at E10.0 from failed trabeculation and AVMs. Interestingly, vascular but not cardiac defects in these mice could be rescued by the insertion of *Bmp9* into the *Bmp10* locus [140]. Together, these data suggest that BMP9 and BMP10 are endocrine ALK1 ligands, and that BMP9 can functionally compensate for BMP10 in the vasculature if expressed in a BMP10-like spatiotemporal pattern.

In zebrafish, morpholino oligonucleotide mediated knockdown of *bmp9* is not lethal but results in a failure of the caudal vein to properly remodel [143]. These embryos do not develop enlarged cranial shunts similar to those observed in *alk1* mutants [92, 121]. Like in mice, *bmp10* is expressed earlier than *bmp9* and concomitant knockdown of *bmp10* and *bmp10-like* (a zebrafish *bmp10* paralog) results in large cranial shunts and is embryonic lethal [135]. Together with the data from the mouse models, these results suggest that in early development, BMP10 is necessary for embryonic vascular development and BMP9 and BMP10 ultimately function redundantly to maintain normal vasculature.

Type II receptors that complex with ALK1

Ligand binds to a heterotetrameric complex of type I and type II receptors. Type II receptors are thought to be constitutively active and phosphorylate the type I receptors when they are brought into a complex together by ligand binding. BMPs have been shown to preferentially interact with ActRIIA, ActRIIB or BMPRII [109].

1.4   ZEBRAFISH AS A MODEL SYSTEM FOR STUDYING HHT-ASSOCIATED

AVMS AND ALK1 SIGNALING

1.4.1   General attributes of the zebrafish model

Zebrafish are an excellent model system for the study of vertebrate development. External fertilization, small size, and optical clarity allow for the observation of development from the 1-cell stage. Development occurs rapidly, with gastrulation occurring at 6 hpf, heartbeat beginning at 24 hpf and circulation through the head and tail of the embryo by 27 hpf [144]. Furthermore, using confocal or two-photon microscopy, development or particular organ systems can be monitored with high spatiotemporal resolution in live transgenic embryos expressing fluorescent proteins under the control of cell type-specific promoters.

Zebrafish are also amenable to genetic manipulation. DNA and RNA can be injected easily into 1-cell stage zebrafish embryos to ectopically express genes in a tissue-specific manner or globally, respectively. In addition, genes of interest can be knocked down transiently using morpholino-modified antisense oligonucleotides. These short (~25 bases) oligos are highly stable and contain a morpholine ring in place of the deoxyribose ring and non-ionic phosphorodiamidate group in place of the anionic phosphodiester linkages between bases [145]. They are designed to target specific mRNA sequences and through steric inhibition block either translation of the message or proper mRNA splicing [146, 147].

Forward genetic screens using *N*-ethyl-*N*-nitrosourea (ENU) mutagenesis, viral insertion mutagenesis or transposon-mediated gene disruption have generated thousands of genetic mutants that are used to study gene functions and signaling cascades important for embryonic

and larval development [148]. More recent advances in reverse genetics have allowed for the targeted disruption of genes using TALEN and CRISPR/Cas9 technology [149, 150].

In addition to genetic approaches, zebrafish are easily manipulated using pharmacological approaches. Addition of soluble small molecules to the water in which the embryos are reared allows researchers to perturb specific biochemical pathways using previously characterized drugs, and to perform large scale, medium throughput chemical screens to identify novel small molecules that perturb particular signaling pathways or developmental processes. [148]. Together, these attributes make zebrafish an extremely powerful system for the study of vertebrate vascular development in a physiologically relevant in vivo setting.

1.4.2 Zebrafish *alk1* mutants develop cranial AVMs

1.4.2.1 Zebrafish cranial blood vessel development:

Embryonic zebrafish vascular morphology has been studied in great detail, first through the use of confocal microangiography and then through live time-lapse imaging of transgenic embryos expressing fluorescent proteins under the control of endothelial-specific promoters [6, 144]. Microangiography specifically highlights vessels that are lumenized and carrying plasma/blood flow, while imaging of transgenics allows assessment of development both prior to and subsequent to lumen formation. By utilizing both techniques, a complete understanding of vessel formation and maturation can be gained. .

1.4.2.2 *alk1*^{-/-} AVMs arise via a two-step process

The spatial and temporal predictability of shunt formation in *alk1*^{-/-} zebrafish embryos make them an ideal model for studying the molecular and cellular missteps that lead to AVM formation. In the absence of Alk1 signaling, zebrafish embryos develop grossly enlarged cranial arteries that contain supernumerary endothelial cells: *alk1*^{-/-} embryos have a 1.2-fold increase in the number of endothelial cells in the BCA/PCS beginning at 32 hpf and a 1.8-fold increase by 48 hpf [92, 121, 135]. By 40 hpf, AVMs form downstream of these arteries, between the BCA and PMBC (anterior shunt) and/or the BA and PHBC (posterior shunt) [92]. Thus, arterial enlargement precedes shunt formation. Time-lapse confocal microscopy has revealed that AVMs are the result of failed regression of one or more transient BCA/PMBC or BA/PHBC connections. These connections are retained in *alk1* mutants only in the presence of blood flow, suggesting that the increased shear stress caused by cranial arterial enlargement triggers an adaptive response aimed at normalizing hemodynamic force [92]. In sum, these data support the idea that AVM development in *alk1* mutants is not genetically determined but instead represents a two-step process that involves genetically programmed arterial enlargement followed by an Alk1-independent response to changes in the hemodynamic environment [92].

1.4.3   *alk1* expression is regulated by blood flow

Alk1 is expressed in arteries that are proximal to the heart in zebrafish embryos. Beginning at 26 hpf, *alk1* expression can be observed in the AA1 and the LDA, vessels that are a part of the initial circulatory loop. Shortly thereafter, expression within the ICA can be detected followed by CaDI and BCA expression at 30 hpf. It is interesting to note that *alk1* is not expressed in the

PCS or BA, and is restricted in the cranial arterial endothelium to arteries that are proximal to the heart and experience the highest magnitude of hemodynamic forces [92, 121]. In silent heart (*sih*) embryos, which lack heartbeat and therefore blood flow, overall vascular patterning is normal; however, *alk1* is not expressed, indicating that flow is required for *alk1* expression. Additionally, pharmacological inhibition of heartbeat also inhibits *alk1* expression [92]. Maintenance of *alk1* expression is also highly dependent on flow. In experiments where flow was stopped after *alk1* expression had been initiated, expression quickly faded in a distal-to-proximal pattern. Upon restoration of heartbeat, *alk1* expression was detectable within an hour in the AA1 and completely restored by 8 hours (Jim Donovan, unpublished data). In *gata1* mutant embryos, which lack erythrocytes, *alk1* expression is unaffected, indicating that expression is not dependent on endothelial-cell/red blood cell interaction [92].

1.4.3.1 Alk1 lies downstream of blood flow in phosphorylation of Smad1/5/9

Alk1 activity within the vascular endothelium can be assayed by assessing pSmad1/5 [110, 133, 134], which is absent in alk1 mutants and in sih morphant embryos lacking blood flow (and therefore also lacking alk1 expression) [135]. Stable transgenic expression of alk1 driven by a flow-independent vascular endothelial promoter is able to rescue pSmad1/5 in alk1 mutants but not sih morphants, suggesting that flow is necessary for Alk1 activity as well as expression [135]. Accordingly, injection of recombinant human BMP10 protein directly into the base of the CaDI of flow-deprived embryos ectopically expressing alk1 was able to restore pSmad1/5, suggesting that blood flow is required to activate Alk1 signaling by circulating Bmp10, which is produced in the heart [135] (Figure 5).
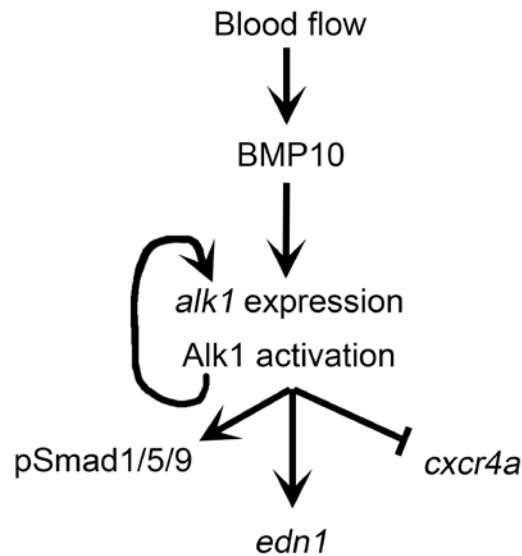
Figure 5: Blood Flow/BMP10/Alk1 Schematic

BMP10 is a circulating angiogenic factor and is delivered to the Alk1 receptor upon the onset of flow. This results in the activation of Alk1, Alk1-dependent phosphorylation of Smads 1/5/9 in the arterial endothelium, and increased expression of *alk1* and *edn1* and the repression of *cxcr4a*.

1.4.3.2 Alk1 lies downstream of blood flow in expression of some shear stress responsive genes

A subset of genes that is known to be regulated by shear stress is dysregulated in *alk1*^{-/-} embryos. Endothelin-1 (Edn1), a vasoactive peptide expressed within the vascular endothelium and/or vascular smooth muscle, has been shown to be negatively regulated by laminar shear stress and positively regulated by cyclic strain [151-153]. Interestingly, vascular *edn1* expression is restricted to *alk1*-positive arteries in the developing zebrafish. In the absence of Alk1 signaling

or blood flow, *edn1* expression is lost, indicating that *alk1* is either directly or indirectly required for *edn1* expression. Cxcr4a is a promigratory chemokine receptor and has been shown to be negatively regulated by laminar shear stress [154]. *cxcr4a* expression is increased in *alk1*-postive arteries in the absence of Alk1 or blood flow (Figure 5).

Not all flow responsive genes are dysregulated in *alk1*$^{-/-}$ embryos. *klf2a*, a transcription factor known to integrate shear stress-responsive pathways, is positively regulated by shear stress [70, 151] and expression is completely lost in zebrafish embryos lacking blood flow [92]. However, *klf2a* expression is unaffected in *alk1*$^{-/-}$ embryos [92]. These results suggest that Alk1 signaling may act upstream of *edn1* and *cxcr4a* in a *klf2a*-independent flow responsive pathway required to limit endothelial caliber upon the onset of flow. In support of this hypothesis, BMP10 protein injection coupled with transgenic, flow-independent *alk1* expression restored *cxcr4a* and *edn1* expression and endothelial cell number to wild type levels in the absence of blood flow [135] (Figure 5).

1.5   NOTCH SIGNALING AND AVMS

With its membrane bound ligand and receptors, Notch signaling allows communication between neighboring cells. It is a fundamentally conserved signaling pathway that is used reiteratively in the development of many different tissues and has been shown to regulate proliferation, apoptosis, self-renewal and differentiation. Notch signaling is highly context specific and therefore it is unwise to make generalized predictions on how Notch signaling will influence the development of one cell type based on results of another [155]. Throughout much of the

introduction, I have touched on Notch signaling and its key roles in angiogenesis, specifically in tip and stalk cell determination, regulation of VEGF signaling and arterial-venous identity. Notch signaling is implicated in the formation of AVMs, and there is also a large amount of evidence suggesting that a Notch and Alk1 interaction is important for proper vascular development.

1.5.1   Notch pathway summary

Notch receptors are single-pass transmembrane proteins that contain an extracellular ligand binding domain and an intracellular domain critical for Notch signal transduction. Notch ligands are transmembrane proteins from the Delta-like ligand (Dll) and Jagged families. Of these, Dll4 has the most prominent role in vascular development. The notch intracellular domain (NICD) is processed upon ligand binding by ADAM metalloproteases [156], which activate the receptor, and then further cleaved by γ-secretase enzymes that release the activated NICD into the cell [157]. The intracellular domain of the Notch receptor binds to CSL (Cp-binding factor 1 (CBF-1), Suppressor of hairless [Su(h)], and Lag-1), also known as recombination signal sequence-binding protein-J kappa (RBPJκ) [158]. In the absence of NICD, RBPJκ acts as a transcriptional repressor. Binding of NICD to RBPJκ converts the complex to a co-activator and results in the transcription of Notch target genes, including the *hairy and enhancer of split-1* (*HES1*) family [155, 159].

1.5.2 Perturbation of Notch signaling results in AVMs

Arterial/venous specification and its role in AVM prevention are evidenced by Notch perturbations resulting in these vascular malformations in zebrafish and mice. In zebrafish, mutations in the *mindbomb (mib)*, a regulator of Notch ligand endocytosis, results in the formation of AVMs as well as impaired arterial/venous specification [30, 160]. While mutations in hey2 results in defects in dorsal aorta due to altered arterial/venous identity [160, 161]. Similarly in mice, decreased expression of the Notch ligand, *dll4* or endothelial specific deletion of *RBPJκ* results in loss of arterial specification and AVMs that are small in caliber and appear atretic [162, 163]. Ectopic activation of Notch signaling also results in improper A/V specification and vascular abnormalities. Zebrafish ectopically overexpressing the NICD in the vascular endothelium have enlarged vessels and decreased expression of venous *ephB4* [164, 165], and expression of a constitutively active Notch4 (Notch4CA*)* in the mouse endothelium results in venous expression of arterial markers and AVMs in the liver, uterus, skin, brain and lung of adult mice [166-169]. Brain AVMs that result from inducible transient expression of Notch4CA are reversible: when the transgene is turned off, vessels shrink back to normal size and A/V marker expression is restored [170]. While AVMs resulting from decreased Notch signaling are small in caliber, Notch overexpression AVMs are large and contain an increased number of endothelial cells [31, 166, 168, 171, 172].

1.5.3   Evidence for Notch/Alk1 interactions

Evidence from cultured endothelial cells demonstrates that Smad1/5 can bind to the promoters of the canonical notch target genes, *hey1*, *hey2* and *hes1* and enhance expression [173], and Alk1 activation increases expression of some Notch targets [32, 174, 175], In addition, Notch target gene expression is synergistically increased by simultaneous Notch and Alk1 pathway activation [175].   BMP9/ALK1 effects were found to be independent of RBPJκ suggesting that Alk1 signaling through Smad1/5 may function to reinforce arterial identity independent of NICD/ RBPJκ [175].   Phenotypic evidence of an interaction between Notch and Alk1 signaling is less convincing.   While inhibition of both pathways separately has been shown to enhance VEGF-stimulated angiogenesis both in cell culture and in vivo, combined inhibition does not appear to have an additive effect [175].   Similarly, constitutively active Notch or Alk1 has been shown to inhibit sprouting with no increased effects of combined pathway activation [174].   And lastly, the inhibition of either pathway does not alter phenotypic effects of activation of the other [174].   A better understanding of how each of these pathways function and interact is required to understand why an apparent genetic synergy does not translate into a phenotypic synergy.

1.6   SUMMARY AND DISSERTATION AIMS

Patients with HHT2 develop AVMs due to a mutation in *ALK1* [91, 112, 113], but the function of ALK1 in endothelial cells and the natural history of AVMs is unknown. Zebrafish *alk1* mutant embryos develop enlarged arteries containing supernumerary endothelial cells, causing a change

in hemodynamic environment that leads to AVMs [92, 121, 135]. The source of the additional endothelial cells has been thought to be a result of increased proliferation and/or migration, supporting the hypothesis that Alk1 signaling is antiangiogenic and contributes to vessel stabilization [132, 176]. Here, I show that the increase in endothelial cell number in the cranial arterial endothelium is due to an improper distribution of cells. Arteries proximal to the heart experience a decrease in cell number due to an accumulation of cells in the more distal arteries. These data suggest that Alk1 is required for directed endothelial cell migration towards the heart and in opposition to blood flow.

In addition, an interaction between Alk1 and Notch signaling pathways has been thought to be important for proper vascular development and AVM prevention [175, 177]. Here I demonstrate that Alk1 and Notch signaling have context specific interactions in the regulation of the expression of some Notch target genes, but there are only weak phenotypic interactions between the two pathways in vivo.

2.0 ALK1 ALLOWS ARTERIAL ENDOTHELIAL CELLS TO RESIST MIGRATION IN THE DIRECTION OF BLOOD FLOW

ALK1, a TGF-β type I receptor serine/threonine kinase, is critical for proper vascular development. Heterozygous loss of ALK1 results in the vascular disorder, hereditary hemorrhagic telangiectasia type 2 (HHT2), which is characterized by the development of arteriovenous malformations (AVMs) and affects 1:8000 people worldwide. *alk1*$^{-/-}$ zebrafish develop embryonic lethal AVMs which form via a two-step mechanism. First, loss of alk1 results in an increase in endothelial cell number in cranial arteries, which results in increased vessel caliber. In the second step, normally transient connections between arteries and veins are maintained as an adaptive mechanism to cope with an increased hemodynamic load. Using zebrafish as a tool to study the AVM formation due to loss of Alk1 signaling, I have found that Alk1 is required for directed arterial endothelial cell migration in opposition to blood flow. Embryos lacking alk1 experience a redistribution of cells, with endothelial cells failing to efficiently migrate against the direction of blood flow and accumulating in more distal regions of alk1-dependent arteries. This altered cellular distribution causes an increase in arterial caliber and consequent retention of downstream arteriovenous connections, resulting in fatal AVMs.

2.1 INTRODUCTION

Hereditary hemorrhagic telangiectasia (HHT) is a haploinsufficiency characterized by a predisposition to development of arteriovenous malformations (AVMs). These fragile, direct connections between arteries and veins can lead to hemorrhage or stroke. HHT is caused by defects in transforming growth factor-beta (TGF-β) superfamily signaling. Specifically, mutations in the type III accessory receptor, endoglin *(ENG)*, cause HHT1; mutations in the type I receptor serine threonine kinase, activin receptor-like kinase 1 *(ACVRL1,* or *ALK1)*, cause HHT2; and mutations in the signaling mediator, *SMAD4*, cause a combined syndrome of juvenile polyposis with HHT [99-101]. Together, mutations in these three genes account for approximately 85% of HHT. Despite the fact that these gene products all participate in TGF-β signaling, whether mutations affect one or more discrete pathways and how these pathways function to prevent AVMs remain poorly understood.

Based on histological observation of cutaneous AVMs (telangiectasias) from HHT patients, it has been postulated that the first step in AVM development is focal dilation of a postcapillary venule, followed by arteriole dilation and subsequent loss of intervening capillaries [90]. However, these conclusions were reached from static observations of independent lesions and not from longitudinal analysis. In *Alk1-* and *Eng*-deleted adult mice, wound-induced subdermal AVMs develop via angiogenic elongation of both arteries and veins, with *de novo* arterial-venous connections developing prior to vessel dilation [117, 120]. Although these findings represent a longitudinal analysis, imaging of vascular growth was performed only once per day and was not at cellular resolution. Therefore, the aberrant cell behaviors that lead to AVMs could not be elucidated.

Zebrafish are an excellent model for the study of both normal and pathological vascular development because signaling pathways that control endothelial cell differentiation and vessel patterning are conserved from fish to mammals, and because optically transparent transgenic zebrafish embryos allow real-time imaging of vessel development at cellular resolution. Zebrafish *alk1* mutants develop AVMs at a predictable time (approximately 40 hours post-fertilization, hpf) in a predictable location (beneath the midbrain or hindbrain) and therefore serve as an excellent model for exploring the cellular basis of HHT-associated AVM development [92, 121, 135].

In zebrafish, *alk1* is expressed after the onset of blood flow in cranial arterial endothelial cells closest to the heart, including (in ordered series) the outflow tract and first aortic arch (AA1), internal carotid artery (ICA), caudal division of the internal carotid artery (CaDI), and basal communicating artery (BCA). We previously reported increases in arterial endothelial cell number in and diameter of the contiguous CaDI, BCA, and posterior communicating segments (PCS) in *alk1* loss-of-function mutants as early as 32 hpf [92, 135]. Between 32-40 hpf, BCA/PCS endothelial cell number increases similarly in the absence of *alk1* function or in the absence of blood flow, and blood flow is required for *alk1* expression [92]. These data suggest that Alk1 transmits a flow-based signal that limits arterial caliber. In *alk1* mutants, high-flow shunts develop by 40 hpf downstream of enlarged arteries, connecting either the BCA to the primordial midbrain channel (PMBC) or the downstream *alk1*-negative basilar artery (BA) to the primordial hindbrain channel (PHBC). These shunts represent aberrant retention of normally transient arteriovenous connections that initiate development of and serve as early drainage for the nascent arterial system [92, 121]. In *alk1* mutants, late increases in endothelial cell number (40-48 hpf) and AVM development require blood flow [92], suggesting that these effects are

36

secondary to enlargement of *alk1*-positive cranial arteries closest to the heart and represent an adaptive response of downstream vessels to altered hemodynamics. Therefore, I focused this study on defining the primary role of Alk1 in arterial endothelium in limiting arterial caliber.

Results demonstrate a defect in arterial endothelial cell distribution within lumenized vessels as the primary effect of loss of Alk1 function. With the onset of blood flow, wild type cranial arterial endothelial cells in the lumenized AA1, ICA, and CaDI migrate in a distal-to-proximal fashion towards the heart, against the direction of blood flow. Some cells originally located in AA1 or the ICA enter the heart and incorporate into ventricular endocardium. In contrast, cells distal to the ICA/CaDI junction generally remain in place after the onset of blood flow, and there is little to no mixing of arterial cells derived from different sprouts or angioblast pools. In *alk1* mutants, endothelial cell distribution is altered, with decreased cranial arterial endothelial cell contribution to endocardium, increased distal migration of endothelial cells, and increased mixing of arterial endothelial cells derived from different sprouts or angioblast pools. Together, these data suggest that loss of *alk1* results in enhanced movement of arterial endothelial cells in the direction of blood flow, resulting in accumulation of cells in and enlargement of cranial arteries distal to the heart.

2.2 ORIGIN AND PATTERNING OF *ALK1*-POSITIVE ZEBRAFISH CRANIAL ARTERIES

Basic development of the cranial vascular system has been described previously [6]. I focus here on a more detailed analysis of the development of the *alk1*-positive cranial arteries. Angioblasts differentiate in the anterior lateral plate mesoderm at the 1-somite stage (~10.5 hpf) and coalesce into two pairs of bilateral clusters by the 7-somite stage (~12.5 hpf). Between the 14 and 18-somite stage (~16 hpf), a pair of ventral, caudally-directed sprouts emerge from the paired rostral clusters (rostral organizing centers, ROCs) and meet with rostrally-directed sprouts from the paired caudal clusters (midbrain organizing centers, MOCs) to form the ICAs. Both ROC- and MOC-derived ICA sprouts dive medially and form a transient left-right connection directly below the forming CaDI. The ROCs also launch dorso-posteriorly directed sprouts around this time navigate around the hypothalamus to form the bilateral CaDIs, which meet at the midline at ~23 hpf. Finally, cells from the MOCs migrate medially around the 20-somite stage (~19 hpf) to form the first aortic arches (AA1), which connect the outflow tract of the heart to the lateral dorsal aortae and ICA. Although this cranial arterial system is in place by 24 hpf, flow does not commence in these vessels until around 26 hpf, when primordial midbrain channel (PMBC)-derived sprouts connect to the apex of the CaDI and allow drainage (see Chapter 3). At this point, the apex of the CaDI compacts along the anterior-posterior axis and elongates along the left-right axis to become the BCA. The outflow tract, AA1, ICA, CaDI, and BCA become *alk1*-positive with the onset of blood flow [92], and there are no patterning defects in this cranial arterial system in *alk1* mutants.
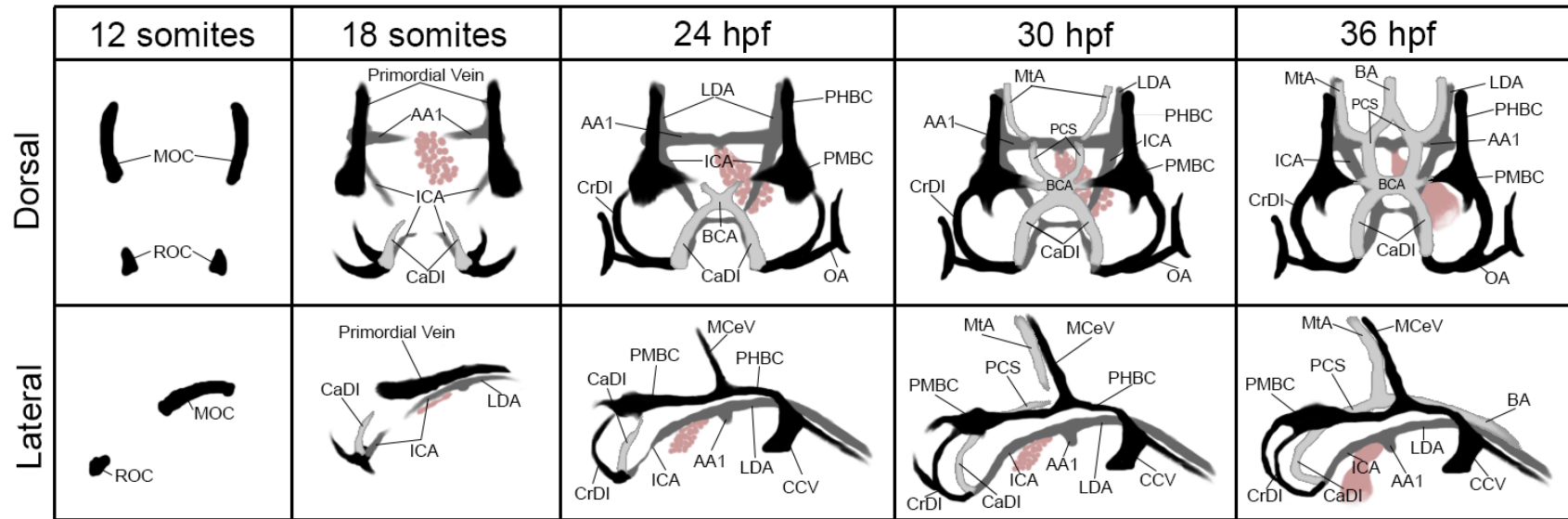
Figure 6: Zebrafish cranial blood vessel development

By 12 somites, 2 bilateral clusters of angioblasts referred to as the midbrain organizing center (MOC) and rostral organizing center (ROC) have formed. By 18 somites, the MOC has begun to sprout anteriorly and posteriorly, with the more dorsal cells giving rise to the cranial veins and the more ventral cells contributing to the first aortic arch (AA1), lateral dorsal aortae (LDA) and the internal carotid arteries (ICA). The ROC has also begun to sprout and form the cranial division of the internal carotid artery (CrDI), the optic artery (OA), the caudal division of the internal carotid artery (CaDI) and the ICA. By 24 hpf, the heart has begun to beat and the final cranial connections are being made in anticipation of circulation. At 30 hpf, transient connections between the basal communicating artery (BCA) and the primordial midbrain channel (PMBC) are carrying flow and providing the only circulatory outlet until the connections between the metencephalic arteries (MtA), posterior communicating segments (PCS) and the basilar artery (BA) become patent at ~36 hpf

2.3   PROXIMAL AND DISTAL ARTERIAL ENDOTHELIAL CELL NUMBERS ARE

DIFFERENTIALLY AFFECTED IN ALK1 MUTANTS

Our laboratory previously reported an increase in endothelial cell number in *alk1* mutant embryos compared to wild type embryos in the combined BCA/PCS [92, 121, 135] and CaDI [135]. Increases in BCA/PCS cell number were significant from 32-48 hpf, whereas CaDI cell number was examined only at 36 hpf. To better understand the origin of these increases in cell number, I investigated the development of and endothelial cell number in (from proximal to distal, with respect to the heart) AA1, ICA, CaDI, and BCA between 24 and 36 hpf. Because these vessels form a contiguous arterial system, I defined the boundaries of each based on their parent vessels, according to the diagrams in Figure 7 and Figure 11.

In wild type embryos, the number of endothelial cells in the proximal regions of AA1 (shaded in gray in Figure 6) decreased steadily between 24 hpf and 36 hpf (15.3± .6 to 12.0± 1.2 cells, mean ± SEM, Students T test, p<0.05 Figure 7A, C). Over this same period of time, AA1 diameters increased slightly, by approximately 5 Figure 7B). Endothelial cell number in the ICA also decreased over this time period in wild type embryos (35.8± 1.3 to 22± .91 cells, mean ± SEM, Students T test, p<0.05 Figure 7A, C)

In *alk1* mutant embryos, AA1 endothelial cell number also decreased over time and was indistinguishable from wild type siblings at 24-28 hpf, but was decreased compared to wild type by 30-36 hpf (16± .46 to 9± .55 cells, mean ± SEM, Students T test, p<0.05 Figure 7A,C). The morphology of AA1 was dynamic and variable in *alk1* mutant embryos: the paired vessels often

developed asymmetrically, with one side dramatically decreasing in diameter (Figure 7A) and in rare cases seemingly disconnecting from the heart outflow tract. In contrast to wild type embryos, in which mean AA1 diameters increased slightly over time, the mean AA1 diameter did not change between 24 and 36 hpf in *alk1* mutants, though variability was very high (Figure 7B**).** In the ICA, endothelial cell number was not different from wild type at 24-26 hpf but failed to decrease, as in wild type, at later times, resulting in a significant increase in cell number compared to wild type between 28 and 36 hpf (31.9 ± 1.7 to 34 ± 1.4 cells, mean $\pm$ SEM, Students T test, $p<0.05$ Figure 7A,C).

In contrast to the steady decrease in endothelial cell number in AA1 and the ICA, endothelial cell number in the more distal CaDI and BCA increased steadily over time in wild type embryos (CaDI: $14.5 \pm .5$ to $25.4 \pm .6$ cells, PCS: 0 ± 0 to $7.9 \pm .7$ cells mean $\pm$ SEM, Students T test, $p<0.05$ Figure 8). Endothelial cell number in the CaDI and BCA was significantly increased in *alk1* mutants compared to wild type siblings from 30-36 hpf (CaDI: $15.3 \pm .7$ to $36.6 \pm .5$ cells, PCS: 0 ± 0 to $7 \pm .5$ cells mean $\pm$ SEM, Students T test, $p<0.05$ Figure 8). These data demonstrate that endothelial cell number in *alk1* mutants is decreased in AA1, the artery most proximal to the heart, but increased in more distal arteries, including ICA, CaDI and BCA.
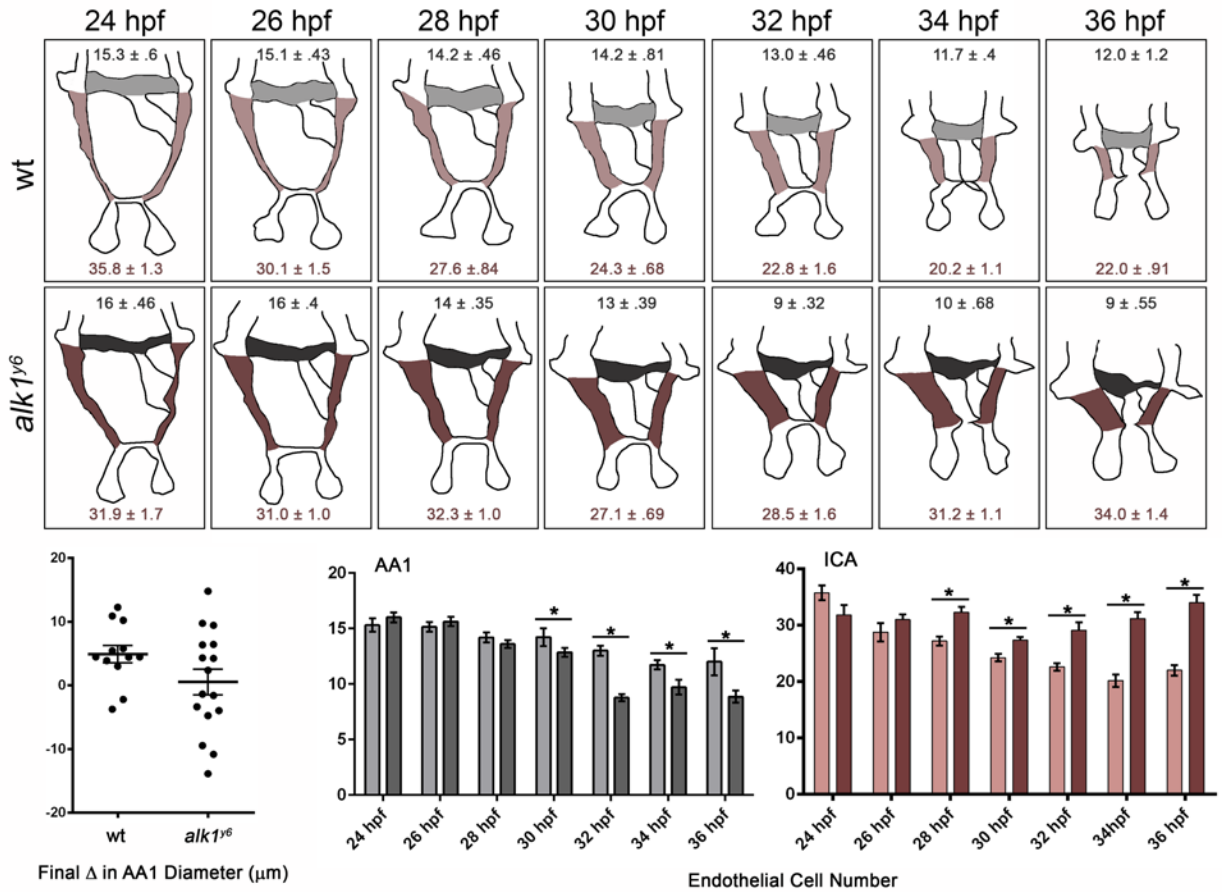
Figure 7: Proximal arteries have altered endothelial cell distribution and vessel morphology in *alk1* mutants

Endothelial cell (EC) number decreases in AA1 between 24-36 hpf and this decrease is significantly higher in alk1[y6/y6] embryos beginning at 30 hpf. The number of ECs decreases in the ICA over time in wt embryos and fails to decrease compared to wt siblings beginning at 28 hpf in alk1[y6/y6] embryos. **A**, wire diagrams of the dorso-frontal view of the ventral cranial arterial system between 24-36 hpf of wt and an alk1[y6/y6] sibling. The boundaries for each vessel are shaded in gray (AA1) and maroon (ICA) and correlate with data presented in **C**. Colored numbers in **A** represent the average number of cells ± SEM in the AA1 or ICA at each time point. **B**, The change in AA1 diameter between 24 and 36 hpf is increased by 5 μm on average in wt embryos and is highly variable in alk1[y6/y6] embryos. **C**, Values are mean ± SEM, significance was determined by Students T test, *p<0.05 for individual comparisons.

2.4 ARTERIAL ENDOTHELIAL CELL NUMBER CHANGES IN ALK1 MUTANTS DO NOT RESULT FROM CHANGES IN PROLIFERATION OR APOPTOSIS

alk1 mutants have fewer arterial endothelial cells in AA1 but more in the ICA and CaDI. Because all of these endothelial cells are *alk1* positive, it seems unlikely that these changes could be caused by enhanced apoptosis in AA1 and increased proliferation or decreased apoptosis in the ICA and CaDI. In support of this reasoning, no differences in apoptosis or proliferation were identified in these vessels in *alk1* mutants versus wild type siblings by time-lapse (having analyzed 8 wt/control morpholino time-lapse movies and 12 *alk1^{y6}/alk1* morpholino time-lapse movies). In fact, we detected almost no proliferation or apoptosis in this vessel system regardless of genotype. These data suggest that a fixed number of differentiated endothelial cells distribute themselves over time in a stereotypical way within these contiguous arteries, and that this distribution is altered in *alk1* mutants.
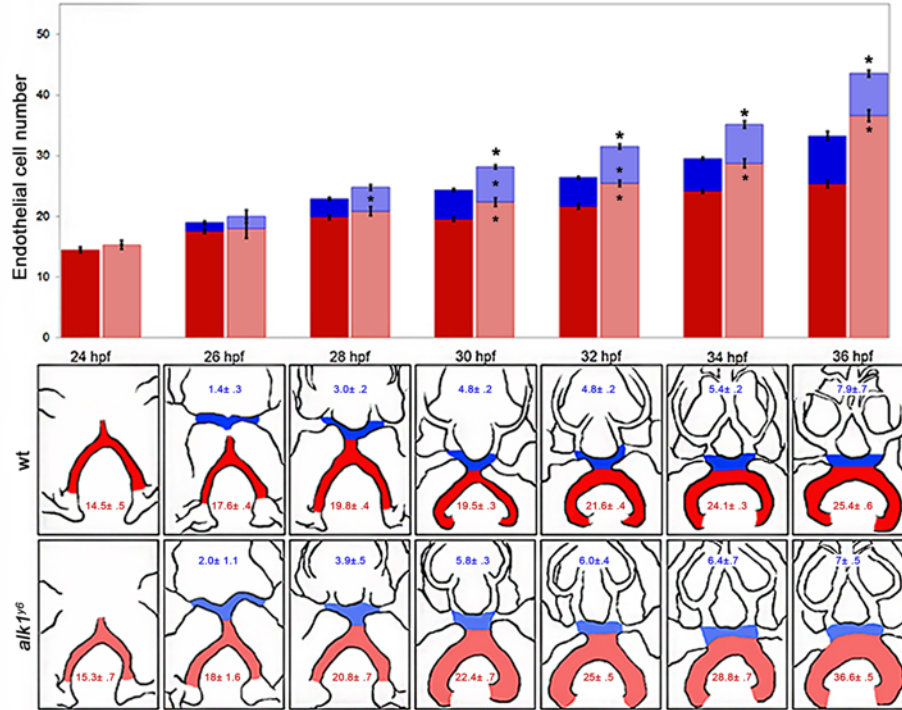
Figure 8: Distal cranial arteries have increased endothelial cell number in alk1 mutants

The CaDI (red) and the BCA (blue) have an increased number of endothelial cells beginning at 28 hpf in the BCA and 30 hpf in the CaDI in alk1[y6] embryos compared to wt siblings. Values are mean ± SEM, significance was determined by Student's T- test, *p<0.05 for individual comparisons. Boundaries for the CaDI and BCA are shaded in red and blue, respectively, in the wire diagrams (frontal views, anterior bottom), 24 to 36 hpf. Colored numbers in the wire diagrams represent the mean number of cells SEM at each time point. Opaque colors (first bar in pair), wild type; transparent colors (second bar in pair), *alk1* mutants.

2.5 ARTERIAL ENDOTHELIAL CELLS PROXIMAL TO THE OUTFLOW TRACT MIGRATE TOWARD THE HEART, AGAINST THE DIRECTION OF BLOOD FLOW

The lack of proliferation or apoptosis in the developing cranial arterial system suggested that cell number changes in wild type cranial arteries from 24-36 hpf (decreased cell number in AA1 and ICA, increased cell number in CaDI) resulted from a redistribution of endothelial cells. To better appreciate the cell movements that generate the cranial arterial system, I performed time-lapse two-photon microscopy of *Tg(fli1a:negfp)^{y7};Tg(fli1a.ep:mRFP-CAAX)^{pt504}* embryos, which express GFP in endothelial cell nuclei and mRFP in endothelial cell membranes. Imaging between 23 and 33 hpf revealed a striking net movement of AA1 endothelial cells toward the heart beginning at approximately 24-25 hpf, just after the onset of heartbeat and blood flow (Figure 9A-B). Tracking of individual endothelial cells (Figure 9B-B') demonstrated that on average 6-10 cells entered the heart from AA1 (red arrows), 3-6 cells entered AA1 from the ICA/LDA (blue arrows) and the rest of the cells remained in AA1 while migrating towards the heart (black arrows) during this window of development.

To confirm this observation, I performed fate mapping using *Tg(fli1a:GAL4FF;UAS:kaede)* embryos which expresses a photoconvertible fluorescent protein in the vascular endothelium. All cells in either the left or right AA1 were photoconverted from green to red at 24 hpf using a 405 nm laser, and photoconverted cell locations were recorded at 48 hpf (Figure 10). Nearly all embryos showed photoconverted cells in the outflow tract and heart, with approximately 60% of embryos having photoconverted cells within the proximal portion of the ventricle, adjacent to the atrioventricular canal. Approximately 20% of embryos had photoconverted cells remaining in AA1 but no embryos had photoconverted cells more distal
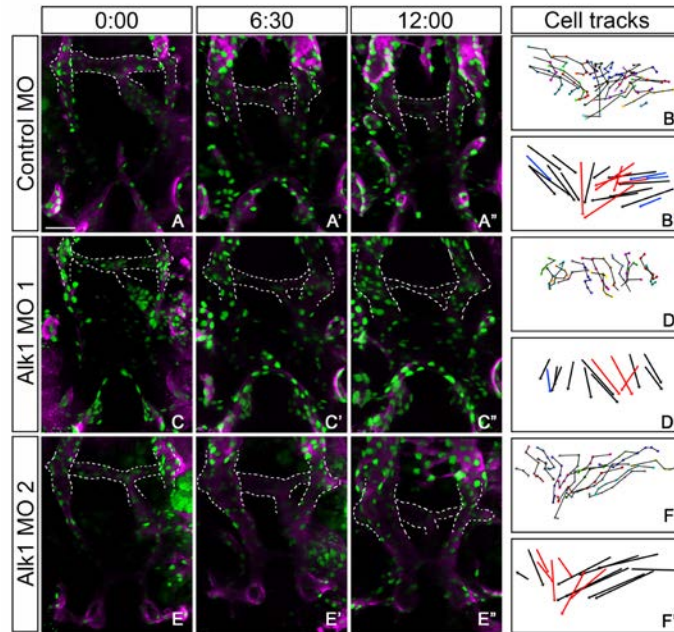
Figure 9: AA1 EC migration towards the heart is impaired in *alk1* morphants.

Time-lapse analysis of *tg(fli1a.ep:neGFP)^y7^;(fli1a.ep:mRFP-CAAX)^pt504^* embryos injected with either a control MO or Alk1 MO. The AA1 and where it intersects with the LDA/ICA and the heart is outlined in white dashed lines. Control MO: **A**-**A''**, *alk1* MO 1: **C**-**C''** and *alk1* MO 2: **E**-**E''**. Individual cells were manually tracked over a 12 hour time period, with the cell paths labeled every 2 hours (**B**, **D**, and **F**). The net migration, representing the distance between the initial and final position of each cell is charted in **B'**, **D'** and **F'**. In control MO embryos (**A**), cells steadily march towards the heart, with cells that were originally proximal to the heart entering over the 12 hours. Cells from the ICA/LDA enter the AA1 as the vessel decreases in length, maintaining normal vessel caliber and morphology. In *alk1* MO embryos, the migration patterns are highly variable and result in abnormal AA1 morphology. In *alk1* MO1 (**C**), cells demonstrate a less steady migration towards the heart. No new cells enter the vessel over the 12 hour time period and the vessel caliber decreases significantly. In *alk1* MO 2 (**E**), cells on one side of the AA1 quickly migrate either towards the heart or the ICA/LDA and no new cells enter the vessel. On the other side, cells demonstrate a slower migration towards the heart, and one cell enters from the ICA/LDA region. This results in the thinning of one side of the vessel and an enlargement of the caliber of the other side of the vessel.
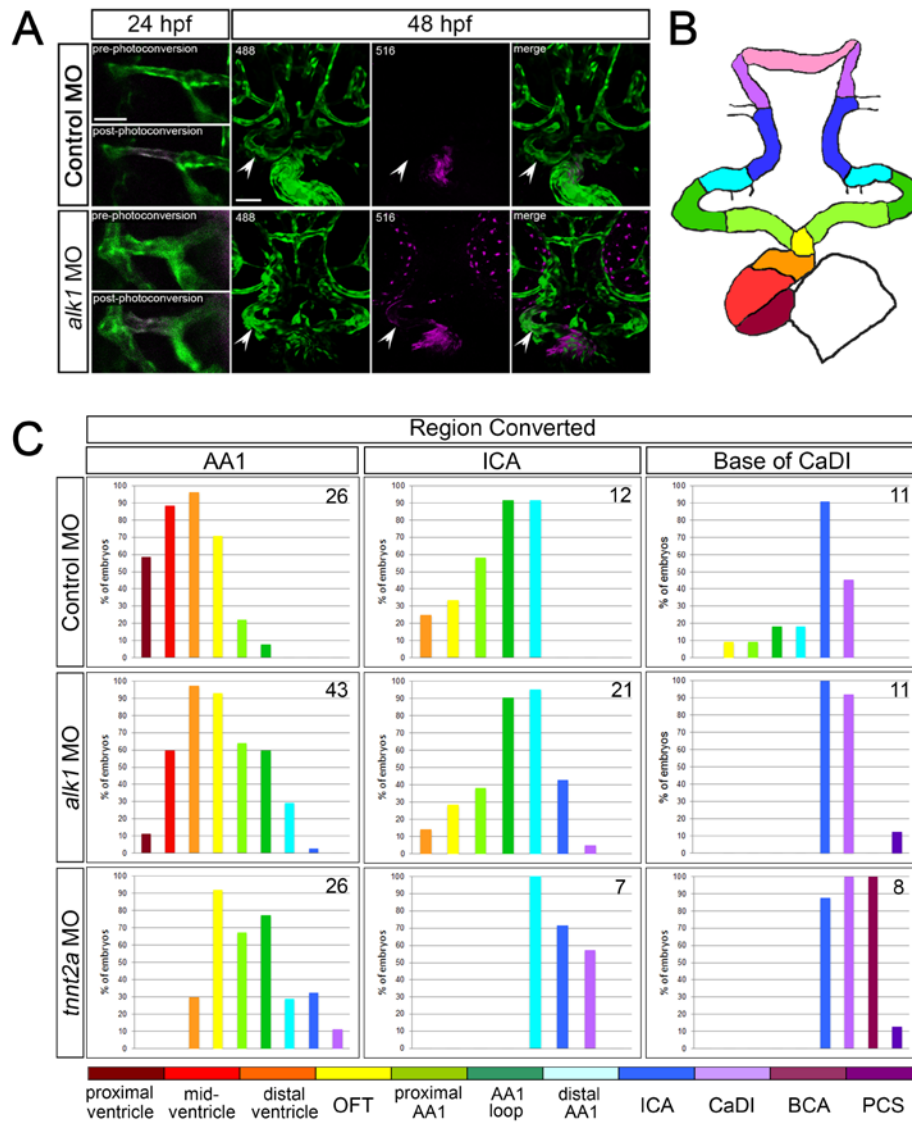
Figure 10: Photoconverted cells in AA1 enter the heart and this migration is altered in alk1 mutants and embryos lacking blood flow

One side of AA1 (A), ICA or base of the CaDI was converted from green to red at 24 hpf *in tg(fli1:gal4FF)^{ubs4};(uas:Kaede)^{rk8}* embryos injected with either a control, *alk1* MO or tnnt2a MO using the 405 laser. The location of the photoconverted cells was imaged at 48 hpf, with the 488 laser exciting the green Kaede cells and the 516 laser exciting the red Kaede cells. In control embryos, the majority of photoconverted cells were located in the heart. In alk1 MO embryos, photoconverted cells were often observed in the AA1 (white arrow head) and the

heart. Images at 24 hpf are single z-stacks, dorsal, anterior down. 48 hpf are two-dimensional confocal projections, frontal with dorsal up. B. The cranial vasculature was divided into regions demarcated on the wire diagram. Cells were converted on one side of AA1, ICA or CaDI at 24 hpf and the location of the converted cells was scored at 48 hpf and the percentage of embryos with cells in each vessel region was calculated and graphed (C). The distribution of cells is shifted away from the heart in alk1 and tnnt2a morphants. Numbers in the top right hand corner of each graph represents the number of embryos assayed for each condition.

than the middle (loop) region of AA1 (Figure 10). Additional photoconversion experiments revealed that cells in the ICA at 24 hpf either remain in the ICA or have moved toward the heart, against the direction of blood flow, by 48 hpf. However, ICA cells reach only distal regions of the ventricle (22% of embryos). Endothelial cells at the base of the CaDI also move toward the heart and contribute to the ICA in nearly all cases (90% of embryos) but only rarely to more proximal arteries (10-18% of embryos) and never to the heart. Together, these data demonstrate that endothelial cells initially residing in lumenized arteries most proximal to the heart migrate towards the heart, against the direction of blood flow, in wild type embryos.

In *tnnt2a* morphants, which lack a heartbeat and blood flow, converted cells within one half of AA1 at 24 hpf did not migrate efficiently into the heart by 48 hpf (Figure 10). The location of these converted cells were shifted more distally when compared to the control morpholino embryos, with only 30% of embryos having cells located in the most distal region of the ventricle (versus 90%), ~90% in the outflow tract and 10% of embryos with cells located as distally as the CaDI. Photoconversion of the ICA and base of the CaDI revealed similar trends, with embryos having photoconverted cells present in more distal vessels at 48 hpf when

compared to control morpholino siblings. These results indicate that blood flow triggers the migration of endothelial cells towards the heart between 24 and 48 hpf.

In *alk1* morphants, which completely phenocopy *alk1* mutants, there was high variability in the migratory behavior of AA1 endothelial cells. In the Alk1 MO1 example (Figure 9C-D), 3 cells entered the heart from AA1, only 1 cell entered AA1 from distal vessels, and in general the migration was less directed. In the Alk1 MO2 example (Figure 9E-F), 6 cells entered the heart, 2 cells exited AA1 toward distal vessels, (migrating in the direction of blood flow) and no new cells entered AA1 from the LDA/ICA. These trends are also observed in additional experiments (n=6 for control morpholino and 8 for *alk1* morpholino). Additionally, in kaede conversion experiments, the distribution of arterial endothelial cells was shifted distally compared to control siblings: a lower percentage of embryos showed AA1-derived photoconverted cells in the proximal ventricle (10% versus 60%), and a higher percentage showed photoconverted cells remaining in proximal (62% versus 21%) and distal (30% versus 0%) regions of AA1. Arterial endothelial cells residing at 24 hpf in the ICA and CaDI were also shifted distally in *alk1* morphants compared to control siblings at 48 hpf (Figure 10). Together, with proliferation and apoptosis data, these data demonstrate that 1) the loss of arterial endothelial cells from wild type AA1 and ICA over time is due to proximal migration of these cells into the heart; and 2) the changes in arterial endothelial cell number in *alk1* mutants (decreased in AA1, increased in ICA and CaDI) are likely due to decreased proximal migration (against the direction of blood flow) and/or increased distal migration (with the direction of blood flow).

To directly determine whether increased distal migration contributes to increased endothelial cell number in the CaDI in *alk1* morphants, I performed time-lapse two-photon microscopy to image endothelial cell contributions to this vessel in *Tg(fli1a:negfp)* embryos, 24-

36 hpf. In 24 hpf control embryos, the ROC-derived bilateral CaDIs (red nuclei) have surrounded the hypothalamus and connected dorsally, and the PMBC-derived sprouts (dark blue nuclei) are connecting to the apex of the CaDI (Figure 11A). The arterial CaDI-derived cells become the anterior portion of the BCA, whereas the venous PMBC-derived cells become the posterior portion of the BCA. By 27-28 hpf, bilateral metencephalic artery-derived sprouts (pink nuclei) have connected to the PMBC-derived cells, and by 31-32 hpf, these cells migrate posteriorly to form the posterior communicating segments (PCS). The PCSs meet at the midline and drain into the developing primordial hindbrain channel-derived basilar artery (BA) [178] by approximately 36 hpf. Thus, this elegant cranial arterial system is derived from two arterial sources (ROC, MtA) and two venous sources (PMBC, PHBC) and there is little to no mixing of these cells once connections have been made. Between 24 and 36 hpf, an average of 3 cells entered the CaDI from the ICA but remain at the base of these vessels, most likely reflective of the changing morphology of the vessels and supporting the idea of limited net migration in the direction of blood flow (Figure 11A, B).

In *alk1* morphants, timing of development and basic patterning of this cranial arterial system is unchanged, but more cells enter the CaDI from the ICA and more distally, supporting the idea that increased distal migration is responsible for CaDI enlargement in these embryos (Figure 11). Furthermore, although the number of cells contributing to the developing arterial system from the PMBC and MtA is not different in *alk1* morphants compared to controls, there is aberrant mixing of arterial- and venous-derived cells, with CaDI-derived cells reaching into territory normally occupied by PMBC-derived cells, and PMBC-derived cells reaching into territory normally occupied by MtA-derived cells. In summary, enhanced distal migration of *alk1*-dependent cells results in increased endothelial cell number in and caliber of the CaDI and

disrupts the "boundaries" between venous-derived and arterial-derived endothelial cells. The increased arterial caliber alters the hemodynamic load within the vasculature and precipitates flow-dependent shunt formation.
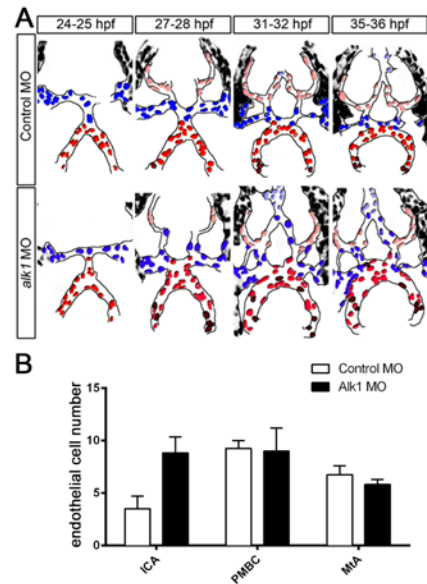
Figure 11: Endothelial cell migration in the distal cranial vasculature

 A. Time-lapse analysis of **Tg**(*fli1a.ep:neGFP)^{y7}* injected with either control or *alk1* MO between 24-36 hpf. Red cells originate from the ICA (originally the ROC), blue cells from the PMBC, pink cells from the MtA and light blue cells from the PHBC. Maroon cells are cells that have entered the CaDI from the ICA after the start of the movie. Wire diagrams were created from two dimensional confocal projections and pseudo-colored in Photoshop. **B.** Quantification of the number of cells that have entered the cranial arterial system from the ICA, PMBC and the MtA over the course of the movie. The increase in cell number in *alk1* MO embryos can be attributed to an increase in the number of cells entering from the ICA.

2.6   ARTERIAL ENDOTHELIAL CELLS REPRESENT A NOVEL SOURCE OF

ENDOCARDIAL CELLS

The contribution of arterial endothelial cells to the heart has not previously been reported. To determine which cardiac cell type these AA1-derived endothelial cells become, I performed double immunofluorescence on *Tg(alk1e5:egfp)* embryos for EGFP and MF20.   EGFP expression in *Tg(alk1e5:egfp)* embryos marks *alk1*-positive endothelial cells in AA1 at 24 hpf but is not detectable in the heart at 48 hpf. MF20 marks sarcomeric myosin heavy chain and only labels the myocardium [179]. Preliminary analysis indicates that these cells do not contribute to myocardium and are likely therefore endocardial, as would be expected by their endothelial origin (Figure 12). Future work is required to clearly identify the fate of these cells.
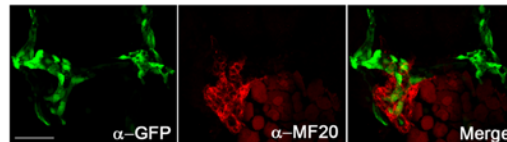
Figure 12: Endothelial cells migrating into the heart appear to become a part of the endocardium

Tg(alk1e5:egfp)^{pt517} marks alk1-positive endothelial cells with gfp, but is to faint to visualize without antibody staining before ~32 hpf. MF20 labels sarcomeric myosin heavy chain and will specifically label myocardium. EGFP expressing (green) cells do not colocalize with MF20 (red) but are present inside the myocardium, indicating these cells are in the endocardium. Images are 2D confocal projections of 30 µM cryosections, dorsal view, anterior downward. Scale bar, 50 µm.

2.7   DISCUSSION

Alk1 signaling functions to transmit a flow-based signal that is required to limit arterial endothelial cell number and vessel caliber [92]. Here I demonstrate that upon the onset of flow, endothelial cells within the first aortic arch (AA1) migrate in opposition to flow and enter the heart, likely contributing to the endocardium. The cranial arterial system is derived from cells of both arterial and venous origins. Due to the carefully coordinated timing of the migration of these cells to their final destination, there is rarely any cell mixing and these cells generally cease to migrate after the onset of flow. In the absence of *alk1*, endothelial cell distribution is altered, with fewer cells in AA1 and more cells in the more distal ICA, CaDI and BCA. Because there was no observed endothelial cell apoptosis or differences in proliferation, these data suggest that the primary defect in *alk1* mutants is due to aberrant migration and allocation of a fixed number of arterial endothelial cells. Arterial endothelial cells proximal to the heart fail to migrate in opposition to flow and/or migrate with flow, resulting in an accumulation of cells in distal cranial arteries.

We have previously reported that *alk1* mutant zebrafish embryos develop AVMs via a two-step mechanism. The first step occurs independent of blood flow and results in an increased number of endothelial cells in the CaDI, resulting in an increased vessel caliber. In the second flow-dependent step, transient connections between arteries and veins are maintained as an adaptive response to the increased flow through the system due to the increased CaDI caliber [92, 135]. In this work, I have demonstrated that the increase in endothelial cell number that is central to the first step in AVM development occurs due to aberrant endothelial cell migration in what are normally *alk1*-positive arteries. Furthermore, I show through time-lapse analysis that

Alk1 signaling does not influence endothelial cell proliferation and increased proliferation does not account for the increase in arterial cell number in *alk1* mutants (data not shown), as has been previously speculated [176, 180]. However, EDU and TUNEL staining are required to confirm proliferation and apoptosis time-lapse observations.

3.0 CONTEXT-SPECIFIC INTERACTIONS BETWEEN NOTCH AND ALK1 CANNOT EXPLAIN ALK1-ASSOCIATED ARTERIOVENOUS MALFORMATIONS

Notch and activin receptor-like kinase 1 (ALK1) have been implicated in arterial specification, angiogenic tip/stalk cell differentiation, and development of arteriovenous malformations (AVMs), and ALK1 can cooperate with Notch to upregulate expression of Notch target genes in cultured endothelial cells. These findings suggest that Notch and ALK1 might collaboratively program arterial identity and prevent AVMs. I therefore sought to investigate the interaction between Notch and Alk1 signaling in the developing vertebrate vasculature. I modulated Notch and Alk1 activities in zebrafish embryos and examined effects on Notch target gene expression and vascular morphology. Although Alk1 is not necessary for expression of Notch target genes in arterial endothelium, loss of Notch signaling unmasks a role for Alk1 in supporting *hey2* and *ephrinb2a* expression in the dorsal aorta. In contrast, Notch and Alk1 play opposing roles in *hey2* expression in cranial arteries and *dll4* expression in all arterial endothelium, with Notch inducing and Alk1 repressing these genes. Although *alk1* loss increases expression of *dll4*, AVMs in *alk1* mutants could neither be phenocopied by Notch activation nor rescued by Dll4/Notch inhibition. Control of Notch targets in arterial endothelium is context-dependent, with gene-specific and region-specific requirements for Notch and Alk1. Alk1 is not required for arterial identity, and perturbations in Notch signaling cannot account for *alk1* mutant-associated AVMs. These data

suggest that AVMs in HHT patients are not caused by defective arterial specification or altered Notch signaling.

3.1   INTRODUCTION

Notch signaling is critical for cell fate determination in many tissues. When activated by transmembrane ligands of the Delta and Jagged families, the Notch intracellular domain (NICD) is cleaved, translocates to the nucleus, binds to the DNA binding protein, recombination signal binding protein for immunoglobulin kappa J (RBPJ), and induces target gene expression [181]. In the vasculature, delta-like ligand 4 (Dll4)/Notch signaling controls arterial specification and angiogenic tip/stalk cell selection [30, 33, 38, 182], and in mouse and zebrafish models, decreased Dll4/Notch function leads to direct connections between arteries and veins, or arteriovenous malformations (AVMs) [30, 162, 166, 172, 183]. Because Dll4/Notch signaling transcriptionally upregulates the arterial endothelial marker, ephrinb2 (*Efnb2*) [184], and decreased Dll4/Notch signaling results in loss of *Efnb2* and ectopic arterial expression of the venous marker, *Ephb4* [30, 31, 162, 166, 171, 174, 183, 184], AVMs resulting from decreased Dll4/Notch signaling are generally attributed to disruption of arterial-venous identity. Notch loss-of-function (Notch[lof]) generates small caliber AVMs that are associated with thin, nearly atretic arteries [162, 183, 185]. Notch gain-of-function (Notch[gof]), which enhances *Efnb2* and represses *Ephb4*, also results in AVMs in mice [30, 31, 162, 166, 171, 174, 183, 184], and human brain AVMs exhibit increased Notch signaling [168, 186]. AVMs associated with Notch[gof] involve enlarged arteries containing supernumerary endothelial cells [31, 166, 167, 171, 172], suggesting

that failed repulsion mediated by EfnB2/EphB4, which is required for segregation of venous and arterial cells in developing vessels [187, 188], may be responsible for these AVMs. Thus, both Notch[lof and] Notch[gof] result in AVMs associated with disrupted arterial-venous identity, but the morphological characteristics of these AVMs are distinct, with low flow, small caliber shunts associated with Notch[lof] and high flow, large caliber shunts associated with Notch[gof].

Similar to Notch signaling, bone morphogenetic protein (BMP) signaling has also been implicated in AVM prevention. BMP ligands bind to a heterotetrameric complex of type I and type II serine/threonine kinase receptors; non-signaling type III receptors facilitate ligand binding. Upon complex formation, type II receptors phosphorylate type I receptors, which in turn phosphorylate Smad1, Smad5, and/or Smad9. Phosphorylated Smads bind to Smad4, translocate to the nucleus, and bind to DNA to regulate gene expression [189]. In humans, heterozygous loss of endoglin (*ENG*, encoding a type III receptor), activin receptor-like kinase 1 (*ACVRL1* or *ALK1*, encoding a type I receptor), or *SMAD4* results in hereditary hemorrhagic telangiectasia (HHT), a disease characterized by a predisposition to development of telangiectasias and AVMs [98, 101, 190, 191]. *Alk1* mutant mice exhibit decreased *Efnb2* expression in the dorsal aorta (DA) [192], and BMP9/ALK1 transcriptionally induces *EFNB2* in cultured human umbilical artery endothelial cells [174], suggesting that ALK1, similar to Notch, is required for arterial identity. Also like Notch, ALK1 has been implicated in maintenance of stalk cell identity [175]. Because both Notch and ALK1 are required for arterial differentiation, stalk cell fate determination, and prevention of AVMs, ALK1 and Notch might function in a common pathway to control arterial and/or stalk cell identity and prevent AVMs.

Several lines of evidence suggest that Notch and ALK1 interact in endothelial cells. Activation of either DLL4/Notch or BMP9/ALK1 in cultured endothelial cells enhances

expression of canonical Notch targets *HEY1*, *HEY2,* and *HES1,*[32, 174, 175] and simultaneous activation of these pathways synergistically increases expression of *HEY1* and *HEY2* [175]. A less dramatic effect on *HEY2* expression is observed in response to combined stimulation by constitutively active forms of Notch (*NICD*) and *ALK1 (ALK1^{CA}*) [184]. Induction of *HEY1* and *HEY2* by BMP9/ALK1 requires *SMAD4* but not *RBPJ* [175], and BMP9 induces SMAD1/5 binding to *HEY1, HEY2*, and *HES1* promoters in cultured human umbilical vein endothelial cells (HUVECs) [193]. These findings suggest that BMP9/ALK1 directly stimulates canonical Notch targets by a SMAD-dependent and NICD/RBPJ-independent pathway. Notch and ALK1 additively induce *VEGFR1*, a stalk cell marker, and inhibit *APELIN*, a tip cell marker, and mosaic sprouting assays demonstrate that endothelial cells lacking *ALK1*, *SMAD4*, or *HEY2* are more likely to be in the tip position [175]. Together, these results suggest that BMP9/ALK1/SMAD signaling induces canonical Notch targets independently of NICD/RBPJ and reinforces Notch-mediated acquisition of arterial identity and maintenance of stalk cell fate.

Although Notch and ALK1 exhibit synergistic interactions with respect to Notch target gene expression in cultured endothelial cells, evidence for synergy is less compelling for phenotypic endpoints. Both *NICD* and *ALK1^{CA}* dampen endothelial cell sprouting, but simultaneous pathway activation shows no further effects, and inhibition of one pathway does not inhibit effects of activation of the other pathway [174]. Similarly, both ALK1 and Notch inhibition enhance VEGF-stimulated tube formation in HUVECs and increase vascular area in the postnatal retina; however, combined inhibition of these pathways shows less than additive effects [175]. Thus, the synergy between Notch and ALK1 in controlling gene expression may not directly translate to synergistic effects on endothelial cell behavior.

To better understand the interaction between Notch and Alk1 in arterial endothelium, I assayed expression of Notch target genes and vascular phenotype in zebrafish embryos with altered Notch and/or Alk1 activity. Abrogation of Alk1 signaling did not decrease arterial endothelial expression of Notch targets, demonstrating that Alk1 is not necessary for maintenance of Notch target gene expression or arterial identity in vivo. However, concomitant inhibition of Notch and Alk1 revealed context-dependent interactions, with these two pathways cooperatively maintaining *hey2* and *efnb2a* in the DA, yet exhibiting opposing roles in controlling *hey2* expression and no role in controlling *efnb2a* expression in cranial arteries. In addition, I observed increased *dll4* expression in both trunk and cranial arterial endothelium in the absence of Alk1 signaling, in contrast to the dramatic loss of expression observed with Notch inhibition. These molecular data suggested that AVMs in *alk1* mutants might arise due to Notch gain-of-function; however, ectopic Notch activation failed to phenocopy and Notch inhibition failed to rescue AVMs associated with loss of *alk1*. Taken together, these data demonstrate that Notch and Alk1 exhibit context-specific and target-specific interactions in controlling Notch target gene expression in vivo, and that AVMs associated with Alk1 deficiency do not result from perturbations in Notch activity.

3.2   NOTCH IS ACTIVE CONCOMITANT WITH ALK1 IN CRANIAL ARTERIAL ENDOTHELIUM

Because my goal was to determine whether Alk1 and Notch signaling interact during vascular development, and because *alk1* plays a critical role in zebrafish cranial arterial development [92,

121, 135], I first assessed Notch activity in cranial endothelium using a double transgenic line, *Tg(tp1:egfp)^{um14};Tg(fli1a.ep:mRFP-CAAX)^{pt504}*. These fish report Notch activity, as visualized by EGFP expression [194], on a background of mRFP-labeled endothelial cells. Embryos were imaged at 36 hpf, a time point when Alk1 is active in cranial arterial endothelium [135]. Notch activity was weak to moderate in cranial arteries, including the first aortic arch (AA1), internal carotid artery (ICA), caudal division of the internal carotid artery (CaDI), optic artery (OA), and basal communicating artery (BCA) [Figure 13A]. All of these arteries are *alk1*-positive at 36 hpf [92]. Notch activity was also detected in the *alk1*-negative posterior communicating segments (PCS) and metencephalic arteries (MtA), but was absent in cranial veins (Figure 13A). These data demonstrate that cranial vascular Notch activity is arterial-specific, and that all *alk1*-positive arteries have active Notch signaling.

Next, I assayed cranial vessel expression of endogenous Notch targets. Hairy and enhancer of split (HES)-related proteins are transcriptional repressors that are induced by NICD/RBPJ [195], and the *HES*-related genes *HES1, HEY1,* and *HEY2* are upregulated by BMP9/ALK1 in cultured endothelial cells [175, 184, 193]. The zebrafish genome contains two *hes1* paralogs, *her6* and *her9* [196]. However, neither these genes nor *hey1* were detectable in endothelium at 24-36 hpf (data not shown). In contrast, *hey2* was expressed in all *alk1*-positive cranial arteries at 36 hpf (Figure 13B). *efnb2a*, another Notch target [184], as well as *dll4*, which encodes a Notch ligand that is positively regulated by Notch signaling [42, 197, 198], were also expressed in all *alk1*-positive cranial arteries at 36 hpf (Figure 13B). *dll4* was additionally expressed in the *alk1*-negative PCS and MtA. These data demonstrate that Notch targets *hey2*, *efnb2a,* and *dll4* are expressed in cranial arterial endothelium concomitant with active Alk1 signaling and are good candidates for cooperative regulation by Notch and Alk1.

60
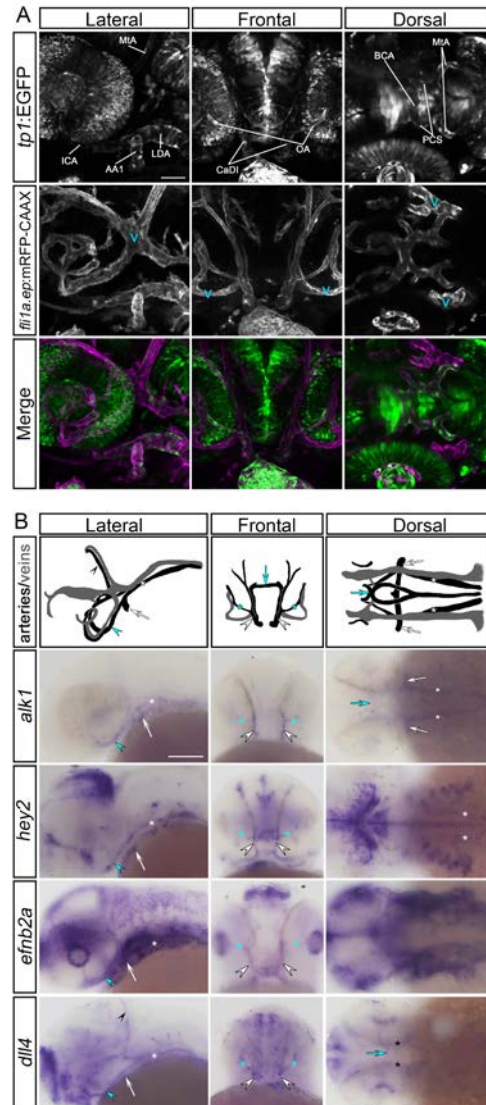
Figure 13: Notch is active concomitant with Alk1 in cranial arterial endothelium

A, Notch activity is detectable in cranial arterial but not venous endothelium ("v") at 36 hpf. Two-dimensional confocal projections of *Tg(tp1:egfp)^jum14* (green in merge) and *Tg(fli1a.ep:mRFP-CAAX) ^pt504* (magenta in merge). alk1-positive arteries: AA1, aortic arch 1; ICA, internal carotid artery; LDA, lateral dorsal aorta; CaDI, caudal division of internal carotid artery; OA, optic artery; BCA, basal communicating artery. alk1-negative arteries: PCS, posterior communicating segment; MtA, metencephalic artery. Images represent N = 20 embryos. Lateral and dorsal views, anterior leftward; frontal view, anterior up. Scale bar, 50 μm. B, Wiring diagrams (arteries black, veins gray) and representative whole mount in situ hybridization for alk1, hey2, efnb2a, and dll4 at 36 hpf. Expression of Notch

targets is detected in the alk1-positive AA1 (white arrow), ICA (blue arrowhead), LDA (white asterisk), CaDI (white arrowhead), OA (blue asterisk), and BCA (blue arrow). *dll4* is also expressed in the alk1-negative PCS (black asterisk) and MtA (black arrowhead). Plane of focus of dll4, frontal view, is deeper than other frontal images because of interfering dll4 brain expression. Images represent N > 63 embryos. Lateral and dorsal views, anterior leftward; frontal view, anterior up. Scale bar, 100 μm.

3.3   NOTCH AND ALK1 COOPERATIVELY REGULATE *HEY2* AND *EFNB2A* BUT OPPOSITELY REGULATE *DLL4* IN THE DORSAL AORTA

To investigate the interaction between Notch and Alk1 in the regulation of Notch targets in vivo, I assayed *tp1:egfp*, *hey2*, *efnb2a*, and *dll4* in embryos with impaired Notch and/or Alk1 signaling. To inhibit Notch signaling, I treated embryos with 10 μmol/L LY411575, a gamma-secretase inhibitor, between 23 and 36 hpf. This time period brackets the critical time period of Alk1 function: *alk1* is first detectable around 26 hpf, and *alk1* mutation results in enlargement of cranial arteries by 32 hpf [92]. LY411575 treatment had no effect on heartbeat or blood flow but resulted in severe trunk curvature (data not shown) as expected in Notch-inhibited embryos [30, 33, 199].

Notch signaling is active in the zebrafish DA throughout embryonic development [30, 161, 182], and despite no obvious requirement for Alk1, *alk1* is indeed expressed in the DA as early as 26 hpf [92]. LY411575 treatment resulted in complete loss of DA *tp1:egfp* expression (Figure 14A), demonstrating effective abrogation of NICD/RBPJ-mediated transcription. However, the effect of Notch inhibition on expression of endogenous Notch targets was variable.

LY411575 treatment had no effect on *hey2*, moderately decreased *efnb2a*, and completely abolished *dll4* (Figure 14A). These observations agree with published data [30, 34] and suggest that among these DA genes, *dll4* is most sensitive to perturbation of Notch signaling, whereas other pathways maintain *hey2* and *efnb2a* in the absence of Notch.

Next, I examined Notch target gene expression in the DA in *alk1^{ft09e}* mutants (Figure 14A). *alk1* mutation had no effect on expression of *tp1:egfp, hey2*, or *efnb2a* in the DA (Figure 14A), demonstrating that Alk1 is not necessary for expression of these arterial-specific Notch targets or for acquisition of arterial identity. In contrast, *dll4* expression was upregulated in the DA in *alk1^{ft09e}* mutants (Figure 14A). This observation was confirmed in *alk1^{y6}* and *alk1^{s407}* mutants and in *alk1* morphants (Figure 15). Furthermore, endothelial-specific expression of *alk1^{CA} (fli1a.ebs:alk1^{CA}-mCherry)* dramatically repressed *dll4* (Figure 15). These data suggest that Alk1 opposes Notch in *dll4* regulation in the DA.

Compared to Notch inhibition alone, combined *alk1^{ft09e}* mutation and Notch inhibition had no effect on *tp1:egfp* or *dll4* expression (Figure 14A), supporting the idea that Notch is required for expression of these genes. In contrast, concomitant abrogation of Alk1 and Notch signaling decreased *hey2* and nearly eliminated *efnb2a* (Figure 14A). *hey2* results, originally obtained in LY411575-treated *alk1^{ft09e}* embryos, were recapitulated in DAPT-treated *alk1^{y6}* mutants and LY411575-treated *alk1* morphants (data not shown). These findings suggest cooperative support of *hey2 and efnb2a* expression by Notch and Alk1 in the DA and agree with published data suggesting that both genes are regulated independently via NICD/RBPJ and ALK1/Smad1, 5 [30, 174, 175, 193].
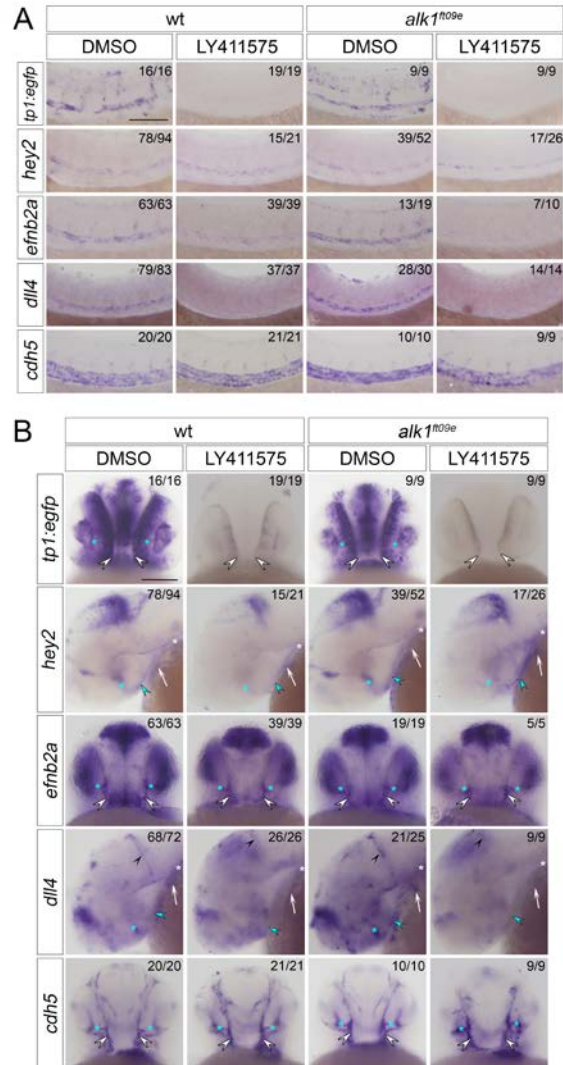
Figure 14: Notch- and Alk1-mediated control of Notch target gene expression is gene-specific and context-dependent

Whole mount in situ hybridization for *tp1:egfp*, *hey2*, *efnb2a*, *dll4*, and *cdh5* in 36 hpf wild type (wt) and *alk1^{ft09e}* embryos treated with 1% DMSO or 10 µmol/L LY411575, 23-36 hpf. **A,** Trunk. Lateral view, anterior leftwards. **B,** Head. AA1, white arrow; ICA, blue arrowhead; LDA, white asterisk; CaDI, white arrowheads; OA, blue asterisks; MtA, black arrowheads. *tp1:egfp, efnb2a, cdh5:* frontal views, anterior up. *hey2, dll4:* lateral views, anterior left. Numbers in upper right corners indicate number of embryos with similar phenotype/total number of embryos assayed. Scale bars, 100 µm.
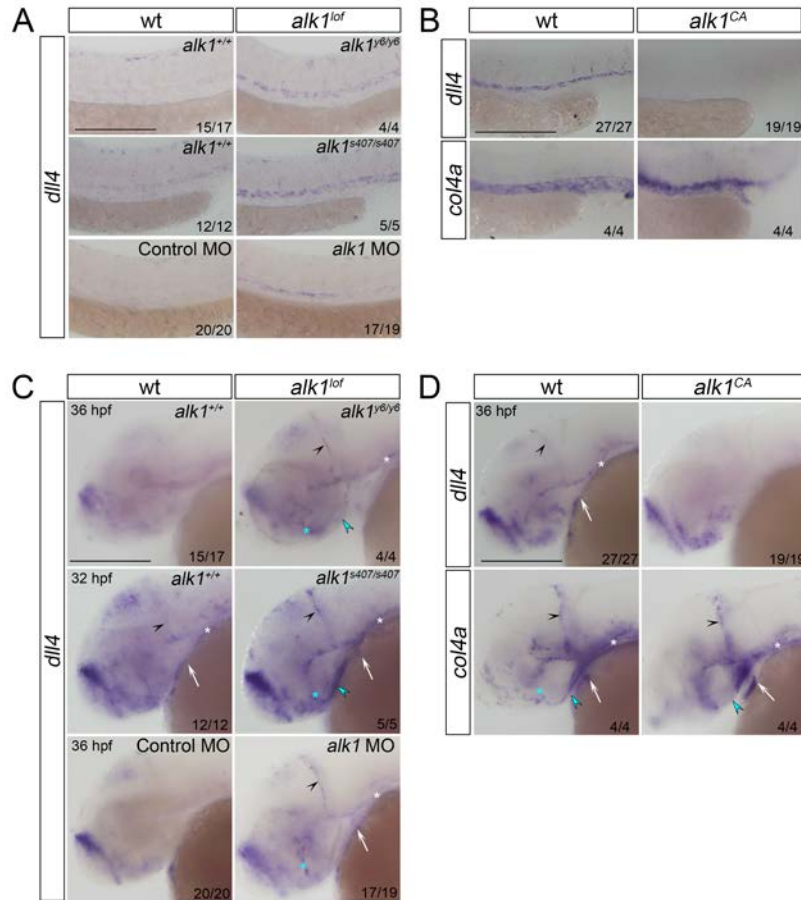
Figure 15: *dll4* is negatively regulated by Alk1 signaling

Whole mount in situ hybridization for *dll4* in *alk1^{y6/y6}* (36 hpf), *alk1^{s407/s407}* (32 hpf) and *alk1* morphants (MO) (36 hpf) in the trunk (**A**) and head (**C**). In the absence of *alk1, dll4* expression is increased in the dorsal aorta (trunk), aortic arch 1 (white arrow), internal carotid artery (blue arrowhead), lateral dorsal aorta (white asterisks), and metencephalic artery (black arrowhead) when compared to wild type (wt) or control MO siblings. *Tg(fli1a.ebs:alk1^{CA}-mcherry)* embryos show no vascular *dll4* expression at 36 hpf in the trunk (**B**) or head (**D**). Expression of collagen type IV alpha1 (*col4a1*), a pan-endothelial marker, demonstrates the presence of vessels in *Tg(fli1a.ebs:alk1^{CA}-mcherry)* embryos. Numbers in lower right corners indicate number of embryos with similar phenotype/total number of embryos assayed. Lateral views, anterior left. Scale bar, 200 μm.

3.4   NOTCH AND ALK1 EXHIBIT GENE-SPECIFIC ANTAGONISTIC INTERACTIONS IN REGULATION OF CRANIAL ARTERIAL ENDOTHELIAL GENE EXPRESSION

I next examined regulation of Notch target genes in cranial arteries, which enlarge upstream of AVMs in *alk1* mutants. LY411575 treatment abrogated *tp1:egfp* expression in cranial arterial endothelium and neural domains (Figure 14B and Figure 16), as expected. However, whereas Notch inhibition dramatically decreased *hey2* in cranial arterial endothelium, *efnb2a* was refractory to this treatment (Figure 14B and Figure 16). These effects were different from those observed in the DA (Figure 14A), suggesting context-specific gene regulation. LY411575 treatment eliminated arterial *dll4* expression in cranial arteries, similar to the DA, but increased *dll4* in neural tissues (Figure 14B and Figure 16). These observations support the idea of a positive feedback loop specific to arterial endothelial cells in which Notch signaling directly regulates *DLL4* expression [34, 42, 197, 198]. As in the DA, in cranial arteries *tp1:egfp, hey2,* and *efnb2a* were unaffected by a*lk1* mutation or knockdown, whereas *dll4* was markedly upregulated, and a *fli1a.ebs:alk1^{CA}-mCherry* transgene dramatically repressed *dll4* (Figure 14B, Figure 15C-D, and Figure 16). Also similar to the DA, loss of *alk1* failed to rescue abrogation of *tp1:egfp* or *dll4* expression induced by LY411575 treatment (Figure 14B and Figure 16). In contrast, *hey2* and *efnb2a* behaved differently in the absence of both Notch and Alk1 signaling in trunk versus cranial arterial endothelial domains. In cranial arteries, *efnb2a* expression proved refractory to combined loss of Notch and Alk1 signaling, whereas this same treatment increased *hey2* expression compared to Notch inhibition alone (Figure 14B and Figure 16). *hey2* results, originally obtained in LY411575-treated *alk1^{ft09e}* embryos, were recapitulated in DAPT-treated

alk1^{y6} mutants and LY411575-treated *alk1* morphants (Figure 17). These results suggest that neither Notch nor Alk1 is necessary for cranial arterial *efnb2a* expression, whereas Notch activates and Alk1 dampens *hey2* expression in cranial arteries, with Alk1 acting either downstream of NICD or independently of Notch. These data support the notion that region-specific regulatory networks control arterial expression of Notch target genes. Effects of Notch and Alk1 manipulation on Notch target gene expression are summarized in Table 1.

Table 1: Qualitative changes in arterial gene expression in response to altered Notch and/or Alk1 signaling

* Embryos were treated with 1% DMSO or 10 µmol/L LY411575, 23-36 hpf, and analyzed by in situ hybridization at 36 hpf. Table indicates increased (up arrows), decreased (down arrows; number of arrows indicates qualitative strength of response), or no change (NC) in expression compared to DMSO-treated wild type embryos.

	Dorsal Aorta			Cranial Arteries		
	wild type	*alk1* mutant/morphant		wild type	*alk1* mutant/morphant	
	LY411575	DMSO	LY411575	LY411575	DMSO	LY411575
tp1:egfp	↓↓↓	NC	↓↓↓	↓↓↓	NC	↓↓↓
hey2	↓↓	NC	↓	↓↓	NC	NC
efnb2a	↓↓	NC	↓↓↓	NC	NC	NC
dll4	↓↓↓	↑	↓↓↓	↓↓↓	↑	↓↓↓
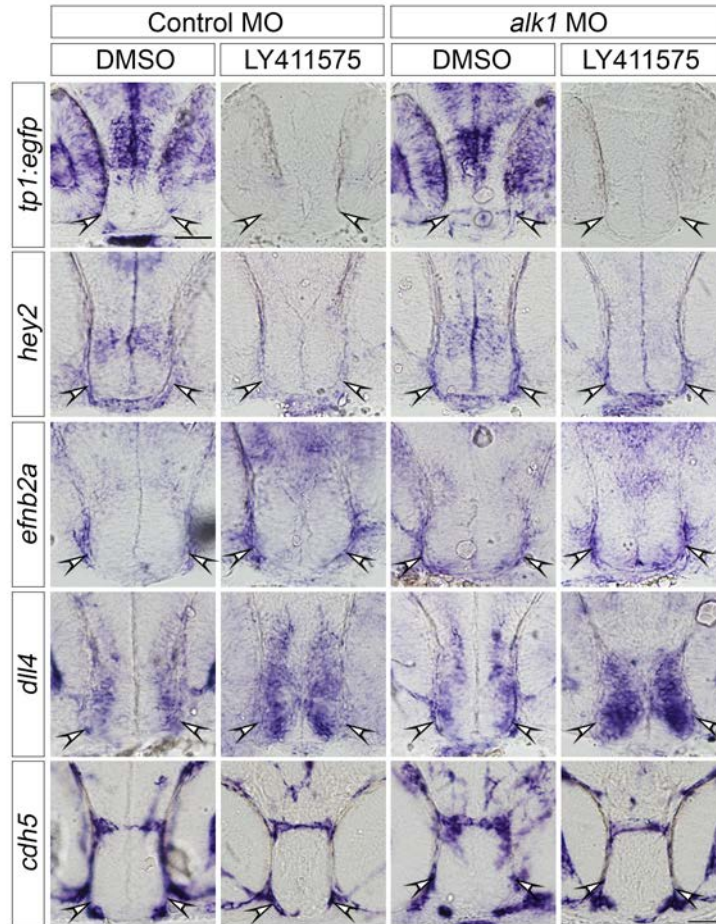
Figure 16: Notch targets are differentially regulated by Alk1 and Notch signaling in cranial arterial endothelium

Transverse cranial vibratome sections (50 µm) of 36 hpf control morpholino- and *alk1* morpholino-injected embryos treated with 10 µmol/L LY411575 or 1% DMSO, 23-36 hpf. Embryos were subjected to whole mount in situ hybridization for Notch-regulated *egfp*, *hey2*, *efnb2a*, *dll4* and *cdh5* prior to sectioning. Arrowheads, caudal divisions of the internal carotid artery. N = 12-20 embryos per treatment. Frontal views, dorsal up. Scale bar, 40 µm.
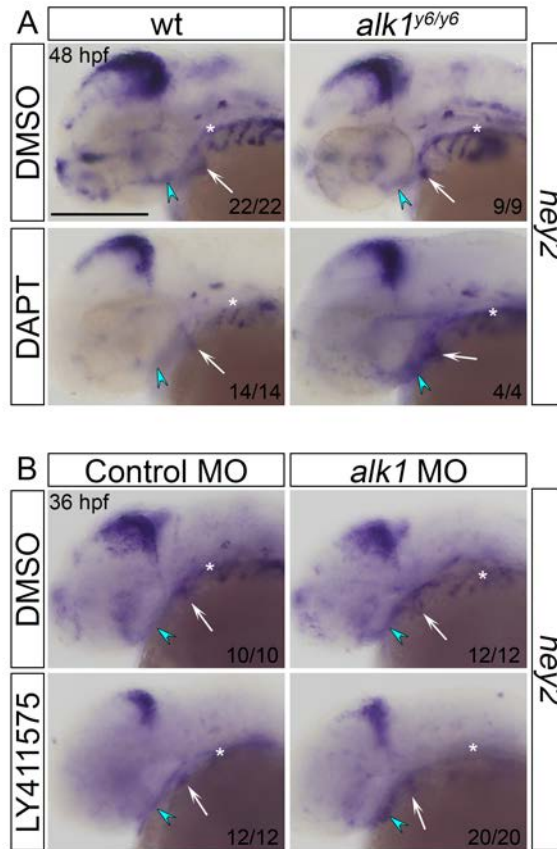
Figure 17: Opposing roles of Alk1 and Notch signaling in cranial arterial *hey2* expression

Whole mount in situ hybridization for *hey2* in 48 hpf wild type (wt) and *alk1*^{y6} mutant embryos treated with 50 µmol/L DAPT, 23-48 hpf (**A**), and 36 hpf control morphant and *alk1* morphant embryos treated with 10 µmol/L LY411575, 23-36 hpf (**B**). *hey2* expression in the first aortic arch (white arrow), internal carotid artery (blue arrowhead), and lateral dorsal aorta (white asterisk) is decreased with Notch inhibition, unaffected by *alk1* loss-of-function, but returned to control levels by concomitant Notch inhibition and *alk1* mutation or knockdown. Numbers in lower right corners indicate number of embryos with similar phenotype/total number of embryos assayed. Lateral views, anterior left. Scale bar, 200 µm.

3.5   *NOTCH^GOF* AND *ALK1^LOF* GENERATE VASCULAR MORPHOLOGI ES WITH SOME PHENOTYPIC OVERLAP BUT WITH INDEPENDENT ETIOLOGIES

My in vivo gene expression studies demonstrated that loss of *alk1* is associated with increased endothelial *dll4* expression. Therefore, I reasoned that enhanced Dll4/Notch signaling might phenocopy cranial AVMs in *alk1* mutants. To investigate this possibility, I compared cranial vascular development in wild type embryos, *Tg(fli1a:GAL4FF)^ubs3;Tg(5xUAS-E1b:6xMYC-notch1a)^kca3* embryos [which ectopically express Notch1a ICD in all endothelial cells; hereafter referred to as *Tg(endo:N1ICD)*], and *alk1* morphant embryos.

In wild type embryos, single sprouts emerged from the most posterior aspect of each bilateral venous primordial midbrain channel (PMBC) ~22 hpf and migrated medially to connect to a sprout emanating from the apex of the paired CaDIs by ~ 26 hpf, forming the BCA. These transient BCA/PMBC connections serve as the primary drainage for the CaDI/BCA between 26-36 hpf but regress thereafter as downstream arteries develop [92].

In *Tg(endo:N1ICD)* embryos, the CaDIs developed and lumenized normally, but sprouting from the PMBC was impaired, with BCA/PMBC connections delayed up to 8 hours compared to wild type [Figure 18, compare A-E, WT to F-J, *Tg*(*endo:N1ICD*)]. Vascular morphology was variable in 36 hpf *Tg(endo:N1ICD)* embryos, with establishment of early alternative drainage connections (for example, BCA to PCS/MtA, Figure 18G-H) associated with relatively normal caliber vessels, and establishment of late connections associated with CaDI/BCA engorgement and enlargement (Figure 18P,Q). Regardless of 36 hpf phenotype, BCA area was not significantly increased compared to control at 48 hpf (Figure 18S), but all

Tg(endo:N1ICD) embryos maintained at least one BCA/PMBC connection, resulting in a small caliber AVM (Figure 18P',Q',T).

Although the *Tg(endo:N1ICD)* phenotype bears some resemblance to the *alk1* mutant phenotype, these phenotypes originate and progress differently. In *Tg(endo:N1ICD)* embryos, delayed venous sprouting compromises early cranial arterial drainage, resulting in variable changes in CaDI/BCA calibers and small AVMs stemming from persistent BCA/PMBC connections (Figure 18F-J, Q, Q'). In *alk1* mutants, venous-derived angiogenic sprouting is not delayed, and all vessel connections develop normally (Figure 18K-O). However, increased endothelial cell number in the CaDI leads to increased caliber and altered hemodynamics, causing downstream vessels to adapt by maintaining normally transient arterial-venous connections (Figure 18T), most often between the BCA and PMBC [92, 121, 135]. Although the *Tg(endo:N1ICD)* phenotype decreases in severity over time (Figure 18Q, Q'), the *alk1* mutant phenotype exacerbates over time (Figure 18R, R'), with progressive increases in vessel caliber both upstream and downstream of the AVM.
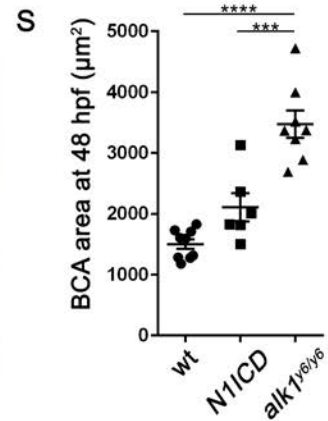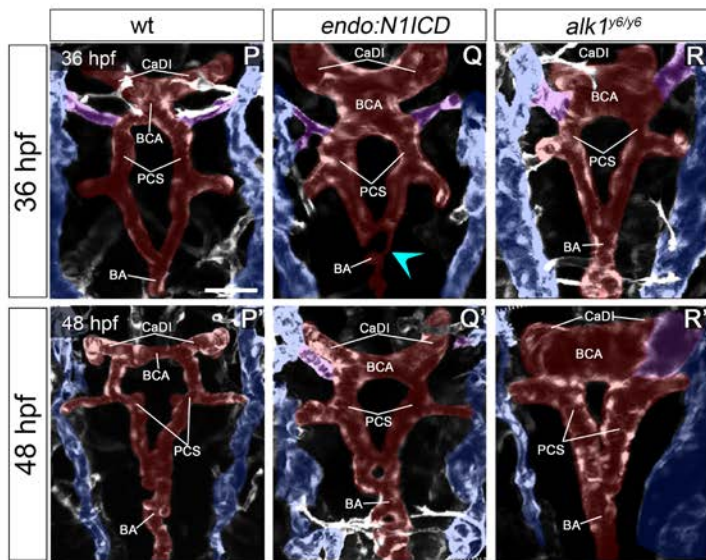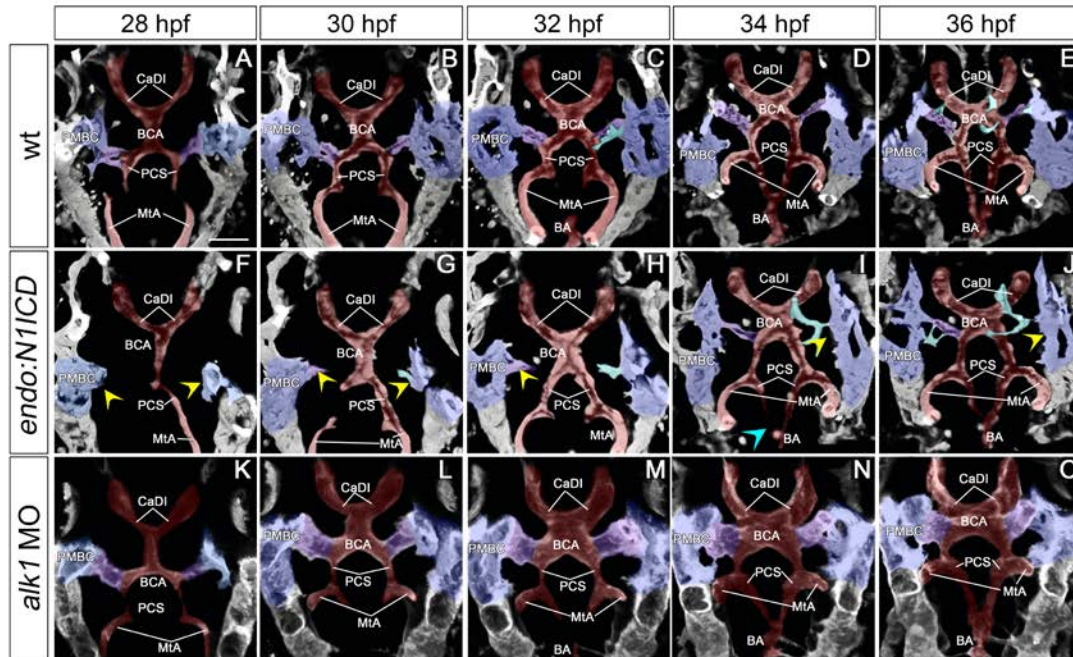
Figure 18*: notch^{gof} and alk1^{lof} cranial AVMs have independent etiologies*

(A-J) Time-lapse analysis of cranial arterial development in wild type (**A-E**), *Tg(endo:N1ICD)* (**F-J**), and *alk1*

morphant (**K-O**) embryos, 28-36 hpf. See also Supplemental material online, Movies S4, 5, 6. In *Tg(endo:N1ICD)*

embryos (**F-J**), PMBC-derived sprouts (yellow arrowheads) are delayed, compromising CaDI/BCA drainage. In

alk1 morphant embryos (**K-O**)**,** all connections form normally, but BCA enlargement is evident as early as 30 hpf. Two-dimensional projections of Z-stacks from two photon/confocal time-lapse imaging, frontal views, anterior up. Images represent N = 8 WT, 6 *Tg(endo:N1ICD)*, 10 *alk1* MO. Endothelial transgenes imaged: WT and *Tg(endo:N1ICD)*, *Tg(fli1a:GAL4FF;UAS:kaede)*; *alk1* MO, *Tg(fli1a:mrfp-caax)^{pt504}*. (**P-R'**) Two-photon imaging of WT (**P, P'**), *Tg(endo:N1ICD)* (**Q, Q'**), and *alk1^{y6}* mutant (**R, R'**) embryos at 36 and 48 hpf. *Tg(endo:N1ICD)* embryos show phenotypic overlap with *alk1* mutants, with variable enlargement of the CaDI at 36 hpf and consistent retention of BCA/PMBC connections at 48 hpf. Two-dimensional projections of Z-stacks, dorsal views, anterior up. Images represent N = 10 WT, 8 *Tg(endo:N1ICD)*, and 8 *alk1^{y6}* mutants.   Imaged transgene is *Tg(kdrl:gfp)^{la116}*. (**A-R**) Pseudocoloring: PMBC, blue; arteries, red; BCA/PMBC connection, purple. Scale bars, 50 μm. (**S**) BCA area is significantly increased in *alk1* mutants but not *Tg(endo:NICD)* at 48 hpf. N = 6-9 for each condition; lines represent mean ± SEM. One-way ANOVA followed by Tukey's post-hoc test, ***P<0.001, ****P < 0.0001. (**T**) Presence of shunts at 48 hpf.
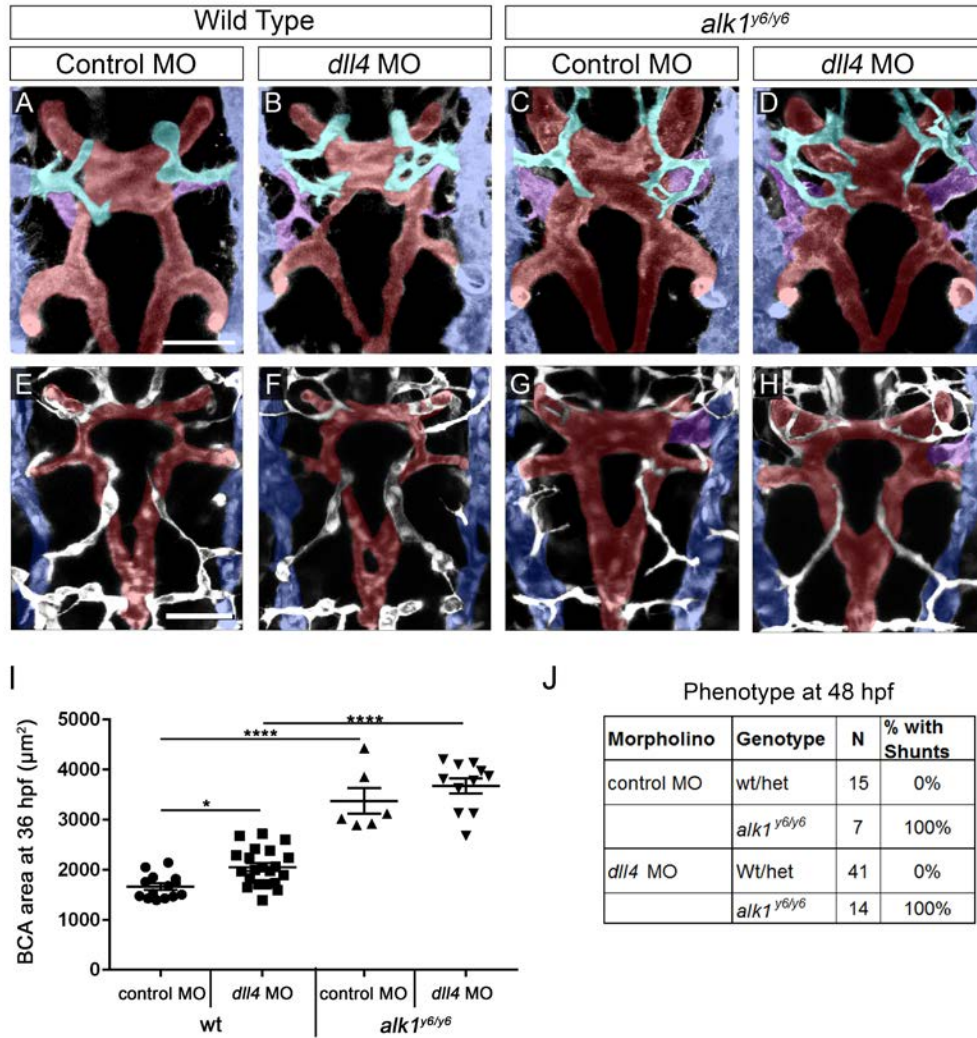
Figure 19: *dll4* expression is not required for AVM development in *alk1* mutants

Embryos from an *alk1^y6/+;^Tg(kdrl:gfp)^la116^* incross were injected at the 1 to 4-cell stage with 15 ng *dll4* MO or 5-bp

mismatch control MO, imaged at 36 (**A-D**) or 48 (**E-H**) hpf, and genotyped. Two-dimensional projections of two-

photon Z-stacks. Pseudo-coloring: PMBC (blue), arteries (red), and BCA/PMBC connection (purple). Dorsal views,

anterior up. Images represent N = 7-41 embryos per condition. Scale bars, 50 μm. (**I**) *dll4* knockdown failed to

rescue increased BCA area in *alk1^y6^* mutants at 36 hpf. Lines represent mean ± SEM, N = 6-21 embryos per

condition. One-way ANOVA followed by Tukey's post-hoc test, * $P<0.05$; ****$P<0.0001$. (**J**) *dll4* knockdown

failed to rescue cranial shunt formation in *alk1^y6^* mutants at 48 hpf.
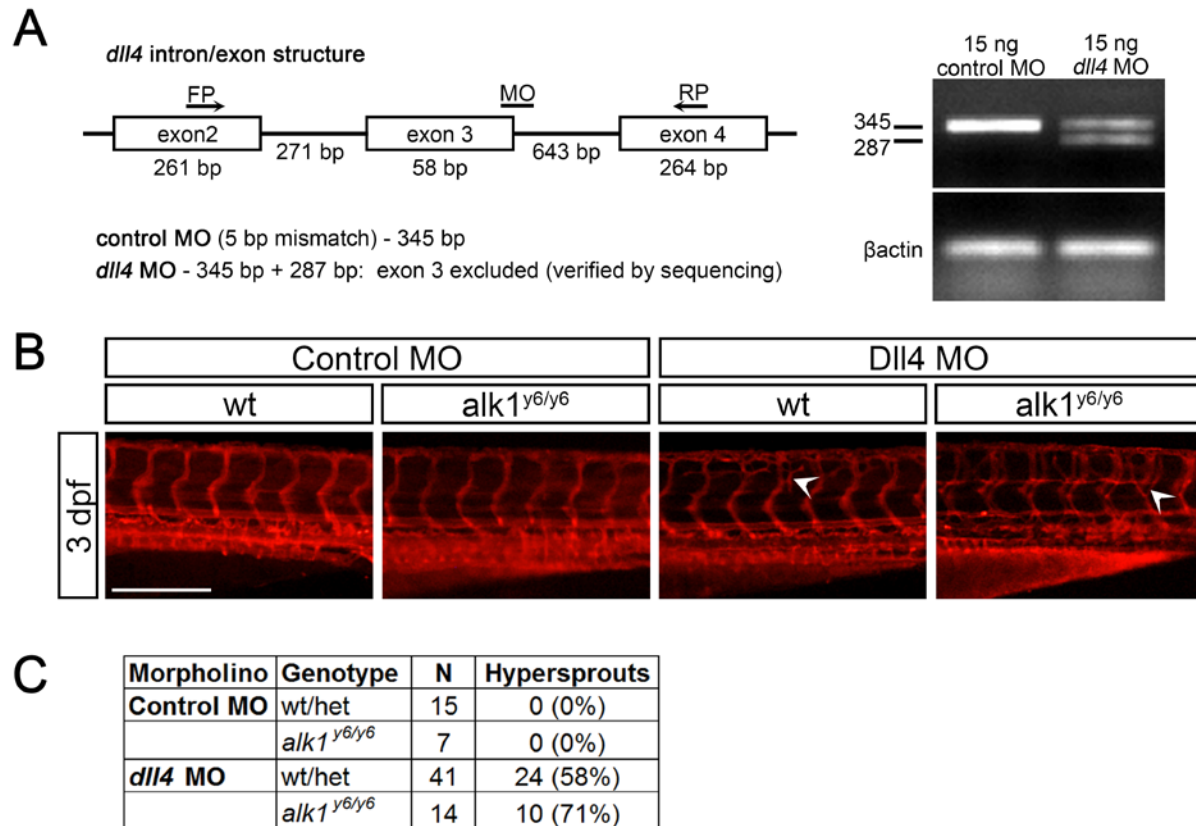
Figure 20: *dll4* morpholino validation

(**A**) RT-PCR following injection of *dll4* MO or 5-bp mismatch control MO (15 ng) using primers flanking the MO binding site. In 3 dpf control morphant cDNA, a single 345 bp band was detected. In 3 dpf *dll4* MO cDNA, *dll4* wild type product was decreased to 37% of control and an additional exon 3-deleted product (287 bp) was detected. Band intensities were normalized to ▯actin and identities were confirmed by sequencing of gel-extracted bands. (**B**) Injection of *dll4* MO but not 5-bp mismatch control MO (15 ng) caused hypersprouting (arrowheads) in trunk intersegmental vessels, 3 dpf, in wild type and *alk1^y6* mutant embryos. Two-dimensional confocal projections, *Tg(fli1a:mrfp-caax)^pt504*, anterior left. Scale bar, 50 µm (**C**) Hypersprouting was present in 63% of *dll4* MO-injected embryos, with similar representation in wild type and *alk1* mutant embryos.

3.6   NOTCH ACTIVITY IS NOT REQUIRED FOR AVM DEVELOPMENT IN *ALK1*

MUTANTS

To further explore the role of enhanced Dll4/Notch in AVM development in the absence of Alk1 function, I inhibited Notch activity in *alk1* mutants and assessed cranial vascular phenotype. First, I injected a splice-blocking *dll4* morpholino[33] into *alk1^{y6}* mutants. The morpholino generated an aberrant splice product that eliminated exon 3, decreased wild type transcript to approximately 37% of control, and resulted in intersegmental vessel hypersprouting [33, 34] in 60% of embryos (Figure 20). Wild type *dll4* morphants exhibited a small but significant increase in BCA area at 36 hpf (Figure 19A, B, I) but normal cranial vessel morphology, with no AVMs, at 48 hpf (Figure 19E, F, J). *dll4* knockdown failed to rescue increased BCA area (36 hpf) or cranial AVMs (48 hpf) in *alk1^{y6}* mutants (Figure 19C, D, G, H, I, J).

Because I could not achieve complete knockdown of *dll4*, I treated *alk1* mutants with LY411575 (beginning at 23 hpf) to eliminate Notch activity and assessed cranial vascular phenotype at 36 and 48 hpf (Figure 21). In DMSO-treated wild type embryos, the anterior central arteries (CtAs) [200] sprouted as the BCA/PMBC connection regressed: one or two sprouts emerged from more anterior aspects of each PMBC and migrated medially, with sprouts interacting ipsilaterally but not contralaterally and ultimately connecting to the BCA by 36 hpf (Figure 21A). Notch inhibition in wild type embryos had no effect on the CaDI/BCA but caused hypersprouting in the PMBC-derived CtAs at 36 hpf, with significant increases in number of PMBC-derived sprouts, connections to the BCA, branch points, and contralateral sprout connections (Figure 21B, Figure 22A-B', E-H).

In contrast to Notch-inhibited embryos, DMSO-treated *alk1* mutants exhibited enlarged CaDIs/BCAs at 36 hpf, as previously reported [92, 121, 135], but PMBC-derived CtAs were unaffected (Figure 21C, Figure 22C-D', E-H). Notch-inhibited *alk1* mutants were indistinguishable from DMSO-treated *alk1* mutants in terms of increased BCA caliber at 36 hpf (Figure 21C, D, I). At 48 hpf, LY411575 treatment decreased PCS caliber in both wild type and *alk1* mutant embryos but failed to rescue *alk1* mutant AVMs (Figure 21E-H, J). Furthermore, despite enhanced *dll4* expression, Notch signaling, as quantified by mean BCA EGFP fluorescence intensity in *Tg(tp1:egfp)^{um14}* embryos, was unchanged in *alk1* morphants compared to control (Figure 23). These data support *dll4* morphant data and suggest that enhanced Dll4/Notch signaling does not underlie AVM development in the absence of *alk1*.

Although Notch inhibition failed to rescue the *alk1* mutant phenotype, *alk1* mutation dampened Notch inhibitor-induced effects on CtAs, decreasing number of PMBC-derived sprouts, number of connections to the BCA, and CtA branch points to levels between wild type DMSO-treated and wild type LY411575-treated embryos (Figure 21A-D and Figure 22). However, effects did not achieve statistical significance. Further studies are required to determine whether this result reflects a genetic interaction between Alk1 and Notch pathways or an effect of altered vascular hemodynamics.
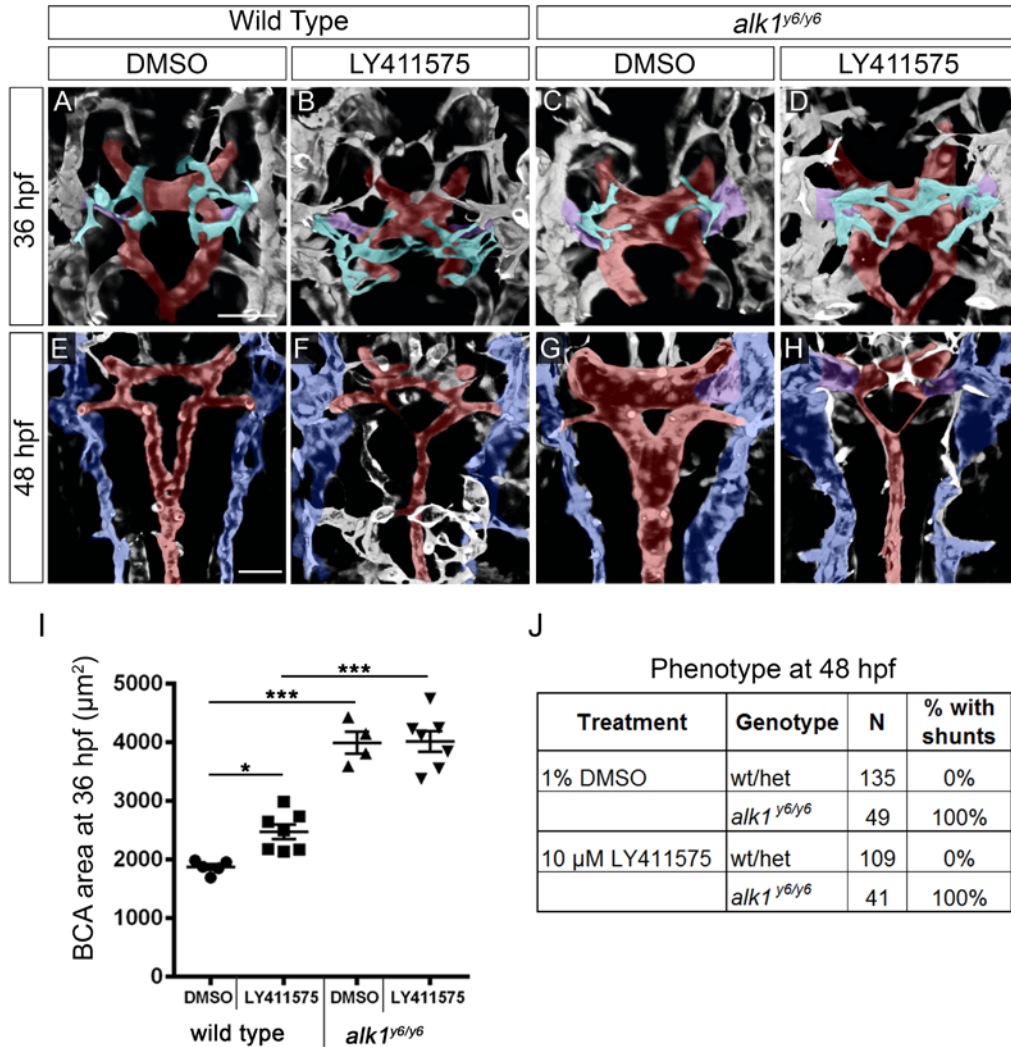
Figure 21: Notch activity is not required for AVM development in *alk1* mutants

Embryos from an *alk1[y6/+];Tg(kdrl:gfp)[la116]* incross were treated with 1% DMSO or 10 μmol/L LY411575 at 23 hpf and cranial vasculature imaged at 36 (**A-D**) and 48 (**E-H**) hpf. Two-dimensional projections of two-photon Z-stacks; in (**E-H**), dorsal planes were removed to highlight BCA/PCS. Pseudo-coloring: PMBC (blue), CtA (cyan); CaDI/BCA/PCS/BA (red), and BCA/PMBC shunt (purple). Dorsal views, anterior up. Scale bars, 50 μm (36 hpf) and 100 μm (48 hpf). (**I**) Notch inhibition failed to rescue increased BCA area in *alk1[y6]* mutants at 36 hpf. Lines represent mean ± SEM, N = 4-7 embryos per condition. One-way ANOVA followed by Tukey's post-hoc test, *$P<0.05$; ***$P<0.001$. (**J**) Notch inhibition failed to rescue cranial shunt formation in *alk1[y6]* mutants at 48 hpf.
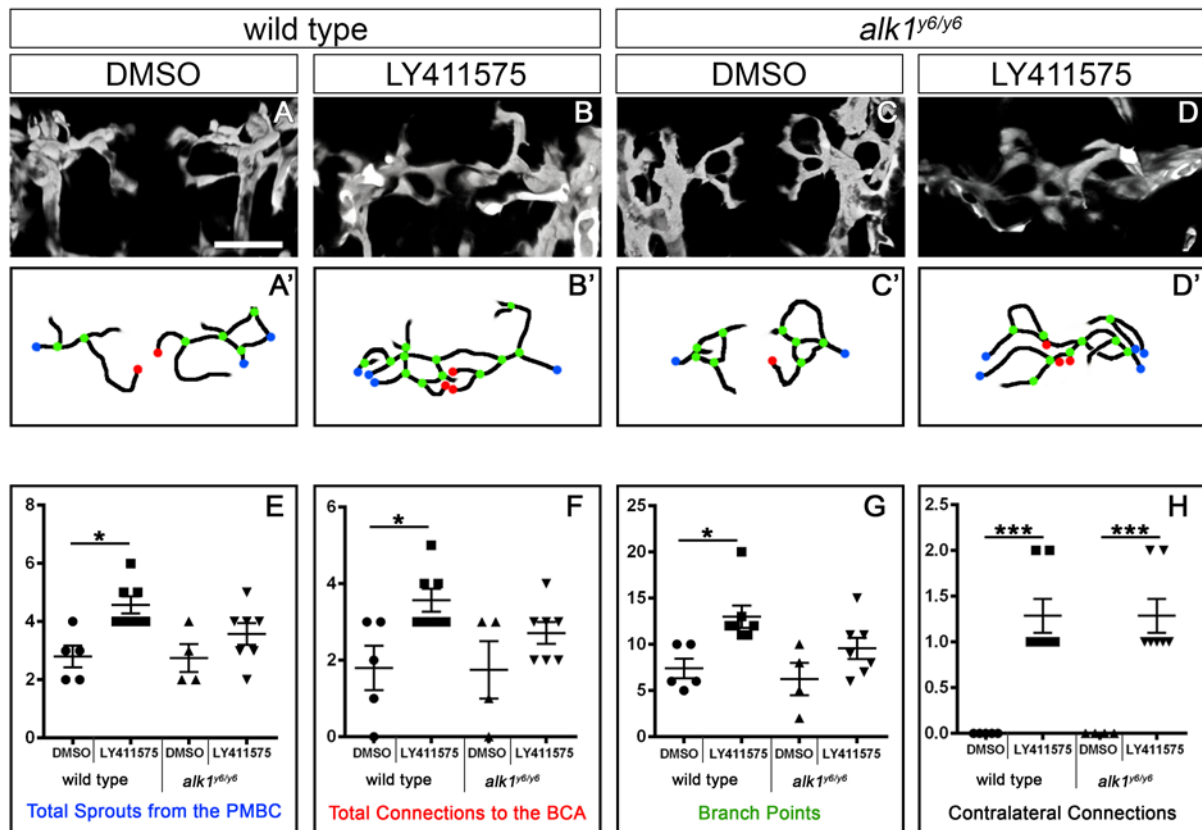
Figure 22: The Notch[lof] hypersprouting phenotype in midbrain and forebrain central arteries is partially rescued by *alk1* mutation

Embryos from an *alk1[y6/+]; Tg(kdrl:gfp)[la116]* incross were treated with 1% DMSO or 10 μmol/L LY411575, 23-36 hpf. Two-dimensional two-photon projections of the 36 hpf vasculature (**A-D**) were traced to generate wiring diagrams (**A'-D'**) of the midbrain and forebrain central arteries (CtA). Blue dots: connections to the primordial midbrain channel (PMBC); red dots: connections to the basal communicating artery (BCA); green dots: branch points. Frontal views, dorso-anterior up. Scale bar, 50 µm. Graphs quantify the number of PMBC-derived sprouts (**E**), CtA/BCA connections (**F**), CtA branch points (**G**), and CtA contralateral connections (**H**). N= 4-7 for each condition; lines represent mean ± SEM. One-way ANOVA followed by Tukey's post-hoc test, *$P<0.05$, ***$P<0.001$.
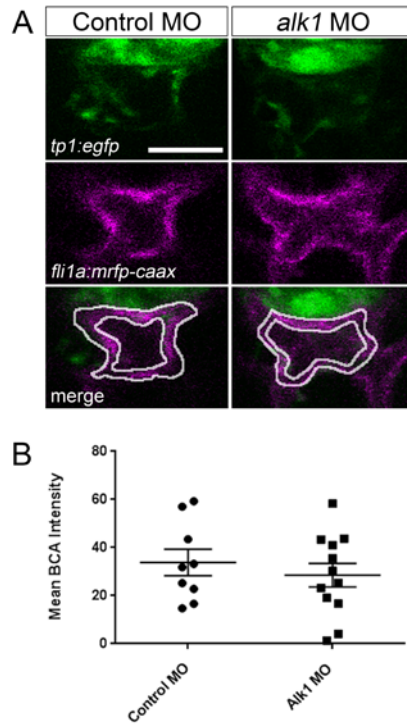
Figure 23: Notch signaling output is unaffected by *alk1* knockdown

(**A**) A single Z-plane through the center of the BCA of 36 hpf *Tg(tp1:egfp)*[um14]*;Tg(fli1a.ep:mRFP-CAAX)*[pt504] control morphant (MO) and *alk1* MO embryos. NICD/RBPJ-driven EGFP is green, endothelial cell membranes are magenta. Dorsal views, anterior up. Scale bar, 50 μm. (**B**) The mRFP channel was used to create a mask of the endothelial cell membrane, and the average EGFP intensity of the BCA was measured. N = 10-12 for each condition; lines represent mean ± SEM. Student's *t*-test: not significant.
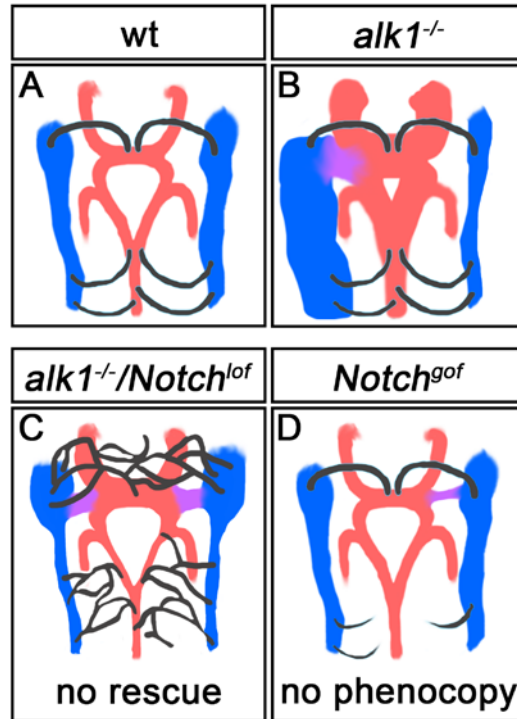
Figure 24: Cranial vessel architecture resulting from Alk1 and/or Notch manipulation

alk1 mutants develop enlarged cranial arteries (red) that drain through an aberrantly-retained connection (purple) to major primitive drainage veins (blue). Although this phenotype is associated with increased arterial *dll4*, *notch^gof* fails to phenocopy and *notch^lof* fails to rescue this defect. *notch^gof* causes impaired venous-derived sprouting (black), whereas *Notch^lof* causes enhanced venous-derived sprouting. 48 hpf, dorsal views, anterior up.

3.7 DISCUSSION

My results in zebrafish embryos demonstrate context-specific effects of Notch signaling on arterial endothelial gene expression. Although Notch inhibition abrogated transcription of a synthetic Notch reporter and endogenous dll4 in both trunk and cranial arteries, other arterial Notch targets were less sensitive to Notch inhibition, suggesting that additional control elements

81

sustain expression of these genes in the absence of Notch. Furthermore, Notch sensitivity of particular genes showed regional variation, suggesting unique regulatory mechanisms in different vascular beds. These data suggest that context-specific regulation, which may be lost or dampened in cultured endothelial cells, plays an important role in the control of Notch target gene expression in vivo.

Based on published work demonstrating cooperative interactions between DLL4/Notch and BMP9/ALK1 in enhancing arterial Notch target gene expression in cultured endothelial cells [175], I had anticipated that combined Notch and Alk1 inhibition might additively if not synergistically decrease Notch target gene expression and impair arterial specification. However, abrogation of Alk1 signaling failed to decrease expression of Notch targets or disrupt arterial (*hey2*, *efnb2a*, *dll4*) or venous (data not shown) identity, and I uncovered only minor cooperative interactions between Alk1 and Notch, with both contributing to maintenance of *efnb2a* and *hey2* expression in trunk but not cranial arteries. Furthermore, I uncovered opposing roles of Notch and Alk1 in expression of the Notch target and arterial marker, *dll4*. Although *dll4* is upregulated in the zebrafish DA in the absence of blood flow [201], lack of blood flow cannot account for increased *dll4* in *alk1* mutants: blood flow remains strong in *alk1* mutants at 36 hpf, with only a subtle redistribution of flow towards cranial vessels [92]. Together with previous data demonstrating increased *cxcr4a* and decreased *edn1* in the absence of blood flow or *alk1* expression [92], these data support the idea that Alk1 mediates a flow-based signal that controls expression of a subset of arterial genes. It is also possible that *dll4* upregulation in the absence of *alk1* might be attributed to the loss of the Smad1/5 target, *id1*. In the DA, *id1* is downregulated in the absence of *alk1* or blood flow (data not shown), and ID1 stabilizes HES1 (Her6 in zebrafish), which in turn represses *DLL4* [177, 202]. Therefore, decreased Id1 might decrease Her6, thereby

resulting in increased *dll4*. However, I was unable to detect *her6* in zebrafish arterial endothelial cells by in situ hybridization.

In addition to the unanticipated opposing effects of Notch and Alk1 on *dll4* expression, I demonstrated a paradoxical interaction with respect to cranial arterial *hey2* regulation, with loss of *alk1* restoring *hey2* to near control levels in Notch-inhibited embryos. This finding suggests that Alk1 may repress *hey2* in cranial arterial endothelial cells either downstream of NICD cleavage or via an independent mechanism. Although it is possible that enhanced blood flow through enlarged, *alk1*-dependent vessels might increase *hey2* expression, this seems unlikely given that *hey2* expression is unchanged in *alk1* mutants with intact Notch signaling (Table 1) or in the absence of blood flow (data not shown). Further studies are required to untangle the relationship between Notch and Alk1 in cranial arterial *hey2* regulation.

Dll4 is a critical arterial endothelial Notch ligand [182, 184] and Notch[gof] and in particular *Dll4* overexpression results in large caliber arteries and AVMs similar in morphology to AVMs in *Alk1* knockout mice [31, 166, 167, 171, 172]. Therefore, my finding that Alk1 inhibited *dll4* expression initially suggested to us that increased Notch signaling might contribute to AVMs in *alk1* mutants. However, multiple lines of evidence fail to support this hypothesis. First, although ectopic endothelial expression of *N1ICD* results in small cranial AVMs involving the same vessels as in *alk1* mutants, the origin and progression of these AVMs differs dramatically. The primary defect leading to AVMs in *N1ICD*-expressing embryos is delayed venous-derived sprouting, whereas the primary defect in *alk1* mutants is increased endothelial cell number in and caliber of upstream arteries [92]. Differences in the spatiotemporal expression of *fli1a*-driven N1ICD versus *alk1* limit the utility of my approach; however, I would expect that earlier N1ICD expression would cause an even more pronounced arterial phenotype

83

if enhanced arterial Notch signaling could serve as a proxy for arterial *alk1* loss. Second, neither *dll4* knockdown nor Notch inhibition rescues *alk1* mutant AVMs. Third, despite increased *dll4* expression, I failed to detect increased canonical Notch activity in *alk1* mutants. Together, these results suggest that AVMs arise independently in Notch^{gof} and Alk1^{lof} embryos.

Although AVMs initiate via independent mechanisms in Notch^{gof} and Alk1^{lof} embryos, both represent retention of normally transient BCA/PMBC connections. In *alk1* mutants, maintenance of BCA/PMBC connections occurs as an adaptive response to increased shear stress caused by enlargement of upstream arteries [92]. In Notch^{gof} embryos, impaired venous-derived sprouting delays CaDI/BCA drainage, which likely alters cranial vascular hemodynamics and affects remodeling. Thus, an adaptive response to altered hemodynamics, downstream of independent primary molecular and cellular defects, may be a unifying factor in development of Notch^{gof} and Alk1^{lof} AVMs.

Although I failed to rescue vascular defects in *alk1* mutants via Notch inhibition, I partially rescued CtA hypersprouting defects in Notch-inhibited embryos via *alk1* mutation, suggesting some interaction between Notch and Alk1 in the cranial vasculature. It is possible that restored *hey2* expression in the absence of both Notch and Alk1 signaling might contribute to this phenomenon, as knockdown of *HEY2* enhances sprouting in cultured HUVECs [175]. However, whether these observations represent a true genetic interaction or a response to changes in vascular hemodynamics remains to be determined.

In summary, my in vivo analysis of Notch and Alk1 signaling demonstrates gene-specific and context-specific interactions, with examples of both cooperative and antagonistic control of gene expression. However, results fail to support the idea that these pathways interact synergistically to control Notch target genes, program arterial identity, and prevent AVMs.

4.0 CONCLUSIONS AND FUTURE DIRECTIONS

The work presented in this thesis provides insight into the role of Alk1 signaling in endothelial cell migration and presents a model for AVM formation caused by pathway disruption. Previous work in the lab had demonstrated that AVMs form via a two-step mechanism upon loss of *alk1*. In the first step, endothelial cell number increases in cranial arteries and this increase is independent of blood flow [92, 121, 135]. As an adaptive response to increased flow, transient connections are maintained forming flow dependent arteriovenous shunts [92]. My work has focused on furthering the understanding of how loss of *alk1* results in an increase in endothelial cell number in cranial arteries in the zebrafish embryo. I show that Alk1 is necessary for directed endothelial cell migration upon the onset of blood flow and that *alk1* mutant AVMs do not form as a result of defects in arterial/venous identity. I have also contributed to the general knowledge of vascular development by describing in detail the formation of the cranial vascular system between 24 and 36 hpf, a key developmental period when cranial circulation begins. To this end, I have found that endothelial cells migrate in opposition to flow and contribute to the endocardium, described the sources of the endothelial cells that contribute to the cranial arterial system, and described how the timing of sprouting is key to forming a normal mature vascular system.

There are many unresolved questions. Whether Alk1 functions as a mechanosensor/transducer is not clear. Alk1-positive arteries do not appear to have primary cilia (B. Roman, unpublished), and the expression of *vegfr* and *vecad* is unaffected in *alk1* mutants (data not shown). However, Alk1 may regulate *vegf* or *vecad* at the translational or post-translational level and experiments testing the role of Alk1 signaling on the localization of Vegfr2 and Vecad protein in the presence of flow would be informative. Based on the observation that endothelial cells are defective in directed endothelial cell migration, it is possible that Alk1 is involved in endothelial cell polarization. In the presence of high magnitude flow endothelial cells polarize with the nucleus downstream of the microtubule organizing center and the golgi apparatus [74]. In preliminary experiments, I was able to inject a GFP tagged centrin construct (centrin is a key protein of the centrosomes) into zebrafish embryos and visualize endothelial cell centrin in AA1 (data not shown). I hope to determine if endothelial cell polarization is affected in *alk1* mutant embryos and in *ALK1*-depleted cultured endothelial cells exposed to shear stress.

Angiogenesis is often viewed as a binary process. A vessel is either actively undergoing angiogenesis (endothelial cell proliferation, migration and degradation of the ECM) or is quiescent (no proliferation or migration and vessels are stabilized through ECM deposition and smooth muscle recruitment). A long standing model in the field suggested that TGFβ1 activation of Alk1 and Alk5 induced activation or stabilization, respectively, and that the relative activation of the two pathways determined the activation state of the endothelium [176, 180, 203, 204]. AVMs were thought to arise due to a disruption in this balance causing aberrant angiogenesis [203, 205]. This model was shown to be inaccurate because in mice and zebrafish, Alk1 and Alk5 are not coexpressed in the vascular endothelium and Alk5 is not required in endothelial

cells for normal vascular development [118, 206, 207]. Subsequent work has postulated that AVMs form in HHT models due to defects in arterial venous identity (as evidenced by decreased *ephrinB2* expression in the DA of mouse *alk1* mutants [114, 121]) or due to focal capillary regression [90].

It is my hope that the work I present in this document provides a more nuanced understanding of angiogenesis and AVM development. ALK1 signaling is neither pro- nor anti-angiogenic, and AVM formation is not the result of "too much" or "too little" angiogenesis. Instead, AVM development involves defects in post-angiogenic endothelial cell behaviors and force-dependent remodeling. Alk1 is important upon the onset of flow to provide a means for endothelial cells to migrate towards the heart in the vessels that experience the highest hemodynamic load. Without this signal, arterial endothelial cells are not able to respond appropriately and while the immediate result is somewhat variable, the final result is a decrease in cells proximal to the heart and an accumulation of cells in downstream arteries. My work has also demonstrated that while Alk1 is not necessary for determining or maintaining arterial identity, there is still much to be understood regarding the relationship and interactions between Alk1, Notch and blood flow.

4.1   CURRENT HHT TREATMENTS

Current HHT treatments focus on treating symptoms. Large PAVMs or BAVMs may be coil-embolized or surgically resected, but these procedures are invasive and risky. The observation that wounding is necessary for adult endothelial-targeted *Eng* (*Eng*-iKO[e]) [120] and inducible

87

knockout *Alk1* (*Alk1*-iKO^e) mice [117] to develop AVMs has led to the hypothesis that sites of active angiogenesis are more susceptible to AVM formation in HHT patients. To this end, anti-angiogenic treatments have been shown to greatly improve *Eng*-iKO^e and *Alk1*-iKO^e mouse vascular phenotypes. Specifically treatment with antibodies designed to block VEGF have reversed vascular abnormalities in these mice and restored levels of key angiogenic factors that had been dysregulated in affected tissues [208, 209]. In addition, HHT patients treated with similar therapies have experience significant improvement in nose bleeds, GI bleeding and liver complications [210-213]. Given that VEGF does not appear to be involved in *Eng*-iKO^e and *Alk1*-iKO^e mouse disease pathology, the mechanism by which anti-VEGF treatment improves HHT symptoms is not understood [107]. In light of my research, I suggest that AVMs develop in immature vessels because of aberrant distribution of arterial endothelial cells that causes arterial enlargement, which results in an altered hemodynamic load and consequent downstream AVM formation to normalize hemodynamic forces. Inhibiting angiogenesis prevents the initiation of a sequence of events that would lead to improper endothelial cell migration and distribution.

5.0 MATERIAL AND METHODS

5.1 ZEBRAFISH LINES AND MAINTENANCE

Adult zebrafish (*Danio rerio*) were maintained according to standard protocols [214]. Embryos were grown at 28.5°C in 30% Danieau [17 mM NaCl, 2 mM KCl, 0.12 mM MgSO$_4$, 1.8 mM Ca(NO$_3$)$_2$, 1.5 mM HEPES]. For imaging, embryo medium was supplemented with 0.003% phenylthiourea (Sigma, St. Louis, MO, USA) at ~8 hpf hours post-fertilization (hpf) to prevent melanin synthesis. Mutant lines *alk1^{ft09e}* (p.Y88X), *alk1^{y6}* (p.L240F), *alk1^{s407}* (g.IVS8-2A>T), *alk1* splice-blocking morpholino, and *alk1^{y6}* genotyping assay have been described [92, 121, 215]. Line *alk1^{ft09e}* was genotyped by dCAPs assay [216] using primers 5'-GTGCTACGTACCTGCTATTCCTGGAGTCTA-3' and 5'-CGAACAACCCAGAAACGAG-3'. The forward primer contains a single mismatch (underlined) that creates an *Xba*I site in the mutant allele. Line *alk1^{s407}* was genotyped using PCR primers 5'-GACAATTTCCAGTCATCCTC-3' and 5'-CTGGGCCTGTGCTGGTC-3' followed by restriction digest with DdeI (cuts wild type only). Transgenic lines *Tg(fli1a:GAL4FF)^{ubs3}*, *Tg(UAS:Kaede)^{rk8}* and *Tg(kdrl:GFP)^{la116}* have been described [217-219]. Two new transgenic lines were created by Gateway cloning (Invitrogen/Life Technologies, Carlsbad, CA, USA) into *tol2* transposon arm-flanked vectors followed by injection into one-cell stage embryos [220-222]. *Tg(fli1a.ep:mRFP-CAAX)^{pt504}* has mRFP-labeled endothelial cell membranes.

Tg(fli1a.ebs:alk1^{CA}-mCherry) expresses constitutively active *alk1* [121] fused to mCherry in all endothelial cells. This transgene is embryonic lethal; therefore, F1 embryos were analyzed from mosaic P0 founders. A previously described troponin T type 2a *(tnnt2a)* morpholino [223] was used to prevent heartbeat and blood flow. A full list and description of transgenic zebrafish used in this work can be found in Table 2.

Table 2: Transgenic zebrafish used in this work

Transgenics	Allele	Description
alk1e5:egfp	pt517	Expresses gfp under the control of an alk1 enhancer element
cmlc2:ndsred2	f2	Expresses dsred in myocardial nuclei
fli1ebs:alk1ca-mcherry	-	Ectopically expresses a constitutively active mcherry tagged alk1 in the vascular endothelium
fli1:gff	ubs4	A gal4 variant: drives uas expression in the vascular endothelium
fli1ep:mRFP-CAAX	pt504	Expresses mRFP in endothelial cell membranes
fli1:nEGFP	y7	Expresses gfp in endothelial cell nuclei
flk1:GFP	la116	Expresses gfp in endothelial cell cytoplasm
flk1:nls-mcherry	is4	Expresses mcherry in endothelial cell nuclei
gata1:dsred	sd2	Expresses dsred in erythrocytes
tp-1MmHb5:eGFP	um14	Expresses gfp under the control of a Notch enhancer element
uas:kaede	rkr8	Expresses a photoconvertible cytoplasmic protein in the presence of gal4
uas:myc-N1ICD	kca3	Expresses a myc tagged intracellular domain of Notch1 in the presence of gal4

5.2   MORPHOLINOS AND MORPHOLINO VALIDATION

Morpholinos were purchased from GeneTools, Philomath, OR, USA. Morpholinos used in this study are listed in Table 3.   Splice blooking morpholinos are denoted as SB and translation blocking is denoted byTB. The control morpholino was injected at the same concentration as the experimental morpholino for each experiment. Dll4 MO was validated by RT-PCR using primers listed in Table 4 according to the published protocol [33].

Table 3: Morpholino sequences used in this study

Morpholinos	Sequence		
alk1	5'-ATCGGTTTCACTCACCAACACACTC-3'	2.5 ng	SB
tnnt2a	5'-CATGTTTCGTCTGATCTGACACGCA-3'	4 ng	TB
dll4	5'-CGAATCTTACCTACAGGTAGATCCG-3'	15 ng	SB
dll4 5-mismatch control	5'-CGAATgTTAgCTAgAGcTAcATCCG-3'	15 ng	
Control	5'-CCTCTTACCTCAGTTACAATTTATA-3'		

5.3   CONFOCAL AND TWO-PHOTON IMAGING

For live imaging, up to 12 embryos were anesthetized in 160 mg/ml tricaine (Sigma) and embedded in 0.5% low melting temperature NuSieve GTG Agarose (Lonza, Rockland, ME, USA)/30% Danieau. Z-series (1.48 mm steps) were collected using a TCS SP5 multiphoton/confocal microscope (Leica Microsystems, Wetzlar, Germany) outfitted with a custom motorized stage (Scientifica, Uckfield, East Sussex, UK), an APO L 20x/1.00 water

immersion objective or an HCX IRAPO L 25x/0.95 water immersion objective, non-descanned

detectors, and spectral detectors, with a 1.7X zoom. EGFP was excited with a Mai Tai DeepSee

Ti:Sapphire laser (Newport/Spectra Physics, Santa Clara, CA, USA) at 900 nm, whereas

mCherry and dsRed were excited with a 561 nm diode. Sequential frame scanning was

performed using a resonant scanner with unidirectional (8000 Hz) or bidirectional (1600 Hz)

scanning and 16x or 32x line averaging. For time lapse experiments, (X,Y) coordinates were set

using the LAS AF "Mark and Find" function, and images were collected every 18-23 minutes,

with z-stack parameters redefined for each (X,Y) coordinate. Images were analyzed using LAS

AF (version 3.0.0 build 834) and Adobe Photoshop CS6. Confocal time series were converted to

QuickTime (.mov) files using LAS AF and annotated using Final Cut Pro and iMovie.

5.4   ENDOTHELIAL CELL TRACKING

Maximum projection z-stacks were compiled using the Leica ASF-AF software and each time

point was saved as an individual tiff. Tiffs were imported into an Adobe Photoshop file, with

each time point occupying a single layer. Individual cells were labeled in Photoshop using the

paint tool and tracked over each layer. 3D projections were referenced in the Leica ASF-AF

software when it became difficult to track an individual cell with certainty.

Table 4: Primers and Assayes used for genotyping and morpholino validation

Allele	Forward Primer 5'-3'	Reverse Primer 5'-3'	Digest	Assay
alk1^{y6}	cacggtccaactaaggcatgaaaacacctt	atggacagagaagtgtaagtaagaaat	BsaJ1	dCAPS; Cuts wt
alk1^{ft09e}	gtgctacgtacctgctattcctggagtcta	cgaacaacccagaaacgag	Xba1	dCAPS; cuts mutant
alk1^{s407}	gacaatttccagtcatcctc	ctgggcctgtgctggtc	DdeI	RFLP; cuts WT
sih^{tc300b}	tatggcctttatgaatttgtctgtaac	gaacataagacttaccctcctgctctc	Xba1	dCAPS; Cuts wt

Transgenics

gfp	tggtgcccatcctggtcgagctgg	aagtcgtgctgcttcatgtg	n/a	1 band for +GFP
fli1ep:gffubs4	ctccgctgactagggcacat	gacggcatctttattcacattatc	n/a	1 band for +gff (200 bp).
mCherry	cctgtcccctcagttcatgt	cccatggtcttcttctgcat	n/a	1 band for +mcherry
uas:Kaede^{rk8}	ttgggagcgaagcctgatgt	caccctcctgcctagatttgtaag	n/a	1 band for +Kaede
uas:notch1ICD^{kca3}	cgtgagtcagtgagttacagct	gtggaggagctcaaagtga	n/a	1 band for NotchICD -350 bp

Dll4 MO validation

dll4	cgtgtctccaggtgactgtatcttt	gaacaactgtcgccgtagtaat	n/a	1 band at 345 bp in control, exon 3 excluded in MO injected resulting in 287 bp product
actinb2	cgtgctgtcttcccatcca	tcaccaacgtagctgtctttctg	n/a	1 band ~100 bp

5.5   KAEDE PHOTOCONVERSION

Up to 12 embryos were embedded in 0.5% low melt agarose at 24 hpf. The Leica "Frap Wizard" software was used for imaging and bleaching. An initial scan was captured with the argon laser set to 28% power, with the 488 nm line at 25%; the 561 nm diode at 25% and the 405 nm laser at 0%, 600Hz laser speed (3x line average) and a 2x zoom. Using this image, a region of interest (ROI) was drawn around the section of vessel that was to be photoconverted. For bleaching all parameters remained the same, with the exception of the 405 laser, which was set to 20%. The "set background to zero" and "use laser settings for all ROIs" options were selected. The bleaching time course consisted of 2 pre-bleach scans, 5 bleach scans, and 2 post-bleach scans. Embryos were removed from the agarose and placed in a 12-well plate and incubated at 28.5°C in the dark until 48 hpf. Embryos were then embedded again and imaged using the 488 nm and 516 nm wavelengths to determine the location of the converted cells.

To quantify the location of photoconverted cells, I divided the vessels into anatomical sections and scored whether or not an individual embryo had a converted cell in that specific region. The data represents the percentage of embryos that had at least one photoconverted cell in each vessel region.

5.6   CRYOSECTIONS AND IMMUNOFLUORESCENCE

Embryos were fixed overnight in 4% paraformaldehyde at 4°C. Embryos were then washed into a 15% and 30% sucrose/PBS solution before being embedded in Tissue Freezing Medium (TFM, Triangle Biomedical Sciences) and stored at -80°C. Cryosectioning was performed on a Leica CM 1850 and 30 µM sections were immediately placed on a Shandon Superfrost Plus positively charged slide (Thermo Scientific), dried at 37°C for 30 minutes and stored at -20°C overnight. Immunohistochemistry was performed using primary antibodies mouse anti-MF20 at 1:500 (sarcomeric myosin, Developmental Studies Hybridoma Bank, Iowa City, IA, USA) or rabbit anti-GFP at 1:500 (Invitrogen, A-11122) and secondary antibodies goat-anti-rabbit Alexa Fluor 488 at 1:1000, and goat-anti-mouse Alexa Fluor 568 at 1:1000. Embryos were washed in a PBS/0.1% triton X-100/0.1% DMSO (PBDT) solution and blocked in 5% goat serum in PBDT. Sections were mounted with Vectashield Fluorescent mounting medium (Vector) and imaged with an Olympus Fluoview 1000 confocal microscope outfitted with a UPFLN 20x oil immersion objective. Two-dimensional projections were generated from Z-series (1 µm steps) using ImageJ 1.45s (National Institutes of Health, USA).

5.7   IN SITU HYBRIDIZATION

All embryos were collected at 36 hpf, fixed in 4% paraformaldehyde/PBS for approximately 36 hours at 4°C, dehydrated in methanol, and stored at -20°C for in situ hybridization. Digoxigenin-labeled riboprobes were generated according to the manufacturer's protocol (Roche,

Indianapolis, IN, USA). *cdh5* plasmid [92], *dll4* plasmid [33], and *efnb2a* plasmid [30] have been described. *hey2* was amplified from zebrafish cDNA and cloned into PCRII-TOPO (Invitrogen/Life Technologies). *egfp* was amplified from plasmid DNA and cloned into pCRII-TOPO. *collagen type IV alpha 1* (*col4a1*) was amplified from zebrafish cDNA using primers appended with T3 (sense) and T7 (antisense) polymerase sites, and the PCR product was column purified (Qiaquick PCR Purification Kit) and used for riboprobe synthesis. Whole mount in situ hybridization was performed in an InSituPro VSi liquid handler (Intavis Inc, Chicago, IL, USA). Briefly, 36 hpf embryos were rehydrated to PBS/0.1% tween-20 (PBT), permeabilized with 50 mg/ml proteinase K for 15 minutes, and the permeabilization terminated with 0.2% glycine/PBT, 5 minutes. Embryos were then post-fixed for 20 minutes with 4% paraformaldehyde/PBS and hybridized at 65°C for 12 hr with riboprobe diluted 1:500 in hybridization buffer (50% formamide, 5x SSC, 5 mg/mL yeast tRNA, 50 mg/ml heparin, 0.1% tween-20). Embryos were then washed with 50% formamide/2x SSC/0.1% tween-20 (2 x 30 minutes, 65°C), 2x SSC/0.1% tween-20 (15 minutes, 65°C), and 0.2x SSC/0.1% tween-20 (2 x 30 mintues, room temperature). Specimens were then blocked with 5% sheep serum (Sigma)/PBT and incubated with embryo-adsorbed anti-digoxigenin-AP, Fab fragments (Roche), 1:5000 in 5% sheep serum/PBT. Embryos were then washed 6 x 15 minutes followed by overnight in PBT, transferred to 6-well plates containing NTMT (100 mmol/L NaCl, 100 mmol/L Tris-HCl, pH 9.5, 50 mmol/L MgCl$_2$, 1% tween-20), and incubated in NBT/BCIP (340 mg/ml nitro blue tetrazolium; 350 µg/ml 5-bromo-4-chloro-3-indolyly phosphate in NTMT) for color development. Embryos were photographed using an MVX-10 MacroView microscope and DP71 camera (Olympus America, Center Valley, PA, USA), scored for expression pattern and relative staining intensity, and then processed for genotyping (Table 4). Stained embryos were embedded in 4% NuSieve GTG

agarose (Lonza, Rockland, ME, USA), sectioned at 50 mm with a VT1000S vibratome (Leica Microsystems, Buffalo Grove, IL, USA), and photographed using a BX51 compound microscope with UPLFLN 20x/0.5 objective and DP71 camera (Olympus). All figures represent embryos that were simultaneously processed for fixation and staining.

5.8   CENTRAL ARTERY SPROUT QUANTIFICATION

Manual tracing (Adobe Photoshop CS6) of maximum projections generated from confocal Z-stacks was used to generate simplified wiring diagrams of the forebrain and midbrain central arteries, which originate from the primordial midbrain channels. From these wiring diagrams, I counted: sprouts emerging from the primordial midbrain channel, sprout connections to the basal communicating artery, branch points, and contralateral connections (midline crossings). Each parameter was averaged within treatment groups and values are presented as mean ± SEM.

5.9   BCA AREA QUANTIFICATION

Approximate basal communicating area measurements were achieved by creating a region of interest on a two dimensional maximal projection around the basal communicating artery. Using the analyze tool in the LAS AF (version 3.0.0 build 8134) software, the area within the ROI was calculated. Areas were averaged within treatment groups and values are presented as mean ± SEM.

5.10 FLUORESCENCE INTENSITY MEASUREMENTS OF NOTCH REPORTER EMBRYOS

Fluorescence intensity of cranial arterial EGFP in $Tg(tp1:egfp)^{um14};Tg(fli1a.ep:mRFP-CAAX)^{pt504}$ embryos was quantified using the LAS AF Version 3.0.0 build 8134 software. An ROI was created based on the mRFP channel (threshold, 55; background, 30), and GFP intensity within the masked ROI was measured and averaged over a single z plane, yielding a mean intensity of GFP fluorescence within the ROI. Mean intensities were averaged across samples (n=10 control morphants, 12 *alk1* morphants), and values expressed as mean ± SEM. Results were verified by manually drawing ROIs over the basal communicating artery, using the mRFP channel as a guide, and averaging the colocalized GFP intensity across an entire stack for two embryos per treatment. This method gave similar results to the automated method.

BIBLIOGRAPHY

1. De Val, S., *Key transcriptional regulators of early vascular development.* Arterioscler Thromb Vasc Biol, 2011. **31**(7): p. 1469-75.

2. Risau, W. and I. Flamme, *Vasculogenesis.* Annu Rev Cell Dev Biol, 1995. **11**: p. 73-91.

3. Patan, S., *Vasculogenesis and angiogenesis as mechanisms of vascular network formation, growth and remodeling.* J Neurooncol, 2000. **50**(1-2): p. 1-15.

4. Fouquet, B., et al., *Vessel patterning in the embryo of the zebrafish: guidance by notochord.* Dev Biol, 1997. **183**(1): p. 37-48.

5. Coffin, J.D. and T.J. Poole, *Embryonic vascular development: immunohistochemical identification of the origin and subsequent morphogenesis of the major vessel primordia in quail embryos.* Development, 1988. **102**(4): p. 735-48.

6. Proulx, K., A. Lu, and S. Sumanas, *Cranial vasculature in zebrafish forms by angioblast cluster-derived angiogenesis.* Dev Biol, 2010. **348**(1): p. 34-46.

7. Anderson, M.J., et al., *Loss of unc45a precipitates arteriovenous shunting in the aortic arches.* Dev Biol, 2008. **318**(2): p. 258-67.

8. Li, P., M. Pashmforoush, and H.M. Sucov, *Mesodermal retinoic acid signaling regulates endothelial cell coalescence in caudal pharyngeal arch artery vasculogenesis.* Dev Biol, 2012. **361**(1): p. 116-24.

9. Paffett-Lugassy, N., et al., *Heart field origin of great vessel precursors relies on nkx2.5-mediated vasculogenesis.* Nat Cell Biol, 2013. **15**(11): p. 1362-9.

10. Kamei, M., et al., *Endothelial tubes assemble from intracellular vacuoles in vivo.* Nature, 2006. **442**(7101): p. 453-6.

11. Blum, Y., et al., *Complex cell rearrangements during intersegmental vessel sprouting and vessel fusion in the zebrafish embryo.* Dev Biol, 2008. **316**(2): p. 312-22.

12. Parker, L.H., et al., *The endothelial-cell-derived secreted factor Egfl7 regulates vascular tube formation.* Nature, 2004. **428**(6984): p. 754-8.

13. Strilic, B., et al., *The molecular basis of vascular lumen formation in the developing mouse aorta.* Dev Cell, 2009. **17**(4): p. 505-15.

14. Zovein, A.C., et al., *Beta1 integrin establishes endothelial cell polarity and arteriolar lumen formation via a Par3-dependent mechanism.* Dev Cell, 2010. **18**(1): p. 39-51.

15. Nielsen, J.S. and K.M. McNagny, *Novel functions of the CD34 family.* J Cell Sci, 2008. **121**(Pt 22): p. 3683-92.

16. Herbert, S.P. and D.Y. Stainier, *Molecular control of endothelial cell behaviour during blood vessel morphogenesis.* Nat Rev Mol Cell Biol, 2011. **12**(9): p. 551-64.

17. Bautch, V.L., *VEGF-directed blood vessel patterning: from cells to organism.* Cold Spring Harb Perspect Med, 2012. **2**(9): p. a006452.

18. Koch, S., et al., *Signal transduction by vascular endothelial growth factor receptors.* Biochem J, 2011. **437**(2): p. 169-83.

19. Marcelo, K.L., L.C. Goldie, and K.K. Hirschi, *Regulation of endothelial cell differentiation and specification.* Circ Res, 2013. **112**(9): p. 1272-87.

20. Bautch, V.L. and K.M. Caron, *Blood and Lymphatic Vessel Formation.* Cold Spring Harb Perspect Biol, 2015. **7**(3).

21. Carmeliet, P., et al., *Abnormal blood vessel development and lethality in embryos lacking a single VEGF allele.* Nature, 1996. **380**(6573): p. 435-9.

22. Karkkainen, M.J., et al., *Vascular endothelial growth factor C is required for sprouting of the first lymphatic vessels from embryonic veins.* Nat Immunol, 2004. **5**(1): p. 74-80.

23. Jeltsch, M., et al., *Hyperplasia of lymphatic vessels in VEGF-C transgenic mice.* Science, 1997. **276**(5317): p. 1423-5.

24. Ito, N., et al., *Identification of vascular endothelial growth factor receptor-1 tyrosine phosphorylation sites and binding of SH2 domain-containing molecules.* J Biol Chem, 1998. **273**(36): p. 23410-8.

25. Koch, S. and L. Claesson-Welsh, *Signal transduction by vascular endothelial growth factor receptors.* Cold Spring Harb Perspect Med, 2012. **2**(7): p. a006502.

26. Fong, G.H., et al., *Role of the Flt-1 receptor tyrosine kinase in regulating the assembly of vascular endothelium.* Nature, 1995. **376**(6535): p. 66-70.

27. Germain, S., et al., *Hypoxia-driven angiogenesis: role of tip cells and extracellular matrix scaffolding.* Curr Opin Hematol, 2010. **17**(3): p. 245-51.

28. Randi, A.M., et al., *Regulation of angiogenesis by ETS transcription factors.* Biochem Soc Trans, 2009. **37**(Pt 6): p. 1248-53.

29. Jakobsson, L., et al., *Endothelial cells dynamically compete for the tip cell position during angiogenic sprouting.* Nat Cell Biol, 2010. **12**(10): p. 943-53.

30. Lawson, N.D., et al., *Notch signaling is required for arterial-venous differentiation during embryonic vascular development.* Development, 2001. **128**(19): p. 3675-83.

31. Trindade, A., et al., *Overexpression of delta-like 4 induces arterialization and attenuates vessel formation in developing mouse embryos.* Blood, 2008. **112**(5): p. 1720-9.

32. Taylor, K.L., A.M. Henderson, and C.C. Hughes, *Notch activation during endothelial cell network formation in vitro targets the basic HLH transcription factor HESR-1 and downregulates VEGFR-2/KDR expression.* Microvasc Res, 2002. **64**(3): p. 372-83.

33. Siekmann, A.F. and N.D. Lawson, *Notch signalling limits angiogenic cell behaviour in developing zebrafish arteries.* Nature, 2007. **445**(7129): p. 781-4.

34. Leslie, J.D., et al., *Endothelial signalling by the Notch ligand Delta-like 4 restricts angiogenesis.* Development, 2007. **134**(5): p. 839-44.

35. De Smet, F., et al., *Mechanisms of vessel branching: filopodia on endothelial tip cells lead the way.* Arterioscler Thromb Vasc Biol, 2009. **29**(5): p. 639-49.

36. Gerhardt, H., et al., *VEGF guides angiogenic sprouting utilizing endothelial tip cell filopodia.* J Cell Biol, 2003. **161**(6): p. 1163-77.

37. Strasser, G.A., J.S. Kaminker, and M. Tessier-Lavigne, *Microarray analysis of retinal endothelial tip cells identifies CXCR4 as a mediator of tip cell morphology and branching.* Blood, 2010. **115**(24): p. 5102-10.

38. Hellstrom, M., et al., *Dll4 signalling through Notch1 regulates formation of tip cells during angiogenesis.* Nature, 2007. **445**(7129): p. 776-80.

39. Suchting, S., et al., *The Notch ligand Delta-like 4 negatively regulates endothelial tip cell formation and vessel branching.* Proc Natl Acad Sci U S A, 2007. **104**(9): p. 3225-30.

40. Lobov, I.B., et al., *Delta-like ligand 4 (Dll4) is induced by VEGF as a negative regulator of angiogenic sprouting.* Proc Natl Acad Sci U S A, 2007. **104**(9): p. 3219-24.

41. Funahashi, Y., et al., *Notch regulates the angiogenic response via induction of VEGFR-1.* J Angiogenes Res, 2010. **2**(1): p. 3.

42. Wythe, J.D., et al., *ETS factors regulate Vegf-dependent arterial specification.* Dev Cell, 2013. **26**(1): p. 45-58.

43.   Pelton, J.C., et al., *Multiple endothelial cells constitute the tip of developing blood vessels and polarize to promote lumen formation.* Development, 2014. **141**(21): p. 4121-6.

44.   Bergers, G. and S. Song, *The role of pericytes in blood-vessel formation and maintenance.* Neuro Oncol, 2005. **7**(4): p. 452-64.

45.   Jain, R.K., *Molecular regulation of vessel maturation.* Nat Med, 2003. **9**(6): p. 685-93.

46.   Gaengel, K., et al., *Endothelial-mural cell signaling in vascular development and angiogenesis.* Arterioscler Thromb Vasc Biol, 2009. **29**(5): p. 630-8.

47.   Vokes, S.A., et al., *Hedgehog signaling is essential for endothelial tube formation during vasculogenesis.* Development, 2004. **131**(17): p. 4371-80.

48.   Swift, M.R. and B.M. Weinstein, *Arterial-venous specification during development.* Circ Res, 2009. **104**(5): p. 576-88.

49.   Lawson, N.D., A.M. Vogel, and B.M. Weinstein, *sonic hedgehog and vascular endothelial growth factor act upstream of the Notch pathway during arterial endothelial differentiation.* Dev Cell, 2002. **3**(1): p. 127-36.

50.   Villa, N., et al., *Vascular expression of Notch pathway receptors and ligands is restricted to arterial vessels.* Mech Dev, 2001. **108**(1-2): p. 161-4.

51.   Wang, H.U., Z.F. Chen, and D.J. Anderson, *Molecular distinction and angiogenic interaction between embryonic arteries and veins revealed by ephrin-B2 and its receptor Eph-B4.* Cell, 1998. **93**(5): p. 741-53.

52.   Kullander, K. and R. Klein, *Mechanisms and functions of Eph and ephrin signalling.* Nat Rev Mol Cell Biol, 2002. **3**(7): p. 475-86.

53.   Adams, R.H., et al., *Roles of ephrinB ligands and EphB receptors in cardiovascular development: demarcation of arterial/venous domains, vascular morphogenesis, and sprouting angiogenesis.* Genes Dev, 1999. **13**(3): p. 295-306.

54.   Krishnan, V., et al., *Identification of a novel sonic hedgehog response element in the chicken ovalbumin upstream promoter-transcription factor II promoter.* Mol Endocrinol, 1997. **11**(10): p. 1458-66.

55.   Pereira, F.A., et al., *The orphan nuclear receptor COUP-TFII is required for angiogenesis and heart development.* Genes Dev, 1999. **13**(8): p. 1037-49.

56.   You, L.R., et al., *Suppression of Notch signalling by the COUP-TFII transcription factor regulates vein identity.* Nature, 2005. **435**(7038): p. 98-104.

57.   Kang, J., et al., *An exquisite cross-control mechanism among endothelial cell fate regulators directs the plasticity and heterogeneity of lymphatic endothelial cells.* Blood, 2010. **116**(1): p. 140-50.

58.   Swift, M.R., et al., *SoxF factors and Notch regulate nr2f2 gene expression during venous differentiation in zebrafish.* Dev Biol, 2014. **390**(2): p. 116-25.

59.   Moyon, D., et al., *Plasticity of endothelial cells during arterial-venous differentiation in the avian embryo.* Development, 2001. **128**(17): p. 3359-70.

60.   Othman-Hassan, K., et al., *Arterial identity of endothelial cells is controlled by local cues.* Dev Biol, 2001. **237**(2): p. 398-409.

61.   le Noble, F., et al., *Flow regulates arterial-venous differentiation in the chick embryo yolk sac.* Development, 2004. **131**(2): p. 361-75.

62.   Roman, B.L. and K. Pekkan, *Mechanotransduction in embryonic vascular development.* Biomech Model Mechanobiol, 2012. **11**(8): p. 1149-68.

63.   Brownlee, R.D. and B.L. Langille, *Arterial adaptations to altered blood flow.* Can J Physiol Pharmacol, 1991. **69**(7): p. 978-83.

64.   Di Stefano, I., D.R. Koopmans, and B.L. Langille, *Modulation of arterial growth of the rabbit carotid artery associated with experimental elevation of blood flow.* J Vasc Res, 1998. **35**(1): p. 1-7.

65.   Kamiya, A. and T. Togawa, *Adaptive regulation of wall shear stress to flow change in the canine carotid artery.* Am J Physiol, 1980. **239**(1): p. H14-21.

66.   Langille, B.L., M.P. Bendeck, and F.W. Keeley, *Adaptations of carotid arteries of young and mature rabbits to reduced carotid blood flow.* Am J Physiol, 1989. **256**(4 Pt 2): p. H931-9.

67.   Langille, B.L. and F. O'Donnell, *Reductions in arterial diameter produced by chronic decreases in blood flow are endothelium-dependent.* Science, 1986. **231**(4736): p. 405-7.

68.   Cecchi, E., et al., *Role of hemodynamic shear stress in cardiovascular disease.* Atherosclerosis, 2011. **214**(2): p. 249-56.

69.   Dekker, R.J., et al., *KLF2 provokes a gene expression pattern that establishes functional quiescent differentiation of the endothelium.* Blood, 2006. **107**(11): p. 4354-63.

70.   Parmar, K.M., et al., *Integration of flow-dependent endothelial phenotypes by Kruppel-like factor 2.* J Clin Invest, 2006. **116**(1): p. 49-58.

71.   Fledderus, J.O., et al., *KLF2 primes the antioxidant transcription factor Nrf2 for activation in endothelial cells.* Arterioscler Thromb Vasc Biol, 2008. **28**(7): p. 1339-46.

72. Hay, D.C., et al., *Activation of NF-kappaB nuclear transcription factor by flow in human endothelial cells.* Biochim Biophys Acta, 2003. **1642**(1-2): p. 33-44.

73. SenBanerjee, S., et al., *KLF2 Is a novel transcriptional regulator of endothelial proinflammatory activation.* J Exp Med, 2004. **199**(10): p. 1305-15.

74. Tkachenko, E., et al., *The nucleus of endothelial cell as a sensor of blood flow direction.* Biol Open, 2013. **2**(10): p. 1007-12.

75. AbouAlaiwi, W.A., et al., *Ciliary polycystin-2 is a mechanosensitive calcium channel involved in nitric oxide signaling cascades.* Circ Res, 2009. **104**(7): p. 860-9.

76. Van der Heiden, K., et al., *Endothelial primary cilia in areas of disturbed flow are at the base of atherosclerosis.* Atherosclerosis, 2008. **196**(2): p. 542-50.

77. Van der Heiden, K., et al., *Monocilia on chicken embryonic endocardium in low shear stress areas.* Dev Dyn, 2006. **235**(1): p. 19-28.

78. Hierck, B.P., et al., *Primary cilia sensitize endothelial cells for fluid shear stress.* Dev Dyn, 2008. **237**(3): p. 725-35.

79. Iomini, C., et al., *Primary cilia of human endothelial cells disassemble under laminar shear stress.* J Cell Biol, 2004. **164**(6): p. 811-7.

80. Nauli, S.M., et al., *Endothelial cilia are fluid shear sensors that regulate calcium signaling and nitric oxide production through polycystin-1.* Circulation, 2008. **117**(9): p. 1161-71.

81. Weinbaum, S., J.M. Tarbell, and E.R. Damiano, *The structure and function of the endothelial glycocalyx layer.* Annu Rev Biomed Eng, 2007. **9**: p. 121-67.

82. Reitsma, S., et al., *The endothelial glycocalyx: composition, functions, and visualization.* Pflugers Arch, 2007. **454**(3): p. 345-59.

83. Thi, M.M., et al., *The role of the glycocalyx in reorganization of the actin cytoskeleton under fluid shear stress: a "bumper-car" model.* Proc Natl Acad Sci U S A, 2004. **101**(47): p. 16483-8.

84. Osawa, M., et al., *Evidence for a role of platelet endothelial cell adhesion molecule-1 in endothelial cell mechanosignal transduction: is it a mechanoresponsive molecule?* J Cell Biol, 2002. **158**(4): p. 773-85.

85. Tzima, E., et al., *A mechanosensory complex that mediates the endothelial cell response to fluid shear stress.* Nature, 2005. **437**(7057): p. 426-31.

86. Dimmeler, S., et al., *Activation of nitric oxide synthase in endothelial cells by Akt-dependent phosphorylation.* Nature, 1999. **399**(6736): p. 601-5.

87.   Jin, Z.G., et al., *Ligand-independent activation of vascular endothelial growth factor receptor 2 by fluid shear stress regulates activation of endothelial nitric oxide synthase.* Circ Res, 2003. **93**(4): p. 354-63.

88.   Morgan, J.T., et al., *Nesprin-3 regulates endothelial cell morphology, perinuclear cytoskeletal architecture, and flow-induced polarization.* Mol Biol Cell, 2011. **22**(22): p. 4324-34.

89.   le Noble, F., et al., *Control of arterial branching morphogenesis in embryogenesis: go with the flow.* Cardiovasc Res, 2005. **65**(3): p. 619-28.

90.   Braverman, I.M., A. Keh, and B.S. Jacobson, *Ultrastructure and three-dimensional organization of the telangiectases of hereditary hemorrhagic telangiectasia.* J Invest Dermatol, 1990. **95**(4): p. 422-7.

91.   Guttmacher, A.E., D.A. Marchuk, and R.I. White, Jr., *Hereditary hemorrhagic telangiectasia.* N Engl J Med, 1995. **333**(14): p. 918-24.

92.   Corti, P., et al., *Interaction between alk1 and blood flow in the development of arteriovenous malformations.* Development, 2011. **138**(8): p. 1573-82.

93.   Laakso, A. and J. Hernesniemi, *Arteriovenous malformations: epidemiology and clinical presentation.* Neurosurg Clin N Am, 2012. **23**(1): p. 1-6.

94.   Ragsdale, J.A., *Hereditary hemorrhagic telangiectasia: from epistaxis to life-threatening GI bleeding.* Gastroenterol Nurs, 2007. **30**(4): p. 293-9; quiz 300-1.

95.   Hershkovitz, D., et al., *RASA1 mutations may cause hereditary capillary malformations without arteriovenous malformations.* Br J Dermatol, 2008. **158**(5): p. 1035-40.

96.   Moalem, S., et al., *Hypotrichosis-lymphedema-telangiectasia-renal defect associated with a truncating mutation in the SOX18 gene.* Clin Genet, 2014.

97.   Chaudhary, M.W. and R.S. Al-Baradie, *Ataxia-telangiectasia: future prospects.* Appl Clin Genet, 2014. **7**: p. 159-67.

98.   McDonald, J., P. Bayrak-Toydemir, and R.E. Pyeritz, *Hereditary hemorrhagic telangiectasia: an overview of diagnosis, management, and pathogenesis.* Genet Med, 2011. **13**(7): p. 607-16.

99.   McAllister, K.A., et al., *Endoglin, a TGF-beta binding protein of endothelial cells, is the gene for hereditary haemorrhagic telangiectasia type 1.* Nat Genet, 1994. **8**(4): p. 345-51.

100.   Johnson, D.W., et al., *Mutations in the activin receptor-like kinase 1 gene in hereditary haemorrhagic telangiectasia type 2.* Nat Genet, 1996. **13**(2): p. 189-95.

101.   Gallione, C.J., et al., *A combined syndrome of juvenile polyposis and hereditary haemorrhagic telangiectasia associated with mutations in MADH4 (SMAD4).* Lancet, 2004. **363**(9412): p. 852-9.

102.   Cole, S.G., et al., *A new locus for hereditary haemorrhagic telangiectasia (HHT3) maps to chromosome 5.* J Med Genet, 2005. **42**(7): p. 577-82.

103.   Bayrak-Toydemir, P., et al., *A fourth locus for hereditary hemorrhagic telangiectasia maps to chromosome 7.* Am J Med Genet A, 2006. **140**(20): p. 2155-62.

104.   Bayrak-Toydemir, P., et al., *Genotype-phenotype correlation in hereditary hemorrhagic telangiectasia: mutations and manifestations.* Am J Med Genet A, 2006. **140**(5): p. 463-70.

105.   Sabba, C., et al., *Hereditary hemorrhagic telangiectasia: clinical features in ENG and ALK1 mutation carriers.* J Thromb Haemost, 2007. **5**(6): p. 1149-57.

106.   Letteboer, T.G., et al., *Genotype-phenotype relationship for localization and age distribution of telangiectases in hereditary hemorrhagic telangiectasia.* Am J Med Genet A, 2008. **146A**(21): p. 2733-9.

107.   Ardelean, D.S. and M. Letarte, *Anti-angiogenic therapeutic strategies in hereditary hemorrhagic telangiectasia.* Front Genet, 2015. **6**: p. 35.

108.   Meurer, S.K., et al., *Endoglin in liver fibrogenesis: Bridging basic science and clinical practice.* World J Biol Chem, 2014. **5**(2): p. 180-203.

109.   David, L., J.J. Feige, and S. Bailly, *Emerging role of bone morphogenetic proteins in angiogenesis.* Cytokine Growth Factor Rev, 2009. **20**(3): p. 203-12.

110.   Schmierer, B. and C.S. Hill, *TGFbeta-SMAD signal transduction: molecular specificity and functional flexibility.* Nat Rev Mol Cell Biol, 2007. **8**(12): p. 970-82.

111.   Tillet, E. and S. Bailly, *Emerging roles of BMP9 and BMP10 in hereditary hemorrhagic telangiectasia.* Front Genet, 2014. **5**: p. 456.

112.   Ricard, N., et al., *Functional analysis of the BMP9 response of ALK1 mutants from HHT2 patients: a diagnostic tool for novel ACVRL1 mutations.* Blood, 2010. **116**(9): p. 1604-12.

113.   Gu, Y., et al., *Functional analysis of mutations in the kinase domain of the TGF-beta receptor ALK1 reveals different mechanisms for induction of hereditary hemorrhagic telangiectasia.* Blood, 2006. **107**(5): p. 1951-4.

114.   Oh, S.P., et al., *Activin receptor-like kinase 1 modulates transforming growth factor-beta 1 signaling in the regulation of angiogenesis.* Proc Natl Acad Sci U S A, 2000. **97**(6): p. 2626-31.

115. Urness, L.D., L.K. Sorensen, and D.Y. Li, *Arteriovenous malformations in mice lacking activin receptor-like kinase-1.* Nat Genet, 2000. **26**(3): p. 328-31.

116. Srinivasan, S., et al., *A mouse model for hereditary hemorrhagic telangiectasia (HHT) type 2.* Hum Mol Genet, 2003. **12**(5): p. 473-82.

117. Park, S.O., et al., *Real-time imaging of de novo arteriovenous malformation in a mouse model of hereditary hemorrhagic telangiectasia.* J Clin Invest, 2009. **119**(11): p. 3487-96.

118. Park, S.O., et al., *ALK5- and TGFBR2-independent role of ALK1 in the pathogenesis of hereditary hemorrhagic telangiectasia type 2.* Blood, 2008. **111**(2): p. 633-42.

119. Tual-Chalot, S., et al., *Endothelial depletion of Acvrl1 in mice leads to arteriovenous malformations associated with reduced endoglin expression.* PLoS One, 2014. **9**(6): p. e98646.

120. Garrido-Martin, E.M., et al., *Common and distinctive pathogenetic features of arteriovenous malformations in hereditary hemorrhagic telangiectasia 1 and hereditary hemorrhagic telangiectasia 2 animal models--brief report.* Arterioscler Thromb Vasc Biol, 2014. **34**(10): p. 2232-6.

121. Roman, B.L., et al., *Disruption of acvrl1 increases endothelial cell number in zebrafish cranial vessels.* Development, 2002. **129**(12): p. 3009-19.

122. Barbara, N.P., J.L. Wrana, and M. Letarte, *Endoglin is an accessory protein that interacts with the signaling receptor complex of multiple members of the transforming growth factor-beta superfamily.* J Biol Chem, 1999. **274**(2): p. 584-94.

123. Alt, A., et al., *Structural and functional insights into endoglin ligand recognition and binding.* PLoS One, 2012. **7**(2): p. e29948.

124. Castonguay, R., et al., *Soluble endoglin specifically binds bone morphogenetic proteins 9 and 10 via its orphan domain, inhibits blood vessel formation, and suppresses tumor growth.* J Biol Chem, 2011. **286**(34): p. 30034-46.

125. Li, D.Y., et al., *Defective angiogenesis in mice lacking endoglin.* Science, 1999. **284**(5419): p. 1534-7.

126. Bourdeau, A., D.J. Dumont, and M. Letarte, *A murine model of hereditary hemorrhagic telangiectasia.* J Clin Invest, 1999. **104**(10): p. 1343-51.

127. Arthur, H.M., et al., *Endoglin, an ancillary TGFbeta receptor, is required for extraembryonic angiogenesis and plays a key role in heart development.* Dev Biol, 2000. **217**(1): p. 42-53.

128. Sorensen, L.K., et al., *Loss of distinct arterial and venous boundaries in mice lacking endoglin, a vascular-specific TGFbeta coreceptor.* Dev Biol, 2003. **261**(1): p. 235-50.

129. Mahmoud, M., et al., *Pathogenesis of arteriovenous malformations in the absence of endoglin.* Circ Res, 2010. **106**(8): p. 1425-33.

130. Torsney, E., et al., *Mouse model for hereditary hemorrhagic telangiectasia has a generalized vascular abnormality.* Circulation, 2003. **107**(12): p. 1653-7.

131. Satomi, J., et al., *Cerebral vascular abnormalities in a murine model of hereditary hemorrhagic telangiectasia.* Stroke, 2003. **34**(3): p. 783-9.

132. Scharpfenecker, M., et al., *BMP-9 signals via ALK1 and inhibits bFGF-induced endothelial cell proliferation and VEGF-stimulated angiogenesis.* J Cell Sci, 2007. **120**(Pt 6): p. 964-72.

133. David, L., et al., *Bone morphogenetic protein-9 is a circulating vascular quiescence factor.* Circ Res, 2008. **102**(8): p. 914-22.

134. Upton, P.D., et al., *Bone morphogenetic protein (BMP) and activin type II receptors balance BMP9 signals mediated by activin receptor-like kinase-1 in human pulmonary artery endothelial cells.* J Biol Chem, 2009. **284**(23): p. 15794-804.

135. Laux, D.W., et al., *Circulating Bmp10 acts through endothelial Alk1 to mediate flow-dependent arterial quiescence.* Development, 2013. **140**(16): p. 3403-12.

136. Bidart, M., et al., *BMP9 is produced by hepatocytes and circulates mainly in an active mature form complexed to its prodomain.* Cell Mol Life Sci, 2012. **69**(2): p. 313-24.

137. Sengle, G., et al., *Prodomains of transforming growth factor beta (TGFbeta) superfamily members specify different functions: extracellular matrix interactions and growth factor bioavailability.* J Biol Chem, 2011. **286**(7): p. 5087-99.

138. Miller, A.F., et al., *Bone morphogenetic protein-9. An autocrine/paracrine cytokine in the liver.* J Biol Chem, 2000. **275**(24): p. 17937-45.

139. Olsen, O.E., et al., *Bone morphogenetic protein-9 suppresses growth of myeloma cells by signaling through ALK2 but is inhibited by endoglin.* Blood Cancer J, 2014. **4**: p. e196.

140. Chen, H., et al., *Context-dependent signaling defines roles of BMP9 and BMP10 in embryonic and postnatal development.* Proc Natl Acad Sci U S A, 2013. **110**(29): p. 11887-92.

141. Neuhaus, H., V. Rosen, and R.S. Thies, *Heart specific expression of mouse BMP-10 a novel member of the TGF-beta superfamily.* Mech Dev, 1999. **80**(2): p. 181-4.

142. Souza, T.A., et al., *Proteomic identification and functional validation of activins and bone morphogenetic protein 11 as candidate novel muscle mass regulators.* Mol Endocrinol, 2008. **22**(12): p. 2689-702.

143.   Wooderchak-Donahue, W.L., et al., *BMP9 mutations cause a vascular-anomaly syndrome with phenotypic overlap with hereditary hemorrhagic telangiectasia.* Am J Hum Genet, 2013. **93**(3): p. 530-7.

144.   Isogai, S., M. Horiguchi, and B.M. Weinstein, *The vascular anatomy of the developing zebrafish: an atlas of embryonic and early larval development.* Dev Biol, 2001. **230**(2): p. 278-301.

145.   Summerton, J. and D. Weller, *Morpholino antisense oligomers: design, preparation, and properties.* Antisense Nucleic Acid Drug Dev, 1997. **7**(3): p. 187-95.

146.   Summerton, J., *Morpholino antisense oligomers: the case for an RNase H-independent structural type.* Biochim Biophys Acta, 1999. **1489**(1): p. 141-58.

147.   Draper, B.W., P.A. Morcos, and C.B. Kimmel, *Inhibition of zebrafish fgf8 pre-mRNA splicing with morpholino oligos: a quantifiable method for gene knockdown.* Genesis, 2001. **30**(3): p. 154-6.

148.   Goessling, W. and T.E. North, *Repairing quite swimmingly: advances in regenerative medicine using zebrafish.* Dis Model Mech, 2014. **7**(7): p. 769-76.

149.   Bedell, V.M., et al., *In vivo genome editing using a high-efficiency TALEN system.* Nature, 2012. **491**(7422): p. 114-8.

150.   Kettleborough, R.N., et al., *A systematic genome-wide analysis of zebrafish protein-coding gene function.* Nature, 2013. **496**(7446): p. 494-7.

151.   Dekker, R.J., et al., *Endothelial KLF2 links local arterial shear stress levels to the expression of vascular tone-regulating genes.* Am J Pathol, 2005. **167**(2): p. 609-18.

152.   Sharefkin, J.B., et al., *Fluid flow decreases preproendothelin mRNA levels and suppresses endothelin-1 peptide release in cultured human endothelial cells.* J Vasc Surg, 1991. **14**(1): p. 1-9.

153.   Wang, D.L., et al., *Cyclical strain increases endothelin-1 secretion and gene expression in human endothelial cells.* Biochem Biophys Res Commun, 1993. **195**(2): p. 1050-6.

154.   Melchionna, R., et al., *Laminar shear stress inhibits CXCR4 expression on endothelial cells: functional consequences for atherogenesis.* FASEB J, 2005. **19**(6): p. 629-31.

155.   Suresh, S. and A.E. Irvine, *The NOTCH signaling pathway in normal and malignant blood cell production.* J Cell Commun Signal, 2015.

156.   Brou, C., et al., *A novel proteolytic cleavage involved in Notch signaling: the role of the disintegrin-metalloprotease TACE.* Mol Cell, 2000. **5**(2): p. 207-16.

157. De Strooper, B., et al., *A presenilin-1-dependent gamma-secretase-like protease mediates release of Notch intracellular domain.* Nature, 1999. **398**(6727): p. 518-22.

158. Gordon, W.R., K.L. Arnett, and S.C. Blacklow, *The molecular logic of Notch signaling--a structural and biochemical perspective.* J Cell Sci, 2008. **121**(Pt 19): p. 3109-19.

159. Andersson, E.R., R. Sandberg, and U. Lendahl, *Notch signaling: simplicity in design, versatility in function.* Development, 2011. **138**(17): p. 3593-612.

160. Weinstein, B.M., et al., *Gridlock, a localized heritable vascular patterning defect in the zebrafish.* Nat Med, 1995. **1**(11): p. 1143-7.

161. Zhong, T.P., et al., *gridlock, an HLH gene required for assembly of the aorta in zebrafish.* Science, 2000. **287**(5459): p. 1820-4.

162. Krebs, L.T., et al., *Haploinsufficient lethality and formation of arteriovenous malformations in Notch pathway mutants.* Genes Dev, 2004. **18**(20): p. 2469-73.

163. Nielsen, C.M., et al., *Deletion of Rbpj from postnatal endothelium leads to abnormal arteriovenous shunting in mice.* Development, 2014. **141**(19): p. 3782-92.

164. Covassin, L., et al., *Global analysis of hematopoietic and vascular endothelial gene expression by tissue specific microarray profiling in zebrafish.* Dev Biol, 2006. **299**(2): p. 551-62.

165. Bussmann, J., S.A. Wolfe, and A.F. Siekmann, *Arterial-venous network formation during brain vascularization involves hemodynamic regulation of chemokine signaling.* Development, 2011. **138**(9): p. 1717-26.

166. Carlson, T.R., et al., *Endothelial expression of constitutively active Notch4 elicits reversible arteriovenous malformations in adult mice.* Proc Natl Acad Sci U S A, 2005. **102**(28): p. 9884-9.

167. Murphy, P.A., et al., *Endothelial Notch4 signaling induces hallmarks of brain arteriovenous malformations in mice.* Proc Natl Acad Sci U S A, 2008. **105**(31): p. 10901-6.

168. Murphy, P.A., et al., *Endothelial Notch signaling is upregulated in human brain arteriovenous malformations and a mouse model of the disease.* Lab Invest, 2009. **89**(9): p. 971-82.

169. Miniati, D., et al., *Constitutively active endothelial Notch4 causes lung arteriovenous shunts in mice.* Am J Physiol Lung Cell Mol Physiol, 2010. **298**(2): p. L169-77.

170. Murphy, P.A., et al., *Notch4 normalization reduces blood vessel size in arteriovenous malformations.* Sci Transl Med, 2012. **4**(117): p. 117ra8.

171.	Kim, Y.H., et al., *Artery and vein size is balanced by Notch and ephrin B2/EphB4 during angiogenesis.* Development, 2008. **135**(22): p. 3755-64.

172.	Krebs, L.T., et al., *Notch1 activation in mice causes arteriovenous malformations phenocopied by ephrinB2 and EphB4 mutants.* Genesis, 2010. **48**(3): p. 146-50.

173.	Morikawa, M., et al., *ChIP-seq reveals cell type-specific binding patterns of BMP-specific Smads and a novel binding motif.* Nucleic Acids Res, 2011. **39**(20): p. 8712-27.

174.	Kim, J.H., et al., *BMP9 induces EphrinB2 expression in endothelial cells through an Alk1-BMPRII/ActRII-ID1/ID3-dependent pathway: implications for hereditary hemorrhagic telangiectasia type II.* Angiogenesis, 2012. **15**(3): p. 497-509.

175.	Larrivee, B., et al., *ALK1 signaling inhibits angiogenesis by cooperating with the Notch pathway.* Dev Cell, 2012. **22**(3): p. 489-500.

176.	Goumans, M.J., et al., *Activin receptor-like kinase (ALK)1 is an antagonistic mediator of lateral TGFbeta/ALK5 signaling.* Mol Cell, 2003. **12**(4): p. 817-28.

177.	Moya, I.M., et al., *Stalk cell phenotype depends on integration of Notch and Smad1/5 signaling cascades.* Dev Cell, 2012. **22**(3): p. 501-14.

178.	Fujita, M., et al., *Assembly and patterning of the vascular network of the vertebrate hindbrain.* Development, 2011. **138**(9): p. 1705-15.

179.	Schumacher, J.A., et al., *tal1 Regulates the formation of intercellular junctions and the maintenance of identity in the endocardium.* Dev Biol, 2013. **383**(2): p. 214-26.

180.	Lebrin, F., et al., *Endoglin promotes endothelial cell proliferation and TGF-beta/ALK1 signal transduction.* EMBO J, 2004. **23**(20): p. 4018-28.

181.	Guruharsha, K.G., M.W. Kankel, and S. Artavanis-Tsakonas, *The Notch signalling system: recent insights into the complexity of a conserved pathway.* Nat Rev Genet, 2012. **13**(9): p. 654-66.

182.	Quillien, A., et al., *Distinct Notch signaling outputs pattern the developing arterial system.* Development, 2014.

183.	Duarte, A., et al., *Dosage-sensitive requirement for mouse Dll4 in artery development.* Genes Dev, 2004. **18**(20): p. 2474-8.

184.	Iso, T., et al., *Dll4-selective Notch signaling induces ephrinB2 gene expression in endothelial cells.* Biochem Biophys Res Commun, 2006. **341**(3): p. 708-14.

185.	Benedito, R., et al., *Loss of Notch signalling induced by Dll4 causes arterial calibre reduction by increasing endothelial cell response to angiogenic stimuli.* BMC Dev Biol, 2008. **8**: p. 117.

186. ZhuGe, Q., et al., *Notch-1 signalling is activated in brain arteriovenous malformations in humans.* Brain, 2009. **132**(Pt 12): p. 3231-41.

187. Herbert, S.P., et al., *Arterial-venous segregation by selective cell sprouting: an alternative mode of blood vessel formation.* Science, 2009. **326**(5950): p. 294-8.

188. Lindskog, H., et al., *Molecular identification of venous progenitors in the dorsal aorta reveals an aortic origin for the cardinal vein in mammals.* Development, 2014. **141**(5): p. 1120-8.

189. Xu, P., J. Liu, and R. Derynck, *Post-translational regulation of TGF-beta receptor and Smad signaling.* FEBS Lett, 2012. **586**(14): p. 1871-84.

190. Johnson, D.W., et al., *Mutations in the activin receptor-like kinase 1 gene in hereditary haemorrhagic telangiectasia type 2.* Nature Genet., 1996. **13**(2): p. 189-95.

191. McAllister, K.A., et al., *Endoglin, a TGF-b binding protein of endothelial cells, is the gene for hereditary haemorrhagic telangiectasia type 1.* Nature Genet., 1994. **8**(4): p. 345-51.

192. Urness, L.D., L.K. Sorensen, and D.Y. Li, *Arteriovenous malformations in mice lacking activin receptor-like kinase-1.* Nature Genet., 2000. **26**(3): p. 328-31.

193. Morikawa, M., et al., *ChIP-seq reveals cell type-specific binding patterns of BMP-specific Smads and a novel binding motif.* Nucleic Acids Res, 2011.

194. Parsons, M.J., et al., *Notch-responsive cells initiate the secondary transition in larval zebrafish pancreas.* Mech Dev, 2009. **126**(10): p. 898-912.

195. Borggrefe, T. and F. Oswald, *The Notch signaling pathway: transcriptional regulation at Notch target genes.* Cell Mol Life Sci, 2009. **66**(10): p. 1631-46.

196. Zhou, M., et al., *Comparative and evolutionary analysis of the HES/HEY gene family reveal exon/intron loss and teleost specific duplication events.* PLoS One, 2012. **7**(7): p. e40649.

197. Caolo, V., et al., *Feed-forward signaling by membrane-bound ligand receptor circuit: the case of NOTCH DELTA-like 4 ligand in endothelial cells.* J Biol Chem, 2010. **285**(52): p. 40681-9.

198. Sacilotto, N., et al., *Analysis of Dll4 regulation reveals a combinatorial role for Sox and Notch in arterial development.* Proc Natl Acad Sci U S A, 2013. **110**(29): p. 11893-8.

199. Jiang, Y.J., et al., *Mutations affecting neurogenesis and brain morphology in the zebrafish, Danio rerio.* Development, 1996. **123**: p. 205-16.

200.	Isogai, S., M. Horiguchi, and B.M. Weinstein, *The vascular anatomy of the developing zebrafish: an atlas of embryonic and early larval development.* Dev. Biol., 2001. **230**(2): p. 278-301.

201.	Watson, O., et al., *Blood flow suppresses vascular Notch signalling via dll4 and is required for angiogenesis in response to hypoxic signalling.* Cardiovasc Res, 2013. **100**(2): p. 252-61.

202.	Bai, G., et al., *Id sustains Hes1 expression to inhibit precocious neurogenesis by releasing negative autoregulation of Hes1.* Dev Cell, 2007. **13**(2): p. 283-97.

203.	Fernandez, L.A., et al., *Hereditary hemorrhagic telangiectasia, a vascular dysplasia affecting the TGF-beta signaling pathway.* Clin Med Res, 2006. **4**(1): p. 66-78.

204.	Lamouille, S., et al., *Activin receptor-like kinase 1 is implicated in the maturation phase of angiogenesis.* Blood, 2002. **100**(13): p. 4495-501.

205.	Fernandez, L.A., et al., *Blood outgrowth endothelial cells from Hereditary Haemorrhagic Telangiectasia patients reveal abnormalities compatible with vascular lesions.* Cardiovasc Res, 2005. **68**(2): p. 235-48.

206.	Seki, T., K.H. Hong, and S.P. Oh, *Nonoverlapping expression patterns of ALK1 and ALK5 reveal distinct roles of each receptor in vascular development.* Lab Invest, 2006. **86**(2): p. 116-29.

207.	Seki, T., J. Yun, and S.P. Oh, *Arterial endothelium-specific activin receptor-like kinase 1 expression suggests its role in arterialization and vascular remodeling.* Circ Res, 2003. **93**(7): p. 682-9.

208.	Han, C., et al., *VEGF neutralization can prevent and normalize arteriovenous malformations in an animal model for hereditary hemorrhagic telangiectasia 2.* Angiogenesis, 2014. **17**(4): p. 823-30.

209.	Ardelean, D.S., et al., *Endoglin and activin receptor-like kinase 1 heterozygous mice have a distinct pulmonary and hepatic angiogenic profile and response to anti-VEGF treatment.* Angiogenesis, 2014. **17**(1): p. 129-46.

210.	Mitchell, A., et al., *Bevacizumab reverses need for liver transplantation in hereditary hemorrhagic telangiectasia.* Liver Transpl, 2008. **14**(2): p. 210-3.

211.	Oosting, S., W. Nagengast, and E. de Vries, *More on bevacizumab in hereditary hemorrhagic telangiectasia.* N Engl J Med, 2009. **361**(9): p. 931; author reply 931-2.

212.	Retornaz, F., Y. Rinaldi, and C. Duvoux, *More on bevacizumab in hereditary hemorrhagic telangiectasia.* N Engl J Med, 2009. **361**(9): p. 931; author reply 931-2.

213.	Bose, P., J.L. Holter, and G.B. Selby, *Bevacizumab in hereditary hemorrhagic telangiectasia.* N Engl J Med, 2009. **360**(20): p. 2143-4.

214.	Westerfield, M., *The zebrafish book : a guide for the laboratory use of zebrafish (Brachydanio rerio).* 1993, Eugene, OR: M. Westerfield.

215.	Jin, S.W., et al., *Cellular and molecular analyses of vascular tube and lumen formation in zebrafish.* Development, 2005. **132**(23): p. 5199-209.

216.	Neff, M.M., et al., *dCAPS, a simple technique for the genetic analysis of single nucleotide polymorphisms: experimental applications in Arabidopsis thaliana genetics.* Plant J, 1998. **14**(3): p. 387-92.

217.	Choi, J., et al., *FoxH1 negatively modulates flk1 gene expression and vascular formation in zebrafish.* Dev Biol, 2007. **304**(2): p. 735-44.

218.	Herwig, L., et al., *Distinct cellular mechanisms of blood vessel fusion in the zebrafish embryo.* Curr Biol, 2011. **21**(22): p. 1942-8.

219.	Hatta, K., H. Tsujii, and T. Omura, *Cell tracking using a photoconvertible fluorescent protein.* Nat Protoc, 2006. **1**(2): p. 960-7.

220.	Kawakami, K., et al., *A transposon-mediated gene trap approach identifies developmentally regulated genes in zebrafish.* Dev Cell, 2004. **7**(1): p. 133-44.

221.	Kwan, K.M., et al., *The Tol2kit: a multisite gateway-based construction kit for Tol2 transposon transgenesis constructs.* Dev Dyn, 2007. **236**(11): p. 3088-99.

222.	Villefranc, J.A., J. Amigo, and N.D. Lawson, *Gateway compatible vectors for analysis of gene function in the zebrafish.* Dev Dyn, 2007. **236**(11): p. 3077-87.

223.	Sehnert, A.J., et al., *Cardiac troponin T is essential in sarcomere assembly and cardiac contractility.* Nat Genet, 2002. **31**(1): p. 106-10.